

**FABRICATION OF LIGHTWEIGHT AND DURABLE THERMOPLASTIC
COMPOSITES FOR INJECTION MOLDING WITH THE INTEGRATION OF
WASTE-DRIVEN REINFORCING MATERIALS**

by

Kuray DERİCİLER

Submitted to the Graduate School of Engineering and Natural Sciences
in partial fulfilment of the requirements for the degree of

Doctor of Philosophy

SABANCI UNIVERSITY

DECEMBER 2023

© KURAY DERİCİLER 2023

All Rights Reserved

ABSTRACT

FABRICATION OF LIGHTWEIGHT AND DURABLE THERMOPLASTIC COMPOSITES FOR INJECTION MOLDING WITH THE INTEGRATION OF WASTE-DRIVEN REINFORCING MATERIALS

Kuray DERİCİLER

Doctor of Philosophy, 2023

Material Science and Nano Engineering

Thesis Advisor: Assoc. Prof. Dr. Burcu SANER OKAN

Keywords: Graphene, Thermoplastic Composites, Polyamide (PA), Waste Derived Reinforcements, Upcycling, Hybrid Composites

Reducing carbon dioxide (CO₂) emissions and adopting lightweighting strategies are crucial aspects of enhancing the sustainability and efficiency of the transportation sector. As sustainability becomes a central focus in the automotive industry, there is a growing demand to use recycled sources in manufacturing processes for part production. Especially for structural parts in automotive part production, polyamides (PAs) are extensively employed as engineering thermoplastics across diverse fields, owing to their ease of processing, good thermal stability, and cost-effectiveness. In PA based compound formulations, short glass fibers are preferred to reinforce PA matrix. However, the higher density of glass fibers and its brittleness during extrusion process can be problematic and high energy demands to produce both fiber and parts are main drawbacks in serial production. At this point, the present thesis aims to replace glass fibers with sustainable solutions by developing new PA compound formulations by using additives coming from recycled sources which are graphene nanoplatelets (GNP) derived from waste tires, spherical graphenes from waste coffee (CWC) and short carbon fiber (CF) bundles coming from plant waste. These additives were successfully incorporated into PA matrix

by using thermokinetic high-shear mixer resulting in high degree of exfoliation and thus high mechanical performance that can compete with conventional compounds. In the case of GNP reinforced PA composites, their tensile and flexural properties improved by 42% and 43%, respectively, by adding optimized loading ratio of 0.3 wt.% GNP in PA6,6. With this amount of GNP, CF based compounds were successfully produced by increasing tensile and flexural properties by 95% and 86%, respectively, in comparison of unfilled PA. Through GNP integration, the absorbed impact energy of this compound improved by 7.7% due to enhanced interfacial interactions between the ternary interfaces. By embracing the evolving trends towards sustainability in major transportation industries, this study strategically navigates the transition from synthetic PA6,6 to semi-synthetic PA6,10 matrix and leveraging the remarkable potential of waste-derived reinforcing materials. Herein, the effects of aspect ratio of waste driven reinforcements, reinforcement size, and loading ratios were investigated to generate a comprehensive interface characterization. Consequently, this thesis demonstrates that using tailored selection of waste-derived reinforcing material, sustainable compounds can replace several synthetic products in the market in terms of both tensile properties, lightweighting, and environmental impact. In addition, CO₂ emission values of both the selected recycled sources and the developed compound formulations were calculated by using life cycle assessment (LCA) analysis. A significant reduction was achieved by reducing 55% CO₂ emission with new recycled additive reinforced PA6,10 formulations over PA6 having 15 wt.% GF available in the market. Therefore, this study extends beyond the material enhancement to encompass a holistic approach that contributes to a circular economy and promotes eco-friendly, high-performance composites for the automotive industry, thereby laying the foundation for incorporation of waste-derived reinforcements into compound formulations to create a future where waste materials are not merely managed but transformed into valuable resources.

ÖZET

ATIKLARDAN ELDE EDİLEN KATKI MALZEMELERİNİN ENTEGRASYONU İLE HAFİF VE DAYANIKLI TERMOPLASTİK KOMPOZİTLERİN ENJEKSİYON KALIPLAMA İÇİN ÜRETİMİ

Kuray DERİCİLER

Doktora Tezi, 2023

Malzeme Bilimi ve Nano Mühendisliği

Tez Danışmanı: Doç. Dr. Burcu SANER OKAN

Anahtar Kelimeler: Grafen, Termoplastik Kompozitler, Poliamid (PA), Atıktan Türetilen Güçlendiriciler, İleri Dönüşüm, Hibrit Kompozitler

Ulaşım sektöründe sürdürülebilirliği ve verimliliği arttırmak için karbon dioksit (CO₂) emisyonlarını azaltma ve hafifletme stratejileri vazgeçilmezdir. Otomotiv endüstrisinde sürdürülebilirlik odak noktası olurken üretim yöntemlerinde geri dönüştürülmüş kaynakların kullanımı için talep de artmaktadır. Özellikle yapısal otomotiv parçalarında poliamidler (PAlar) kolay işlendikleri, iyi termal stabiliteye sahip oldukları, ve düşük maliyetleri sebebiyle bir çok farklı alanda, yaygın bir şekilde kullanılmaktadır. PA bazlı kompond formülasyonlarında matrisi güçlendirmek amacıyla kısa cam fiberler daha çok tercih edilmektedir. Ancak cam fiberlerin yüksek yoğunluğu ve ekstrüzyon esnasındaki gevreklikleri problem yaratmaktadır. Bununla beraber cam fiber ve parça üretimi esnasında yüksek enerji gerekmesi de seri üretimde karşılaşılan problemlerdendir. Bu noktada, bu tez çalışması atık lastiklerden elde edilen grafen nanotabakalar (GNP), atık kahveden üretilen küresel grafenler (CWC) ve fabrika atıklarından elde edilen kısa karbon fiberler (CF) katkı malzemesi olarak kullanılıp PA bazlı kompond formülasyonları geliştirilerek cam fiberlerin yerine sürdürülebilir çözümler sunmayı hedeflemektedir. Bu katkı malzemeleri PA matris içerisine yüksek kayma kuvvetli

termokinetik karıştırıcı ile dağıtılarak tabakaların ayrılmış ve konvansiyonel kompozitler ile yarışabilecek mekanik performans elde edilmiştir. Optimize edilmiş yüklenme oranlarıyla ağırlıkça %0.3 GNP katkılı kompozitler çekme ve eğme özelliklerinde sırasıyla %42 ve %43 iyileşme görülmüştür. Aynı GNP miktarıyla hazırlanan CF katkılı kompozitler de başarı ile üretilmiş ve çekme ile eğme özelliklerinde katkısız polimere göre sırasıyla %95 ve %86 artış yakalanmıştır. GNP entegrasyonu sayesinde üçlü arayüz etkileşimleri pekiştirilmiş ve kompozitin darbe enerjisi emme özelliği de %7.7 artmıştır. Ulaşım endüstrisindeki sürdürülebilirlik yönünde gelişen trendleri de yakalayarak bu çalışma bünyesinde sentetik PA6,6'dan yarı sentetik PA6,10'a geçiş stratejik bir biçimde sağlanmış ve atık malzemelerden elde edilen katkıların kayda değer potansiyeli de kullanılmıştır. Burada, atık malzemelerden elde edilen katkıların en/boy oranı, boyutu ve yüklenme miktarı kontrol edilerek arayüze etkileri detaylı bir şekilde incelenmiştir. Dolayısıyla bu tez, atık malzemelerden elde edilen katkıların dikkatli seçimi elde edilen sürdürülebilir kompozitlerin piyasadaki sentetik ürünlerin mekanik özellikler, hafiflik ve çevresel etki bakımından yerine geçebileceklerini göstermektedir. Ek olarak, hem atık malzemelerden elde edilen katkı malzemelerinin, hem de geliştirilen kompozit formülasyonlarının CO₂ emisyon değerleri yaşam döngüsü değerlendirme (LCA) ile analiz edilmiştir. PA6,10 bazlı kompozitler ile CO₂ emisyonunun piyasadaki ağırlıkça %15 cam fiber katkılı PA6 bazlı kompozitlere oranla %55 azaltılmıştır. Böylece, bu çalışma malzeme geliştirmenin ötesine geçerek tamamlayıcı bir yaklaşımla dögüsel ekonomi ve otomotiv endüstrisi için çevre dostu yüksek performanslı kompozitler geliştirilmesine katkı sağlamış, bu sayede de atık malzemelerden elde edilen katkıların kompozit formülasyonlarına entegre edilmesi ile atıkların sadece yönetilmesinden ziyade değerli kaynaklara dönüştürüldüğü bir gelecek oluşturma konusunda bir temel oluşturmaktadır.

Dedicated to my family...

ACKNOWLEDGEMENTS

I would like to express my deepest gratitude to my dissertation supervisor, Assoc. Prof. Dr. Burcu Saner Okan, for her invaluable guidance, unwavering support, and insightful feedback throughout the entire research process. Her expertise and motivating guidance played a pivotal role in shaping this thesis.

I extend my sincere appreciation to the esteemed members of the jury; Asst. Prof. Dr. Hatice Sinem Şaş Çaycı, Prof. Dr. Emre Erdem, Prof. Dr. Cengiz Kaya, and Assoc. Prof. Dr. Bertan Beylergil, for their time, expertise, and constructive input, which significantly enriched the quality of this work.

Special thanks go to my friends and flatmates, Nargiz Aliyeva, Gizem Semra Arıtürk, and Sina Khalilvandi Behrouzgar, for their unwavering support, encouragement, and shared moments that provided much-needed balance during the demanding phases of this research.

I would also like to acknowledge the support of my colleagues; Sinem Elmas, Yeşim Yeniuyurt Sepici, Nihan Birgün, Asu Ece Ateşpare, Saeed Salamat Gharamaleki, Taha Behroozi Kohlan, Ceren Yıldırım, Abdulrahman Al-Nadhari, Yağız Özbek, Dr. Isa Emami Tabrizi, Sasan Karimi, Amin Balazadeh Koucheh, Faraz Ganjdoust, Mohammad Hasan Joudivand Sarand, Salman Zafar, Hadi Mohammadjafari Sadeghi and countless others who have contributed to the intellectual vibrancy of our academic community.

My heartfelt appreciation goes to the past and present members of the BSO Research group, particularly Atakan Koçanalı, Dr. Semih Doğan, Dr. Havva Başkan Bayrak, Dr. Mohammad Sajad Sorayani Bafqi, Dr. Marjan Hezarkhani, Ramisa Yahyapour, Saher Gül, İlayda Berktaş, and Mostafa Mehdipour Aghbolagh, whose collaboration and shared insights have played a pivotal role in the development of this research.

To my sport buddies, Ogeday Rodop, Cahit Orhun Şenol, and Sercan Akgün, thank you for the camaraderie and support on and off the field, providing a welcome balance to the academic journey.

Heartfelt gratitude is extended to my parents, Fikret Dericiler and Gülden Dericiler, for their unwavering encouragement, love, and belief in my abilities. Your support has been my anchor throughout this academic pursuit.

I want to express my deepest appreciation to my beloved girlfriend, Mine Ersöz, for her understanding, encouragement, and patience during the challenging phases of this thesis. Your unwavering support has been my constant motivation.

I would like to acknowledge the Sabanci University Faculty of Engineering and Natural Sciences Conference Travel Grant, for providing support to both of my international conference travels.

Finally, I would like to thank the Scientific and Technological Research Council of Turkey (TUBITAK) with project number 118C055 and FARPLAS A.S. for supporting my research and industrial studies.

DECEMBER

Kuray DERİCİLER

TABLE OF CONTENTS

ABSTRACT	iv
ÖZET	vi
ACKNOWLEDGEMENTS	x
TABLE OF CONTENTS	xii
ABBREVIATIONS	xiv
SYMBOLS	xvi
LIST OF TABLES	xviii
LIST OF FIGURES	xx
CHAPTER 1: State of the Art	1
CHAPTER 2: Experimental and numerical investigation of flow and alignment behavior of waste tire-derived graphene nanoplatelets in PA6,6 matrix during melt-mixing and injection	5
2.1. Abstract	5
2.2. Introduction.....	5
2.3. Materials and methods	9
2.3.1. Materials	9
2.3.2. Fabrication of GNP reinforced PA6,6 nanocomposites by thermokinetic mixer.....	10
2.3.3. Characterization	11
2.4. Results and Discussion.....	11
2.4.1. Mechanical performance of GNP reinforced PA6,6 nanocomposites	11
2.4.2. Thermal and crystallinity properties of GNP based PA6,6 nanocomposites	15
2.4.3. The effect of GNP as a reinforcement on the rheological behavior of PA6,6 nanocomposites	18
2.4.4. Cross-sectional analysis of GNP reinforced PA6,6 nanocomposites	21
2.5. Conclusions.....	23
CHAPTER 3: The effect of reinforcement aspect ratio on the performance of PA6,6 composites with recycled carbon fiber and upcycled graphene nanoplatelets: An interface characterization from process to modelling	24
3.1. Abstract	24
3.2. Introduction.....	24
3.3. Materials and Method	27

3.3.1. Materials	27
3.3.2. Fabrication of recycled carbon fiber reinforced PA6,6 and recycled carbon fiber-GNP reinforced PA66-based composites	28
3.3.3. Characterization	30
3.4. Results & Discussion	31
3.4.1. Mechanical properties of PA6,6 composites reinforced with recycled carbon fiber and recycled carbon fiber-GNP	31
3.4.2. Thermal and crystallinity properties of recycled carbon fiber reinforced PA6,6 and recycled carbon fiber-GNP reinforced PA6,6 composites	35
3.4.3. The effect of recycled carbon fiber and recycled carbon fiber-GNP hybrid reinforcement on the rheological behavior of PA6,6 composites	36
3.4.4. Cross-sectional fracture surface analysis of recycled carbon fiber and recycled carbon fiber-GNP reinforced PA6,6 composites	37
3.5. Conclusions	41
CHAPTER 4: A Comprehensive Dimensional Analysis of Waste-Derived Reinforcements in Interface Interactions with Semi-Bio-Based PA6,10 Composites	43
4.1. Abstract	43
4.2. Introduction	43
4.3. Materials and Methods	46
4.3.1. Materials	46
4.3.2. Fabrication of PA6,10-based composites with different scale reinforcements	47
4.3.3. Characterization	48
4.4. Results and Discussion	49
4.4.1. Structural transformation of waste coffee into upcycled graphene (CWC)	49
4.4.2. The characteristics of waste-driven reinforcements	56
4.4.3. Mechanical performance of sustainable PA6,10-based composites	59
4.4.4. Thermal and crystallinity characteristics of sustainable PA6,10-based composites	68
4.4.5. The effect of reinforcement aspect ratio and morphology on the rheological properties of PA6,10-based composites	70
4.4.6. Morphological analysis of waste-derived reinforcements and cross-sectional analysis of PA6,10-based sustainable composites	73
4.5. Conclusions	75
CHAPTER 5: General Conclusion	78
REFERENCES	87

ABBREVIATIONS

2D	: 2 Dimensional
3D	: 3 Dimensional
AGO	: Acyl chloride functionalized graphene oxide
BFS	: Blast furnace slag
CB	: Carbon black
CF	: Carbon fiber
CNT	: Carbon nanotube
CWC	: Carbonized waste coffee
DSC	: Differential scanning calorimetry
FESEM	: Field emission scanning electron microscope
FTIR	: Fourier transform infrared
GF	: Glass fiber
GNP	: Graphene nanoplatelet
GNS	: Graphene nanosheet
GO	: Graphene oxide
GOS	: Silica functionalized graphene oxide
HNT	: Halloysite nanotube
ISO	: International Organization for Standardization
LCA	: Life cycle assessment
NF	: Natural fiber
PA	: Polyamide

PVA	: Polyvinyl alcohol
rGO	: Reduced graphene oxide
SEM	: Scanning electron microscopy
TAGS	: Tannic acid modified graphene sheets
TEM	: Transmission electron microscopy
TGA	: Thermogravimetric Analysis
UTM	: Universal testing machine
XPS	: X-ray photoelectron spectroscopy
XRD	: X-ray Diffraction

SYMBOLS

T_m	: Melting temperature
T_c	: Crystallization temperature
T_g	: Glass transition temperature
η*	: Complex viscosity
E	: Tensile modulus
ΔH_m	: Heat of Fusion
X_c	: Degree of Crystallinity
wt.	: Weight Fraction
μm	: Micrometer
nm	: Nanometer
mm	: Millimeter
cm	: Centimeter
g	: Gram
mg	: Milligram
°C	: Degree Celsius
N	: Newton
s	: Second
min	: Minute
h	: Hour
mbar	: Millibar
rpm	: Revolutions per Minute

L : Liter
Pa : Pascal
 θ : Theta
w : Angular frequency

LIST OF TABLES

Table 1. Tensile properties and improvements of neat PA6,6 and PA6,6/GNP nanocomposites.....	13
Table 2. Improvement percentages of neat PA6,6 and PA6,6/GNP nanocomposites in flexural properties	14
Table 3. Melting and crystallization parameters of neat PA6,6 and PA6,6/GNP nanocomposites.....	16
Table 4. Crystallinity degrees of neat PA6,6 and its GNP-based nanocomposites obtained from DSC characterization.....	16
Table 5. α_1 and α_2 peak positions of neat PA6,6 and its GNP-based nanocomposites...	17
Table 6. Crystallinity degrees of neat PA6,6 and GNP/PA6,6 nanocomposites were calculated by the software.....	17
Table 7. Compositions of recycled carbon fiber and recycled carbon fiber-GNP reinforced hybrid composites.....	29
Table 8. Tensile properties of neat PA6,6, recycled carbon fiber-based PA6,6 and recycled carbon fiber/GNP-based composites	32
Table 9. Flexural properties of neat PA6,6, recycled carbon fiber-based PA6,6 composites, and recycled carbon fiber/GNP-based PA6,6 composites	34
Table 10. Charpy notched impact test results of neat PA6,6, recycled carbon fiber and recycled carbon fiber-GNP reinforced composites.....	35
Table 11. Thermal parameters and crystallinity degrees of neat PA6,6, and reinforced composites	36
Table 12. Crystallinities of waste coffee and upcycled graphene.....	51
Table 13. A summary of the elemental composition of waste coffee and upcycled coffee and their molecular bonds.....	55
Table 14. Characteristic properties of waste-driven reinforcing materials.....	57
Table 15. Tensile properties of PA6,10-based composites and improvements compared to the neat polymer	63
Table 16. Flexural properties of PA6,10-based composites	66

Table 17. Densities and specific properties of commercial PA6-based compounds and fabricated PA6,10-based composites	67
Table 18. Thermal parameters and crystallinity degrees of neat PA6,10 and reinforced composites	70

LIST OF FIGURES

Figure 1. Summary diagram of the scope of the thesis.....	4
Figure 2. XPS spectrum (a), Raman spectrum (b), XRD pattern (c), SEM image (d), and TEM image (e) of GNP	10
Figure 3. Tensile stress-strain curves of neat PA6,6 and PA6,6/GNP nanocomposites. 13	
Figure 4. Flexural stress/strain curves of neat PA6,6 and its nanocomposites with different GNP loadings	14
Figure 5. First cooling cycle (a) and second heating cycle (b) thermograms of PA6,6 and GNP-based PA6,6 nanocomposites	15
Figure 6. Diffraction patterns of neat PA6,6 and PA6,6/GNP nanocomposites after elongation at break.....	17
Figure 7. Change in complex viscosity with the addition of GNP to the PA6,6 as a function of time and temperature.....	18
Figure 8. Storage Moduli of neat PA6,6 and PA6,6 GNP composites as a function of temperature	19
Figure 9. Change in the shear stress of PA6,6 and its GNP-based nanocomposites with the angular frequency.....	20
Figure 10. Complex viscosity of neat PA6,6 and its GNP-based nanocomposites as a function of angular frequency.....	20
Figure 11. Change in storage moduli (a) and loss moduli (b) of neat PA6,6 and PA6,6/GNP nanocomposites	21
Figure 12. Platelet structure of GNP (a), and freeze-fractured surfaces of neat PA6,6 (b), 0.3 wt.% GNP loaded PA6,6 nanocomposite at different magnifications (c) and (d), and 0.2 wt.% GNP/PA6,6 nanocomposite (e)	22
Figure 13. Heating cycle of the DSC analysis of neat PA6,6 with an extended temperature range	28
Figure 14. TGA analysis of PA6,6-based composites indicating the reinforcement amount in the compounds.....	30
Figure 15. Tensile test curves of neat PA6,6, recycled carbon fiber-based PA6,6, and recycled carbon fiber-GNP reinforced composites.....	32

Figure 16. Flexural test curves of neat PA6,6, recycled carbon fiber-based PA6,6, and recycled carbon fiber-GNP reinforced composites.....	34
Figure 17. First cooling (a) and second heating (b) cycle DSC curves of the neat PA6,6, PA6,6-recycled carbon fiber, and PA6,6-recycled carbon fiber-GNP composites	36
Figure 18. Changes in complex viscosity (a) and storage moduli (b) with the addition of recycled carbon fiber and recycled carbon fiber-GNP to PA6,6 as a function of time and temperature	37
Figure 19. SEM micrographs of recycled carbon fiber bundle at 1.75kx (a), GNP at 75kx, (b), TEM image of GNP at 500kx (c), fracture surface cross sections of neat PA6,6 at 1kx (d), 20% recycled carbon fiber at 1kx (e), and 20% recycled carbon fiber-0.3% GNP at 2.5kx and 50kx (f, g) reinforced composites	39
Figure 20. SEM images of 5% (a), 10% (b), 20% rCF (c), 20% rCF-0.3% GNP (d) reinforced composite ashes	40
Figure 21. Length distribution of fibers in 5% (a), 10% (b), 20% rCF (c), 20% rCF-0.3% GNP (d) reinforced composite ashes	41
Figure 22. TEM images of GNP (a) and CWC (b).....	47
Figure 23. Schematic representation of the fabrication process of PA6,10-based composites	48
Figure 24. Raman spectra of waste coffee and upcycled graphene from coffee	50
Figure 25. XRD patterns of the waste coffee and upcycled graphene.....	51
Figure 26. FT-IR spectra of waste coffee and upcycled graphene	53
Figure 27. XPS survey scans of waste coffee and upcycled graphene	54
Figure 28. Deconvoluted C1s scans of waste coffee (a) and upcycled graphene (b) and deconvoluted O1s scans of waste coffee (c) and upcycled graphene (d)	55
Figure 29. SEM images of waste coffee before (a, b) and after (c, d) flash pyrolysis at 25,000X (a, c) and 75,000X (b, d) magnifications.	56
Figure 30. XRD patterns of waste-driven reinforcing materials	58
Figure 31. Raman spectra of waste-driven reinforcing materials.....	58
Figure 32. EDX Mapping and elemental analysis of CF.....	59
Figure 33. Yield strength (a) and tensile modulus (b) of PA6,10-based composites with respect to reinforcement loading ratios.....	61
Figure 34. Tensile stress-strain curves of GNP-reinforced (a), CWC-reinforced (b), and CF-reinforced (c) composites	62

Figure 35. Flexural strength (a) and modulus (b) of PA6,10-based composites with respect to reinforcement loading ratios.....	64
Figure 36. Flexural stress-strain curves of GNP-reinforced (a), CWC-reinforced (b), and CF-reinforced (c) composites	65
Figure 37. Cooling (a) and second heating (b) DSC traces of neat PA6,10 and PA6,10-based composites	69
Figure 38. Changes in shear stresses (a) and complex viscosity (b) with the addition of 1 wt.% waste-derived reinforcements as a function of angular frequency	71
Figure 39. Changes in storage moduli (a) and loss moduli (b) with the addition of 1 wt.% waste-derived reinforcements as a function of angular frequency	72
Figure 40. The window of improvement in crystallinity and lightweighting potential of sustainable compounds	73
Figure 41. SEM images of GNP (a), 0.5 wt.% GNP-PA6,10 (b), CWC (c), 20 wt.% CWC-PA6,10 (d), CF (e), 20 wt.% CF-PA6,10 (f)	75
Figure 42. Key materials and findings of this thesis.....	79
Figure 43. Compound formulations and major achievements within the scope of the thesis	82
Figure 44. Global warming potential of matrix materials (a), reinforcing materials (b), comparative analysis of developed PA6,10-based compounds and commercial PA6-based compounds (c), and developed PA6,6-based and PA6,10-based compounds (d)	85
Figure 45. Comparison of sustainable compounds against state of the art.....	86

CHAPTER 1: State of the Art

Polymer matrix composites (PMCs) play a pivotal role in the automotive industry especially in structural parts such as body panels, interior features, and exterior trims by offering strength, lightweight, and design flexibility. However, to provide desired strength and durability depending on the specific area of application, these materials often incorporate high amounts of reinforcement, which in turns negatively affect the weight of the part. Advanced composites with multi-material constructions overcome these challenges by incorporating micro and nanoscale additives such as graphene or other 2D layered materials to reduce the amount of high-density reinforcements such as glass fiber or glass beads, potentially offering lightweight and durability at the same time. Nevertheless, there are significant fundamental challenges such as heterogenous dispersion, compatibility, scalability, fabrication processes, and sustainability that needs to be addressed to integrate these novel materials to existing production and assembly lines to create a synergy between the elements of multi-material constructions. To this end, ground-breaking research accomplished throughout this thesis identifies and addresses these challenges through intricate investigation of interface interactions between the polymer chains.

The philosophy behind this thesis study is based on addressing the challenges in utilization of conventional polyamides (PAs) and integration of multi-scale reinforcing materials using industry-standard fabrication methods within the automotive industry through a systematic exploration of innovative solutions for enhancing the performance and sustainability. By embracing the evolving trends towards sustainability in major transportation industries, this study strategically navigates the transition from synthetic PA6,6 to semi-synthetic PA6,10 matrix and leveraging the remarkable potential of waste-derived reinforcing materials such as waste tire-driven graphene nanoplatelets (GNP), carbonized waste coffee (CWC), and waste carbon fibers (CF). This material combination not only promotes sustainability, but also provides a novel approach to tailor composites properties through careful selection of reinforcement aspect ratio and scale. Furthermore, critical investigation of matrix and reinforcement interface as well as the chemical

structure and surface composition of the reinforcing materials shed light on the mechanisms behind significant performance improvement and dispersion behavior of reinforcements in the matrix supported by correlations established between reinforcing material characteristics and composite performance. Moreover, the philosophy extends beyond the material enhancement to encompass a holistic approach that contributes to a circular economy and promotes eco-friendly, high-performance composites for the automotive industry, thereby laying the foundation for incorporation of waste-derived reinforcements into compound formulations to create a future where waste materials are not merely managed but transformed into valuable resources.

This dissertation is based on five chapters in total, each based on studies that are linked with each other and provide significant outcomes on their respective subjects. In the first chapter, a state of the art is presented, including challenges, motivations, and research gaps providing a basis for the novelty of this study.

The second chapter involves the fabrication of waste tire-driven graphene nanoplatelets (GNP) reinforced PA6,6 nanocomposites with very low loading ratios. The current literature on this field is mainly focused on mechanochemical exfoliation in ball mill from commercial graphite [1], double extrusion with graphene oxide (GO) [2], or in situ polymerization with GO [3] which are not scalable fabrication methods nor they utilize the sustainable aspects of waste tire-driven graphene nanoplatelets. Due to outstanding properties and unachieved potential of GNP in combination with commonly used engineering thermoplastic for the automotive industry, this study sets lower and upper limits of GNP integration into PA6,6. Therefore, this study contributes to the literature by developing novel compound formulations and determining an optimal loading ratio for this specific combination of GNP/PA6,6 nanocomposite through extensive characterization methods which results in significant mechanical performance gains.

The third chapter further revolutionized the optimized compounds by integrating an extra reinforcement such as waste carbon fiber (CF) with significantly different size and aspect ratio. The most recent studies in this field demonstrate either significant mechanical performance improvement, however, utilize continuous GF mats coated by melt mixed commercial graphene and polymer, and their layer by layer assembly [4], focus on spray coating epoxy-based prepregs with commercial GNP suspensions [5], or GO fabrication through Hummers' method and deposition on short CF surface followed by extrusion [6], which significantly increase composite fabrication duration with several steps, thus, not

scalable, and do not utilize the sustainable aspects of waste-based reinforcements while achieving similar improvements. This hybrid reinforcement with GNP and CF not only enhances the sustainability aspect of these compounds, but also opens up new opportunities for advanced application fields with further improvements on the mechanical performance. A comprehensive understanding with regards to the effect of co-reinforcement and the interactions between binary and ternary interfaces were provided through key characterization techniques that are widely used in the industry.

The fourth chapter revolves around the idea of replacing commercial synthetic PA6-based compounds with a semi-bio-based counterpart, PA6,10, which has very similar characteristics as PA6 in terms of thermal and mechanical properties, and development of a novel reinforcement material (CWC) from a widely generated organic waste source, coffee. Carbonization of waste coffee in rotary furnace turned out to be a chemical-free, rapid, and scalable approach to fabricate sustainable reinforcing materials, as proven by detailed structural, chemical, elemental, and morphological analysis. By considering the previous expertise in PA-based GNP and CF reinforced compounds, sustainable compounds reinforced individually by waste derived resources (GNP, CWC, and CF) with different aspect ratios and sizes were developed. Lower and upper limits of nanoscale reinforcement and its optimization, reinforcement efficiency, strengthening mechanisms and key characteristics were demonstrated for sustainable compounds through extensive characterization in terms of mechanical performance, thermal and rheological properties, and cross-sectional analysis. Furthermore, lightweighting potential of these compounds with regards to specific tensile strength and modulus were benchmarked against target PA6-based commercial compounds and proven that sustainable compounds that were developed within the scope of this thesis can already replace several commercial products in the market in terms of lightweighting and stiffness.

The last chapter provides a general conclusion to the studies within this thesis and gives a future outlook for possible improvements on these subjects. Several key advances have been made in terms of integrating nano-, micro-, and macroscale waste derived reinforcements, their single and multiscale incorporation and general evaluation. By addressing the gaps in the literature, promoting the sustainability aspect, and hurdling the challenges, this thesis lays a foundation for developing novel sustainable reinforcements

and compounds with maximized performance to replace synthetic compounds available in the market. The summary diagram of the scope of the thesis is provided in Figure 1.

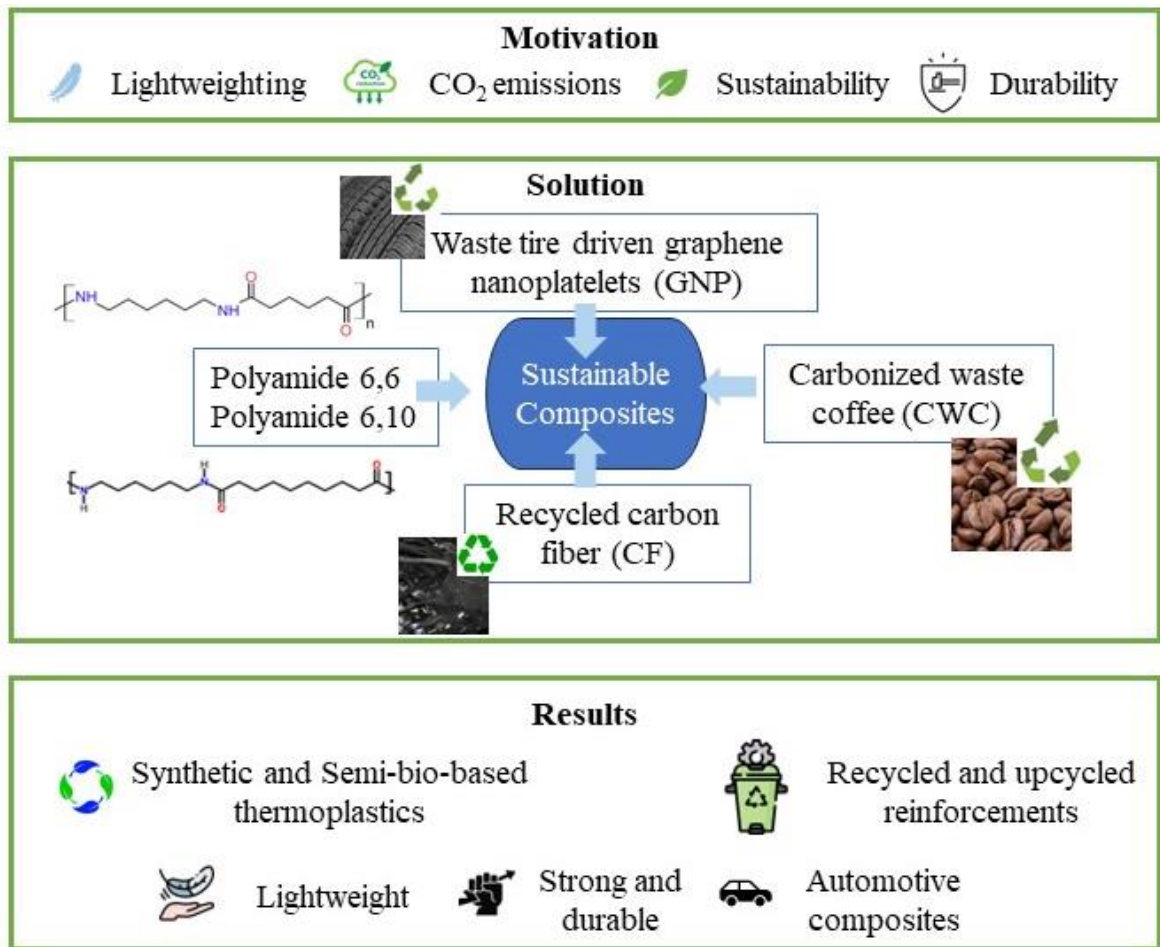


Figure 1. Summary diagram of the scope of the thesis

CHAPTER 2: Experimental and numerical investigation of flow and alignment behavior of waste tire-derived graphene nanoplatelets in PA6,6 matrix during melt-mixing and injection

2.1. Abstract

Homogeneous dispersion of graphene into thermoplastic polymer matrices during melt-mixing is still challenging due to its agglomeration and weak interfacial interactions with the selected polymer matrix. In this study, an ideal dispersion of graphene within the PA6,6 matrix was achieved under high shear rates by thermokinetic mixing. Graphene nanoplatelets (GNP) produced from waste-tire by upcycling and recycling techniques having high oxygen surface functional groups were used to increase the compatibility with PA6,6 chains. This study revealed that GNP addition increased the crystallization temperature of nanocomposites since it acted as both a nucleating and reinforcing agent. Tensile strength and modulus of PA6,6 nanocomposites were improved at 30% and 42%, respectively, by the addition of 0.3 wt.% GNP. Flexural strength and modulus were reached at 20% and 43%, respectively.

2.2. Introduction

Non-aromatic polyamides (PAs) are widely used as engineering thermoplastics in various fields such as aerospace, food packaging, and especially preferred in the automotive industry as engine compartments, bearings, oil pans, and various under-the-hood parts [7] due to their easy processability, good thermal stability, favorable price range, relatively high mechanical properties, superior wear resistance, and low density [8]. Among PAs, PA6,6 has taken great attention due to less water and moisture absorption than PA6, since moisture uptake affects the composites' mechanical performance and rheological properties adversely. In other words, the humidity absorption and low dimensional stability of PAs caused by intrinsic hydrophilic amide groups, along with their sensitivity to shock and relatively low impact resistance, limits their usage [9, 10].

In the literature, numerous studies have been reported on the enhancement of mechanical properties of PA-based composites by compounding with micro/nano additives such as montmorillonite [11], SiO₂ [12], and carbon-based materials such as carbon black [13], multi-walled carbon nanotubes [14], and exfoliated graphite [15] as well as by blending with other polymers such as high-density polyethylene [16], and polyphenylene sulfide [17]. However, high anisotropy and aggregation of carbon nanotubes (CNTs), stacking problems of exfoliated graphite, and brittleness in the presence of carbon black do not meet the requirements in the compounding process. Meanwhile, in recent years graphene is a prominent alternative to micron/nano additives due to its outstanding mechanical, thermal, and electrical properties and its 2D structure that provides ease of dispersion in the polymer matrix [18].

Several methodologies have been proposed for the effective incorporation of graphene and its derivatives as the main reinforcement into polyamide-based composites by in situ polymerization, solution mixing, and melt compounding. Fu et al. distributed few-layer graphene powders in PA6 matrix by in situ polymerization and achieved an increase of 13%, 44%, and 47% in the tensile strength, flexural strength, and impact strength, respectively, with 0.5 wt.% loadings [19]. Li et al. fabricated foam-like structures from graphene oxide by hydrothermal method then utilized in situ polymerization of polymeric precursors to obtain 3D-Graphene/PA6 nanocomposite, which resulted in an increase of 400% in the thermal conductivity of composite at 2 wt.% loading as well as improved anti-dripping properties for heat-retardance applications [20]. Besides, Duan et al. used graphite oxide powder and in situ polymerization method to produce reduced graphene oxide (rGO)/PA6,6 nanocomposites, and with 0.75 wt.% loadings, they obtained 9% and 6% increase in yield strength and Young's modulus, respectively, while maintaining the impact strength [21]. Although the in-situ polymerization technique promotes good dispersion of graphene in the polymer, its adaptation to produce nano-integrated compounds at the industrial amounts has limitations due to scale-up inefficiency and economic issues.

There are several challenges in integrating graphene and its derivatives as the main reinforcement into the polymer matrix. Poor dispersion of graphene in the polymer causes agglomeration of the 2D layers and induces weak interfacial connection, which hinders obtaining theoretical superior composite properties. In order to overcome this problem, researchers have made modifications to the graphene and polymer matrix. For instance,

Sarno et al. described a supercritical CO₂-assisted process to develop GO-loaded polymer membrane supercapacitors [22]. The authors indicated that the supercritical process aided to prevent agglomeration of GO particles even at 90% loading for the aerogels. In another study, Scaffaro et al. utilized modified Tour's method [23] to obtain graphene oxide (GO), then modified graphene oxide with nanosilica (GOS) and fabricated GOS/PA6 composites by batch compounding method, which yielded 180% and 210% increase in Young's modulus and tensile strength at 0.5 wt.% GOS loading, respectively [24]. Moreover, Wang et al. exfoliated graphene sheets in the liquid phase and modified them with tannic acid to fabricate tannic acid-modified graphene sheets (TAGS)/PA66 composite by solution mixing and drying method and obtained 15.9% and 118% improvement in Young's modulus and tensile strength at 0.5 wt.% TAGS loading, respectively [25]. In another study, Cai et al. prepared graphene oxide by Hummers' method [26], mixed GO with PA12,12 in the liquid phase, dried, and melt compounded to fabricate the composite in a two-step manner, which demonstrated an improvement of 10% in yield strength at 0.7 wt.% loading [27]. Furthermore, Gong et al. prepared GO by modified Hummers' method, modified the GO with polyvinyl alcohol (PVA) and fabricated PVA modified GO/PA6 composites by solution mixing technique, obtaining 34% and 41% increase in yield strength and Young's modulus, respectively, for 2 wt.% GO loading [28]. Therefore, it is critical to employ some form of modification to improve the interfacial connection between graphene and the polymer interface.

In addition to graphene utilization as the main reinforcing agent, graphene carries a significant potential for co-reinforcement with commercial reinforcements such as glass fiber (GF) in the compounding process. In one of the studies, Pan et al. investigated the effect of graphene nanosheets (GNS) produced by Hummers' method and hydrazine reduction on the fire and mechanical properties of glass fiber PA6 composites having aluminum hypophosphite resulting in the improvement of bending strength by 44% at the cost of a decrease in the tensile strength by 38% by the addition of 1 wt.% GNS [29]. Cho et al. functionalized commercial GO with acyl chloride (AGO) and utilized them together with CNT and in situ polymerization of PA6,6 to coat carbon fibers (CF), resulting in the improvement of interfacial shear strength and tensile strength by 160% and 136%, respectively, at 1 mg AGO and 0.5 mg CNT [30]. Karatas et al. melt compounded commercial graphene nanoplatelets (GNP) together with CF and PA6,6, which yielded a 57% reduction in adhesive wear and 11% improvement in tensile strength with the

addition of 0.5 wt.% GNP [31]. Moreover, Saner Okan demonstrated that, the addition of GNP from recycling and upcycling waste tire to the PA6,6 and compounding them with GF demonstrated 23% improvement in the flexural modulus [32] at 1% GNP loading. To conclude, a synergistic effect of graphene with hybrid composites with GF and CF yields significant improvements in mechanical and tribological properties.

There are challenges in the integration of graphene and its derivatives into a polymer matrix, especially in melt-phase due to their weak interfacial connections between the main reinforcement, inhomogeneous dispersion, and lacking proper functional groups [24, 25, 27, 28, 33]. Rheology is reported as a strong phenomenon to comprehend the reinforcement's dispersion characteristics in the polymer, which depends on the size, shape, and concentration of the graphene and the interaction between the graphene and the polyamide [34]. In one of the studies, Mayoral et al. demonstrated that at low frequencies, neat PA6 exhibits viscous behavior, whereas, at high frequencies, polymer chain entanglements dominate rheological response; however, with the addition of 15% GNP at 240 °C and 1% strain, rheological percolation is achieved, and GNPs start to agglomerate which degrades mechanical properties of melt-mixed GNP/PA6 composite [35]. Furthermore, Pan et al. linked the melt mixed GFPA6 composite's flame resistance property containing aluminum hypophosphite and GNS with the viscosity at 100 rpm and 215 °C. The authors demonstrated that the increase in the torque yields improved viscosity related to anti-dripping behavior for up to 2% GNS loadings [29]. In another study, Canales et al. developed a new rheological model based on solid content in the molten mix and showed that the crystallization process is accelerated considerably, even with the low amounts of graphene concentration dispersed in the "amorphous" PA6 matrix. This valuable outcome reports that the crystallization time and crystallization degree of a polymer system favorably affect mechanical performance [36]. Thus, it is critical to understand the polymer system's rheological behavior to implement the required reinforcements further to achieve desired performance improvements.

Melt-compounding techniques for the formulation development of graphene-based composites carry a significant potential to initiate graphene commercialization in engineering plastics due to its ease of production and economic feasibility. In one of the studies, Cho et al. investigated the addition of rGO produced by modified Hummers' method followed by hydrazine reduction under microwave treatment, and modified by titanate coupling agent and improved the thermal conductivity of PA by 53% with 5 wt.%

loading [37]. In another work, Karatas et al. utilized commercial GNP to produce GNP/PA6,6 by melt compounding and obtained significantly lower friction coefficients while increasing the tensile strength by 22% at 0.5 wt.% GNP loading [31]. However, getting useful dispersions in the melt compounding process is challenging and often requires compatibilizer or surface modification to provide a good reinforcement/matrix connection.

In the present study, waste tire-derived GNPs were distributed in the PA6,6 matrix by the thermokinetic mixer in the melt phase by controlling GNP ratios and decreasing the loading ratios down to 0.2 wt.%. The detailed characterization was carried out to monitor GNP's effect on the crystallinity and rheological properties of PA6,6 based nanocomposites.

2.3. Materials and methods

2.3.1. Materials

Graphene nanoplatelets (GNP) derived from waste tires by recycling and upcycling processes were obtained from Nanografen Co., Istanbul, Turkey. The density of the waste tire-derived GNPs is calculated as 2.115 g/cm³. Characterization results of GNP in terms of X-Ray photoelectron spectroscopy (XPS), Raman spectroscopy, X-Ray diffraction (XRD) pattern, scanning electron microscopy (SEM) and transmission electron microscopy (TEM) is given in Figure 2. X-ray Photoelectron Spectroscopy (XPS) shows that the GNPs contain 87 wt.% carbon and 9.1 wt.% oxygen containing surface functional groups (Figure 2a). Characteristic graphene peaks of D and G are located around 1358 and 1580 cm⁻¹ (Figure 2b). XRD pattern of graphene nanoplatelets indicates a crystallinity degree of 24.1% (Figure 2c). SEM image confirms the platelet structure (Figure 2d). Transmission electron microscopy (TEM) image shows that the GNPs have lateral size of around 50 nm (Figure 2e). Polyamide 66 (EP 158, Ravago, Istanbul, Turkey) is a general-purpose polymer with a melt flow rate of 71 g/10 min, good toughness, and high impact properties. PA6,6 was dried in the oven at 80 °C before each usage to remove the moisture.

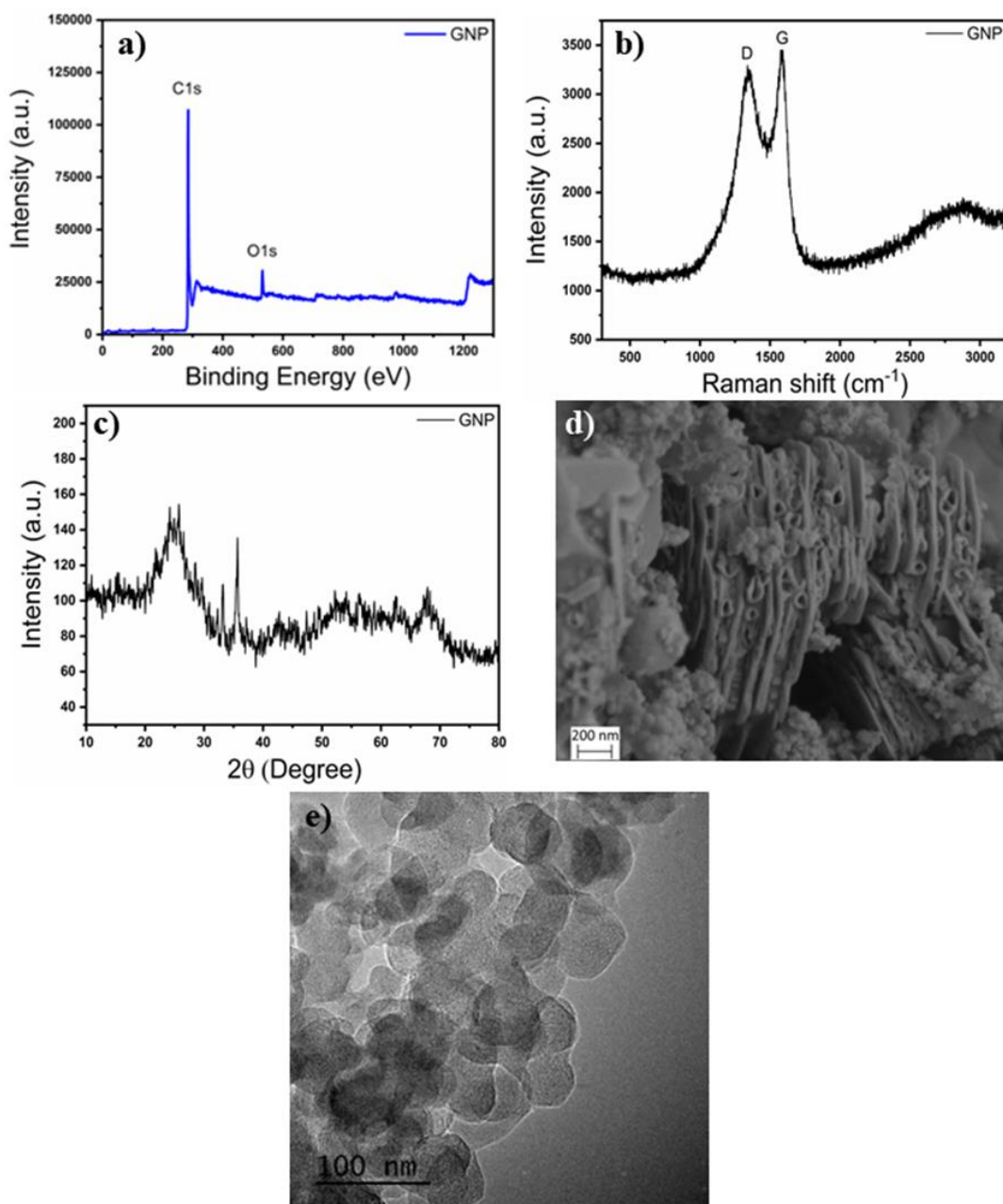


Figure 2. XPS spectrum (a), Raman spectrum (b), XRD pattern (c), SEM image (d), and TEM image (e) of GNP

2.3.2. Fabrication of GNP reinforced PA6,6 nanocomposites by thermokinetic mixer

GNP reinforced PA6,6 composites were prepared by a custom-made Gelimat thermokinetic mixer at a shear rate of ~4700 rpm at 300 °C for 1 min. The loading ratios of 0.2, 0.3, 0.4, 0.5, and 1.0 wt.% GNP were adjusted and mixed with PA6,6 at the melt-phase to attain homogeneous dispersion and provide a high degree of exfoliation through polymer chains. The obtained products were then crushed to granules and injection

molded by a mini-injection molding machine (Xplore, Sittard, The Netherlands) for mechanical tests.

2.3.3. Characterization

Characteristic properties of graphene and its nanocomposites were examined by using various spectroscopic and microscopic techniques. Thermal analysis of polymer composite samples was carried out by Differential Scanning Calorimetry (DSC) method using DSC 3 + 700 (Mettler Toledo, Columbus, OH, USA) under the nitrogen atmosphere from 25 °C to 300 °C. Dried samples were heated and held at 300 °C for 5 min to eliminate the thermal history. An additional heating cycle and cooling cycle were performed at the rate of 10 °C/min to investigate the melting properties, thermal behavior, and crystallization degrees of the samples. STARe software (Mettler Toledo, Columbus, OH, USA) was used in order to obtain the melting enthalpy (ΔH_m), crystallization enthalpy (ΔH_c) as well as melting (T_m), and crystallization temperatures (T_c). In order to carry out the morphological studies, mechanical test specimens were fractured in liquid nitrogen and coated with a thin layer of gold. Surface topography and morphology were investigated using a Leo Supra 35VP Field Emission Scanning Electron Microscope (FESEM, Carl Zeiss AG, Jena, Germany). Crystalline structures of the samples were studied by X-ray Diffraction (XRD) method using a D2 PHASER Desktop diffractometer (Bruker, Billerica, MA, USA) utilizing a $\text{CuK}\alpha$ radiation source. Elemental analysis has been carried out using X-ray Photoelectron Spectroscopy (XPS, Thermo Scientific, Waltham, MA, USA) for graphene samples. The mechanical tests were conducted by using 5982 Static Universal Test Machine (UTM, Instron, Norwood, MA, USA) with 5 kN load cell for ISO 527-2 tensile and ISO 178 three-point bending tests. MCR 702 TwinDrive Rheometer (Anton Paar, Graz, Austria) was used for the rheological characterization of the specimens.

2.4. Results and Discussion

2.4.1. Mechanical performance of GNP reinforced PA6,6 nanocomposites

In the present work, GNP obtained from waste tire used as reinforcement has 9 wt.% surface oxygen groups with a surface area of 130 m²/g and a platelet size of 50 nm. The characterization details of GNP are given in section 2.3.1. Intrinsic oxygenated groups on the surface of GNPs coming from its manufacturing process provides enhanced interfacial interactions with the amino groups in PA6,6 chains. This interfacial interaction allows the

effective load transfer from matrix to strong GNP particles. In a previous work [38], GNP loading ratios were adjusted between 0.5-2.0 wt.%, and significant improvement in both flexural and tensile properties was observed; however, there is a decreasing trend observed by increasing GNP amount higher than 2.0 wt.%. In order to understand the reinforcement and nucleating effects of GNP at low loadings, the GNP amount was decreased down to 0.2 wt.% in the current study. Therefore, GNPs with the loadings of 0.2-1.0 wt.% were mixed with PA6,6 by a high shear thermokinetic mixer. Herein, the thermokinetic mixer provides to increase intercalation of polymer chains through graphene layers leading to the homogeneous dispersion of graphene in the polymer matrix. In order to obtain better dispersion and to determine the optimum loading amount, the tensile and flexural properties of GNP/PA6,6 nanocomposites were characterized in detail.

Figure 3 displays the tensile stress/strain curves of neat PA6,6 and its nanocomposites with different GNP concentrations. By adding GNP in the PA6,6 matrix, stiffness increased significantly compared to neat PA6,6 showing elongated characteristics. Table 1 summarizes the improvements by percentages of tensile strength and tensile modulus and tensile strain at break compared to the neat counterpart. According to tensile test results, the highest tensile strength improvement was obtained as 30.4% with 0.3 wt.% GNP loading, and the highest tensile modulus was provided by incorporating 0.4 wt.% GNP, which is similar to one having 0.3 wt.% GNP. As the GNP amount was increased up to 1 wt.%, there was a decreasing trend in the tensile strength. In other words, at higher loadings, the agglomeration of GNP reduces the interfacial area and creates stress concentration sites leading to an overall decrease in tensile properties [39]. In addition, as polymers' mechanical properties are highly dependent on crystallinity [40], the improvement in tensile properties is a consequence of increased crystallinity, which is also confirmed by DSC analysis in the next section.

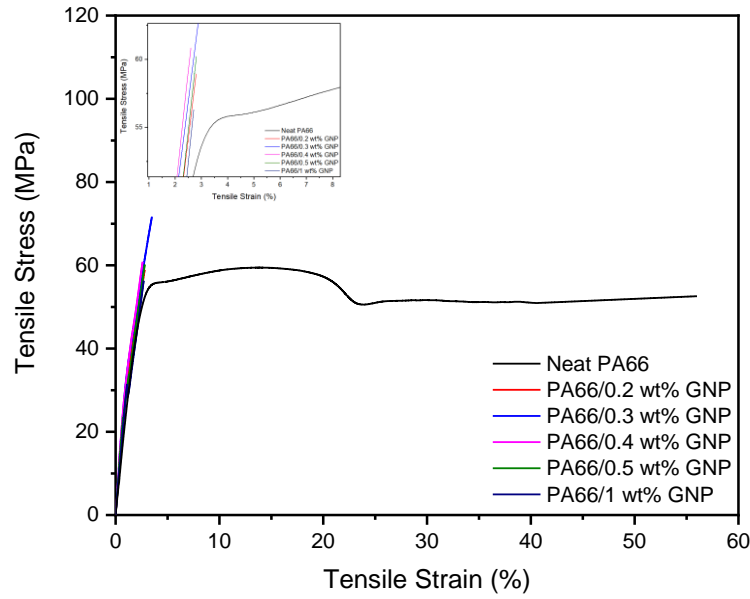


Figure 3. Tensile stress-strain curves of neat PA6,6 and PA6,6/GNP nanocomposites

Table 1. Tensile properties and improvements of neat PA6,6 and PA6,6/GNP nanocomposites

Sample	Tensile Strength (MPa)	Improvement (%)	Tensile Modulus (MPa)	Improvement (%)	Tensile Strain at Break (%)
Neat PA6,6	54.9±6	-	2334±154	-	16.8±21
PA6,6/0.2 wt.% GNP	56.4±10	2.7	3128±150	34.0	2.8±1.2
PA6,6/0.3 wt.% GNP	71.6±1	30.4	3306±50	41.7	3.5±0.2
PA6,6/0.4 wt.% GNP	60.5±1	10.2	3350±143	43.5	2.6±0.1
PA6,6/0.5 wt.% GNP	60.2±4	9.7	3080±64	32.0	2.8±0.1
PA6,6/1.0 wt.% GNP	56.2±12	2.4	3160±513	35.4	2.7±0.4

Figure 4 shows the flexural stress/strain curves of neat PA6,6 and its nanocomposites with different loadings after ISO 178 three-point bending tests. Flexural strength gives insight into a material's resistance to fracture, while flexural modulus indicates a material's tendency to bend [41]. It can be seen that the addition of GNP increased the flexural modulus with the increase of GNP loadings and also improved flexural strength except for 0.2 wt.% loading. The highest flexural strength value was obtained by incorporating 0.4 wt.% GNP as 114 MPa, which resulted in 22.4% improvement compared to neat polymer. Moreover, the addition of 0.3 wt.% GNP achieved a 21.3% improvement in flexural strength as well as improved tensile strength. It is also worth

noting that the flexural moduli have improved at least 40% in each GNP loading. This increase in flexural properties is led by graphene nanoplatelets acting as a nucleating agent in the polymer matrix. The early crystallization start leads to a higher degree of crystallinity, which subsequently improves mechanical properties, as confirmed by DSC analysis later on. Table 2 summarizes flexural strength, strain, modulus, and corresponding improvements of the samples.

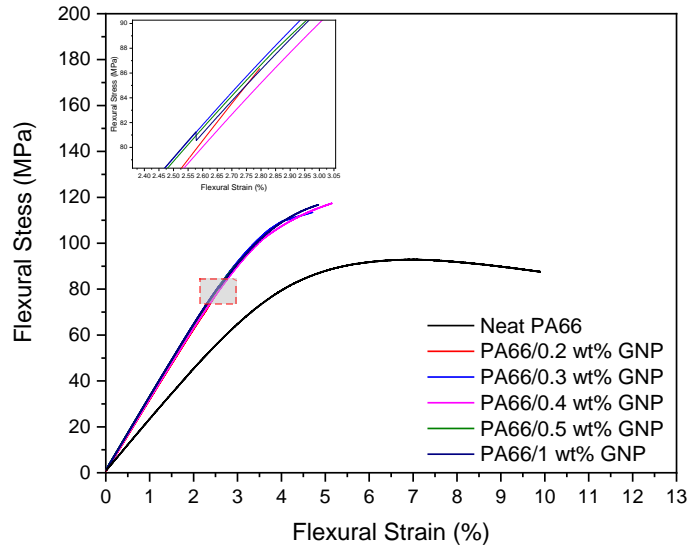


Figure 4. Flexural stress/strain curves of neat PA6,6 and its nanocomposites with different GNP loadings

Table 2. Improvement percentages of neat PA6,6 and PA6,6/GNP nanocomposites in flexural properties

Sample	Flexural Strength (MPa)	Improvement (%)	Flexural Modulus (MPa)	Improvement (%)	Flexural Strain (%)
Neat PA6,6	93.1±2	-	2250.0±68	-	7.05±0.3
PA6,6/0.2 wt.% GNP	83.8±9	-9.9	3170.0±167	40.8	2.79±0.4
PA6,6/0.3 wt.% GNP	113.0±6	21.3	3210.0±100	42.6	4.72±1.4
PA6,6/0.4 wt.% GNP	114.0±10	22.4	3160.0±40	40.4	5.15±1.5
PA6,6/0.5 wt.% GNP	96.30±7	3.4	3220.0±41	43.1	3.25±0.4
PA6,6/1.0 wt.% GNP	108.0±21	16.0	3230.0±54	43.5	4.84±2.0

2.4.2. Thermal and crystallinity properties of GNP based PA6,6 nanocomposites

Thermal properties of neat PA6,6 and GNP-based composites were investigated using the DSC method, which gives insight into the crystallization and melting behavior of the composites. The first cooling cycle for crystallization behavior and the second heating cycle melting curves of neat PA6,6 and PA6,6-GNP composites have been shown in Figure 5a and Figure 5b, respectively. Thermal parameters have been summarized in Table 3. DSC analysis shows no significant changes for the melting behavior of neat PA6,6 and GNP-PA6,6 composites; however, the crystallization temperature increase indicates that GNP in the polymer acts as a nucleating agent and initiated early crystallization. As crystallization starts early, the crystals have more time to grow and increase overall crystallinity. This increase in the crystallization confirmed the improvement in the mechanical properties of GNP-based PA6,6 nanocomposites. Further crystallinity investigation can be conducted using the equation below:

$$X_C = \left(\frac{\Delta H_M}{\Delta H_M^{100\%}} \right) \times 100 \quad (2.1)$$

where X_C is the degree of crystallization, ΔH_m is the melting enthalpy and $\Delta H_M^{100\%}$ is the melting enthalpy of 100% crystalline PA6,6. Neat crystalline PA6,6 has a melting enthalpy of 188.4 J/g [42]. Based on this equation, crystallinity degrees of neat PA6,6 and PA6,6-GNP nanocomposites have been calculated and given in Table 4.

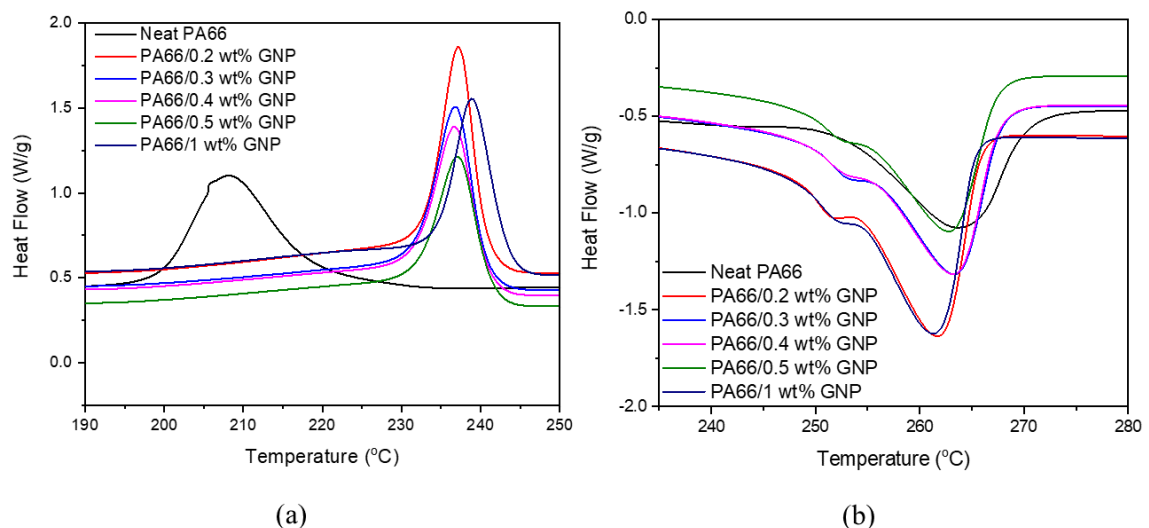


Figure 5. First cooling cycle (a) and second heating cycle (b) thermograms of PA6,6 and GNP-based PA66 nanocomposites

Table 3. Melting and crystallization parameters of neat PA6,6 and PA6,6/GNP nanocomposites

Sample	Melting onset temperature (°C)	Melting peak temperature (°C)	Melting integral, ΔH_m (J/g)	Crystallization onset temperature (°C)	Crystallization peak temperature (°C)	Crystallization integral, ΔH_c (J/g)
Neat PA6,6	250	262	-64.18	219	209	56.56
PA6,6 + 0.2 wt.% GNP	250	260	-83.17	241	238	63.33
PA6,6 + 0.3 wt.% GNP	251	262	-75.25	241	237	57.15
PA6,6 + 0.4 wt.% GNP	250	262	-74.62	241	237	56.56
PA6,6 + 0.5 wt.% GNP	250	262	-68.66	241	237	51.57
PA6,6 + 1.0 wt.% GNP	250	260	-78.21	243	239	59.09

Table 4. Crystallinity degrees of neat PA6,6 and its GNP-based nanocomposites obtained from DSC characterization

Sample	Crystallinity (%)	Amorphous (%)
Neat PA6,6	34.06	65.94
PA6,6 + 0.2 wt.% GNP	44.14	55.86
PA6,6 + 0.3 wt.% GNP	39.94	60.06
PA6,6 + 0.4 wt.% GNP	39.60	60.40
PA6,6 + 0.5 wt.% GNP	36.44	63.56
PA6,6 + 1.0 wt.% GNP	41.51	58.49

XRD also investigated crystalline properties of neat PA6,6 and its nanocomposites to validate GNP's nucleation effect and understand its impact on crystallinity. XRD studies were carried out with the test specimens obtained after the tensile test. Figure 6 shows XRD patterns of neat PA6,6 and its nanocomposites with different GNP loadings. PA6,6 shows two characteristic peaks as α_1 and α_2 around $2\theta=20^\circ$ and $2\theta=24^\circ$ degrees corresponding to (100) and (010)/(110) overlapping peaks, respectively [43]. With GNP incorporation into the matrix, another peak indicating γ (002) phase around $2\theta=14^\circ$ arose, which was previously thermodynamically unstable at room temperature for the neat polymer [44]. The mismatch between crystallization ratios obtained from DSC and XRD results stems from extreme strain shown by the neat PA6,6, and this strain results in distortion of the lattice and change in d-spacings [45]. GNP reinforced PA6,6 composites did not show such strain. Consequently, the resulting mismatch was significantly lower. The discrepancy in crystallinity values from DSC and XRD values is also reported in the literature [46]. The intercalation of GNP between the polymer matrix is indicated by the

separation of α_1 and α_2 peaks. The main peak positions of α_1 and α_2 as well as their ratio, are given in Table 5. Crystallinities of the samples have been calculated by the software given in Table 6.

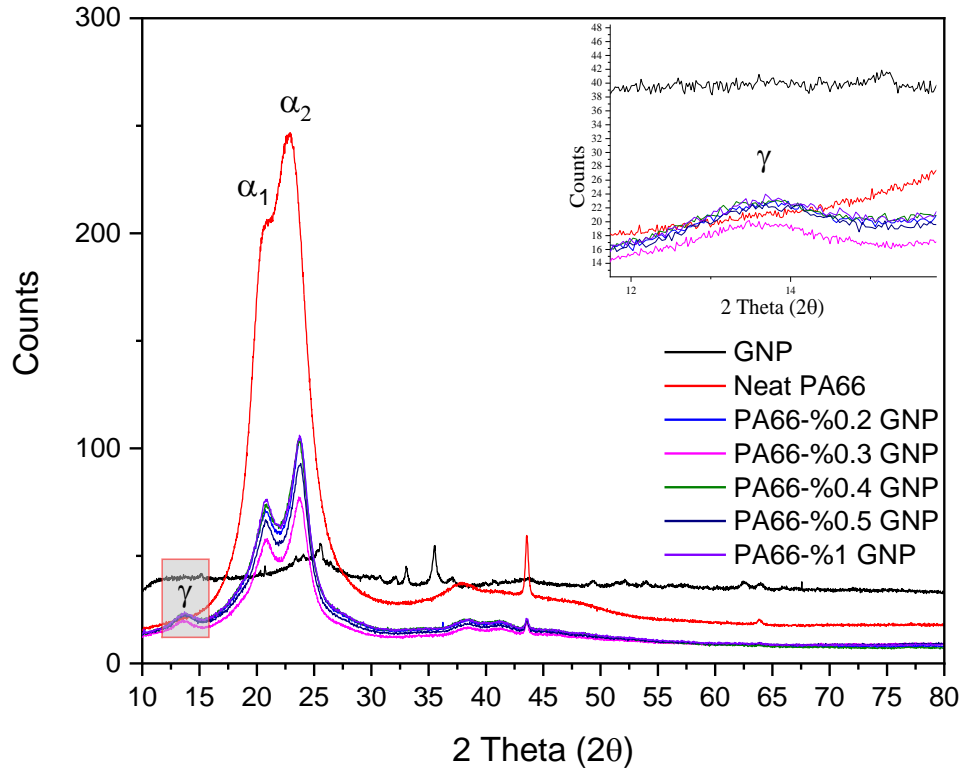


Figure 6. Diffraction patterns of neat PA6,6 and PA6,6/GNP nanocomposites after elongation at break

Table 5. α_1 and α_2 peak positions of neat PA6,6 and its GNP-based nanocomposites

Sample	α_1 Position	α_2 Position	α_1 / α_2 Ratio
Neat PA6,6	20.86	22.93	0.90
PA6,6 + 0.2 wt.% GNP	20.72	23.84	0.86
PA6,6 + 0.3 wt.% GNP	20.90	23.66	0.88
PA6,6 + 0.4 wt.% GNP	20.84	23.56	0.88
PA6,6 + 0.5 wt.% GNP	20.76	23.84	0.86
PA6,6 + 1.0 wt.% GNP	20.88	23.72	0.88

Table 6. Crystallinity degrees of neat PA6,6 and GNP/PA6,6 nanocomposites were calculated by the software

Sample	Crystallinity (%)	Amorphous (%)
Neat PA6,6	51.0	49.0
PA6,6 + 0.2 wt.% GNP	35.4	64.6
PA6,6 + 0.3 wt.% GNP	34.8	65.2
PA6,6 + 0.4 wt.% GNP	35.0	65.0
PA6,6 + 0.5 wt.% GNP	35.9	64.1
PA6,6 + 1.0 wt.% GNP	35.9	64.1

2.4.3. The effect of GNP as a reinforcement on the rheological behavior of PA6,6 nanocomposites

Complex viscosity is an essential parameter for estimating the processability of thermoplastic composites [47]. As the temperature gets close to the polymer's melting point, complex viscosity drops for both neat PA6,6 and GNP-PA6,6 composites. It can be speculated that the long-distance movement of the polymer chains is limited, which is indicated by reaching a stable viscosity value at higher temperatures [48]. Rheological behavior regarding the complex viscosity (η^*) and storage moduli of the neat PA6,6 and PA6,6-GNP composites using temperature sweep method with constant frequency have been given in Figure 7 and Figure 8, respectively. The addition of GNP to the polymer matrix changes the viscosity of the composites, which affects the storage modulus significantly [49]. The storage modulus demonstrates the elasticity portion of the viscoelastic behavior, and it indicates the energy stored before permanent deformation. Decreasing storage modulus at high temperatures shows that the elastic part of the composites, which is the polymer itself, melts and resembles a typical liquid's behavior. High storage moduli of 0.3% and 0.4% GNP loaded PA6,6 composites match the composites' tensile and flexural properties.

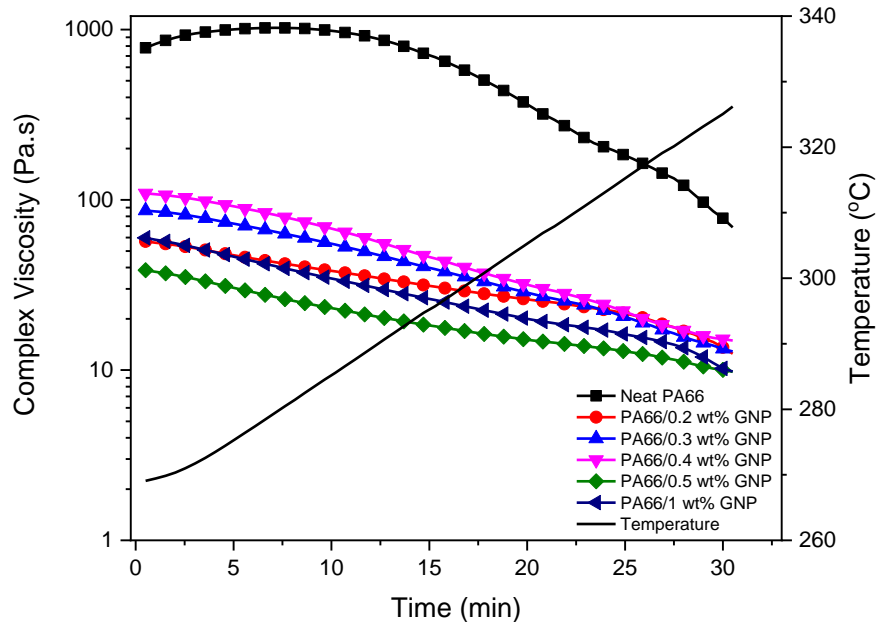


Figure 7. Change in complex viscosity with the addition of GNP to the PA6,6 as a function of time and temperature

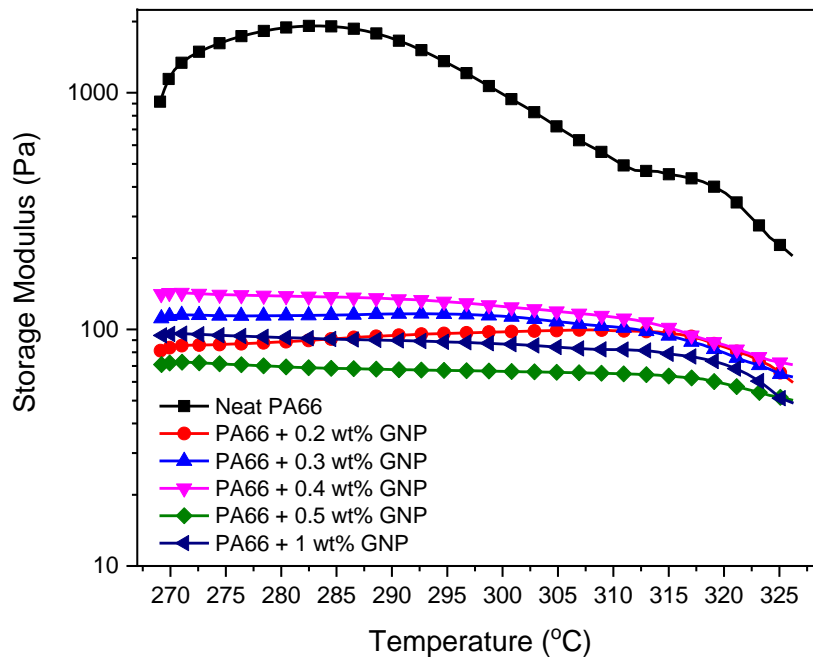


Figure 8. Storage Moduli of neat PA6,6 and PA6,6 GNP composites as a function of temperature

Investigating the rheological behavior of the PA6,6 and its GNP-based nanocomposites at the melt temperature (280 °C) as a function of angular frequency gives insight into the injection molding process dynamics dispersion of the GNP in the PA6,6 matrix. During the injection molding, the flow rates at the center of the mold and the outer layers are different, and this creates a shearing effect on the polymer. Higher shear stresses can cause molecules to break and loss of mechanical properties. Figure 9 shows the shear stresses of PA6,6 and PA6,6/GNP nanocomposites as a function of angular frequency. Here, GNP's addition leads to a decrease in the shear stress, which is confirmed by the increase in the mechanical properties. Figure 10 displays the complex viscosity of the samples. It is seen that both in temperature and frequency sweep, the polymer's viscosity decreases with the addition of GNPs. This behavior resembles the shear-thinning phenomena, and the exfoliation of GNPs can explain the mechanism behind it during the process aiding the slip between the polymer matrix and GNPs [50]. Furthermore, this decrease in the viscosity improves the melt processability of the polymer. Figure 11 displays the storage (a) and loss (b) moduli of the samples. As is expected, storage moduli and loss moduli for all samples increase up to a particular frequency. However, at higher frequencies around 100 rad/s, the storage moduli show a significant decrease for GNP-based PA6,6 composites while loss moduli increase. Thus, due to rigid graphene particles breaking the polymer chains at high frequencies resulting in low energy storage.

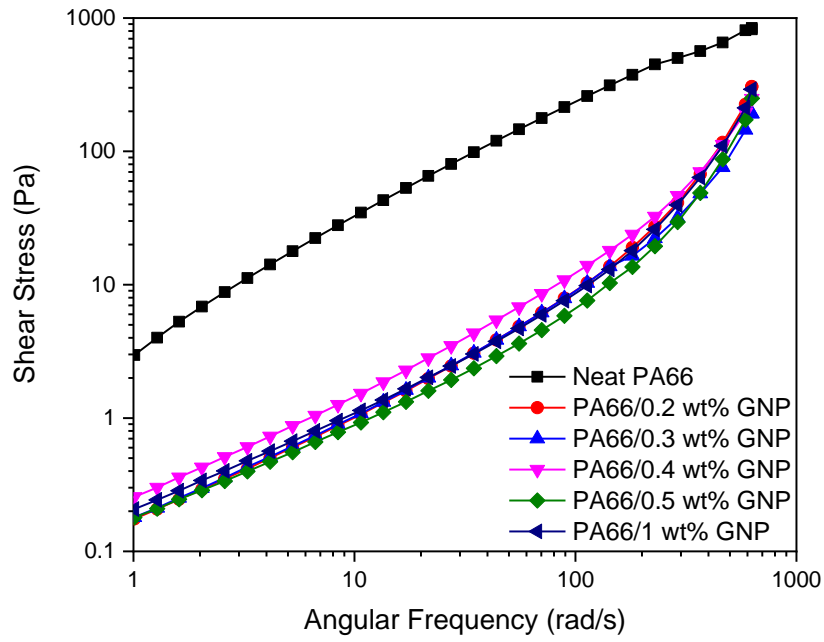


Figure 9. Change in the shear stress of PA6,6 and its GNP-based nanocomposites with the angular frequency

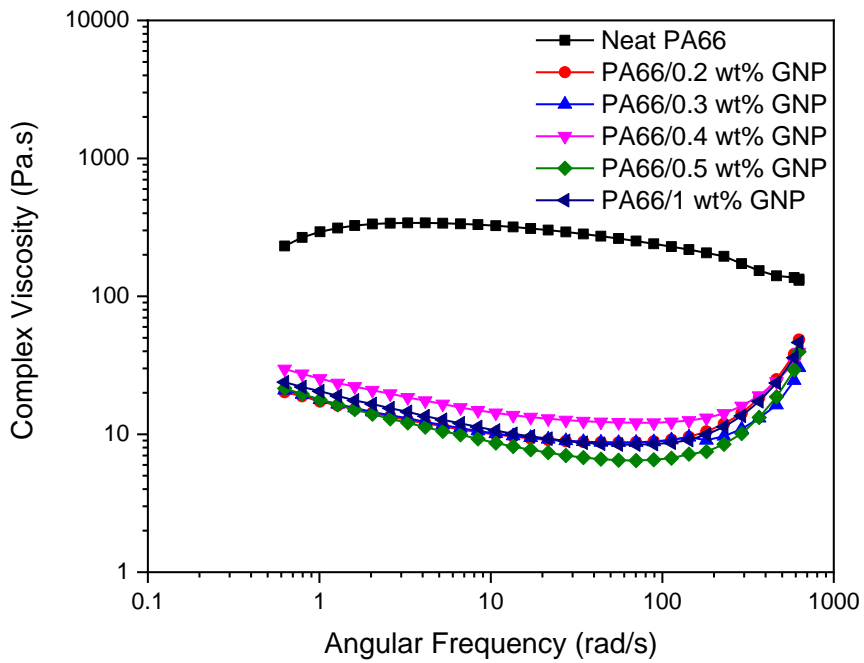


Figure 10. Complex viscosity of neat PA6,6 and its GNP-based nanocomposites as a function of angular frequency

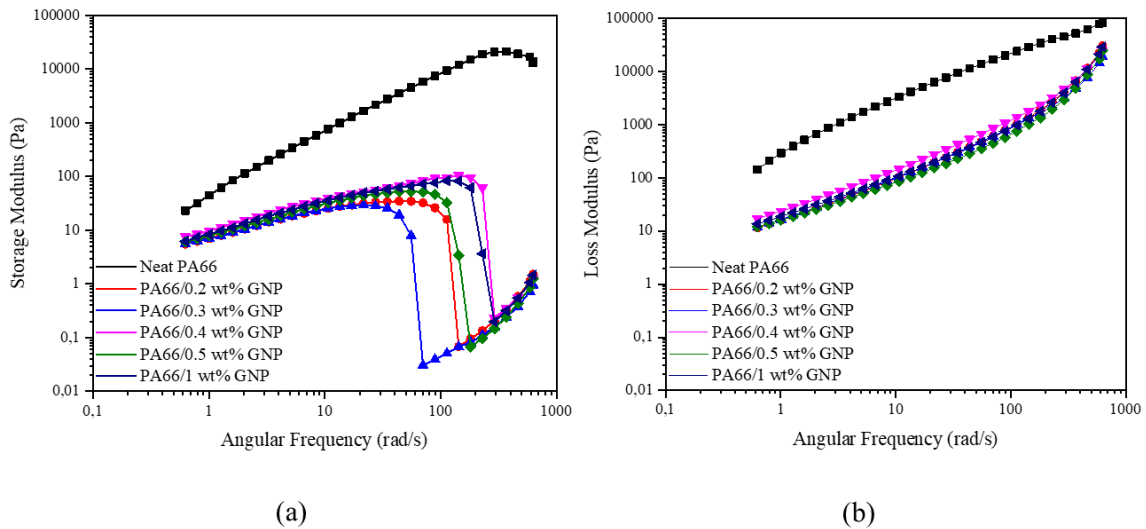
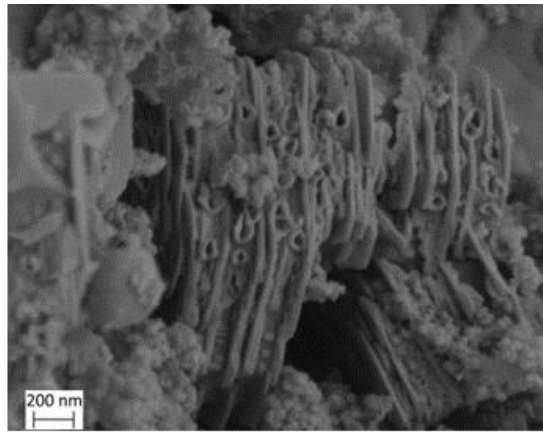


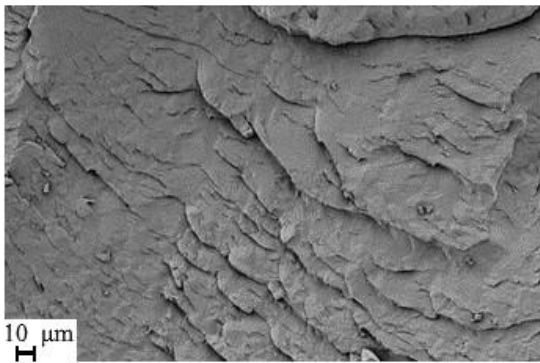
Figure 11. Change in storage moduli (a) and loss moduli (b) of neat PA6,6 and PA6,6/GNP nanocomposites

2.4.4. Cross-sectional analysis of GNP reinforced PA6,6 nanocomposites

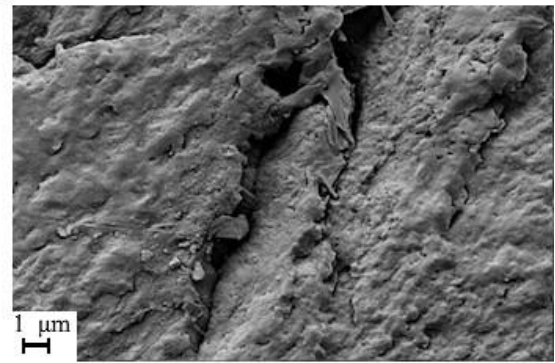
Scanning electron microscopy (SEM) is an important technique to analyze the surface morphology of GNPs, neat PA6,6, and GNP reinforced PA6,6 nanocomposites. The surface topology of the GNPs, as well as, cross-sectional fracture surfaces of freeze-fractured test specimens were investigated by SEM, and the distribution of graphene nanoplatelets in the polymer matrix is observed. This is also a useful technique to observe the distribution of and compare the samples' fracture surfaces. Figure 12a demonstrates the well-defined platelet structure of the waste tire-derived graphene. Figure 12b displays the freeze-fractured surface of neat PA6,6, while Figure 12c shows the freeze-fractured surface of 0.3 wt.% GNP/PA6,6 nanocomposite. The surface of the GNP-based nanocomposite is smoother compared to the neat counterpart. In addition, the fragmented surface on the neat polymer is observed; however, with the addition of GNP, a film-like coating is observed on the surface, preventing the fragmented fracture. Figure 12 also exhibits the freeze-fracture surface of the 0.3 wt.% GNP/PA6,6 (d) at different magnification, and 0.2 wt.% GNP/PA6,6 (e). The fragmented surface is still visible at the 0.2 wt.% loadings; however, a film-like structure is also obtained.



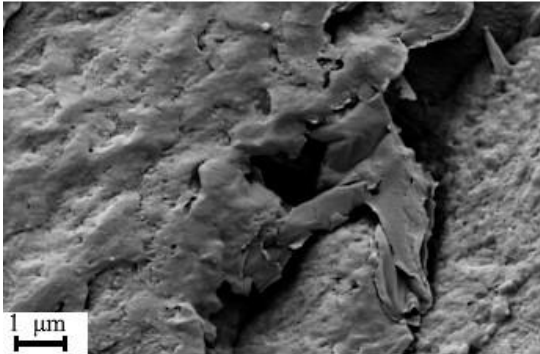
(a)



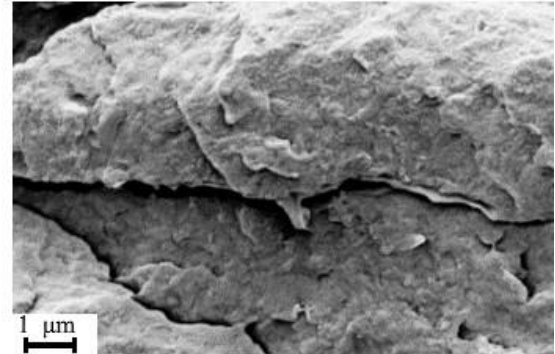
(b)



(c)



(d)



(e)

Figure 12. Platelet structure of GNP (a), and freeze-fractured surfaces of neat PA6,6 (b), 0.3 wt.% GNP loaded PA6,6 nanocomposite at different magnifications (c) and (d), and 0.2 wt.% GNP/PA6,6 nanocomposite (e)

2.5. Conclusions

Graphene, as much as being an outstanding material in numerous aspects, faces several issues regarding the incorporation in polymer matrices. These challenges include non-homogenous dispersion in the polymer matrix and lack of surface functional groups to effectively improve reinforcement/matrix interface. Numerous studies have been reported on graphene/PA composites; however, these main challenges still remain in place. Here, surface oxygen functional groups on GNP surface provided ease intercalation through PA6,6 polymer chains during melt-phase and homogeneous intercalation of GNP in the PA6,6 matrix is confirmed by conducting mechanical, crystalline, and rheological characterization. Additionally, it is important to note that at these small loading amounts, even small changes in the nanocomposite formulation may lead to undesired results and the quality control of the products may prove difficult in terms of thermal and X-ray diffraction.

Overall, this comprehensive and interdisciplinary study proves that the waste tire-derived graphene is a promising reinforcement material, and at lower loadings, significant mechanical property improvements are obtained. Consequently, scalable technologies for introducing graphene into polymer matrices by compounding using conventional techniques such as extrusion and injection processes become viable with the aid of waste tire-derived graphene. Also, converting waste materials into value-added material will contribute to circular economy issues and lower the cost of graphene by using waste tires as a starting material by applying recycling and upcycling technologies for mass production in the plastic industry.

CHAPTER 3: The effect of reinforcement aspect ratio on the performance of PA6,6 composites with recycled carbon fiber and upcycled graphene nanoplatelets: An interface characterization from process to modelling

3.1. Abstract

The use of recycled reinforcements in structural applications is growing due to concerns about the environmental impact and economic costs associated with energy-intensive production techniques of virgin fibers. However, limited research has explored the integration of multiscale reinforcements with different aspect ratios into PA6,6 composites to enhance their performance. In this study, the effect of reinforcement aspect ratio on PA6,6 composites by incorporating recycled carbon fibers and waste tire-derived graphene nanoplatelets (GNP) with oxygen surface functional groups is investigated. The objective of this work is to improve mechanical properties of the composites by promoting nucleation and enhancing the fiber/matrix interface. Through high shear mixing, effective dispersion of the recycled carbon fibers and GNP within the PA6,6 matrix is achieved. The resulting composites demonstrate significant improvements in mechanical properties due to enhanced interfacial interactions, including improved tensile properties up to 94%, flexural properties up to 86% compared to the neat PA6,6. The successful integration of waste tire-driven GNP into the recycled carbon fiber-based composite offers a promising approach to enhance performance. This study contributes to the development of sustainable materials for load-bearing applications, utilizing recycled reinforcements with different aspect ratios.

3.2. Introduction

Fiber-reinforced plastics have a significant impact on both economy and ecology due to production and end-of-life aspects. This impact can be improved by developing recycling concepts [51]. However, the reuse of these materials are challenging due to several factors which include the difficulty of separating materials, deteriorating mechanical properties of both the fiber and the matrix, and shortening of the fibers over each recycling cycle [52]. Nevertheless, the use of recycled fibers in the composite world is showing an

increasing trend and several studies are reporting that the loss of mechanical strength during the recycling process is small enough that it is outweighed by the contribution to the circular economy, reducing global warming potential, energy expenses, and waste production when the recycled fibers are used instead of virgin fibers [53–56].

Polyamides (PAs) have applications in various industries, however, their mechanical properties limit its application in specialty areas [43, 57]. Overcoming the inadequacies of PA6,6 using macro additives such as carbon fibers (CFs), natural fibers (NFs), and Glass Fibers (GFs), and increasing the mechanical properties is a widely researched topic [58–60]. In a recent study Holmström *et al.* investigated the effects of mold flow direction on the mechanical properties of neat and GF reinforced PA6, which demonstrated that significant anisotropy with variations up to 32% and 27% in tensile modulus and strength, respectively occurs with respect to the mold flow direction for 30% GF reinforced PA6 [61]. In another study, Hribersek *et al.* fabricated gears using 30 wt.% GF/PA6,6 with internal lubricants (15% polytetrafluoroethylene and silicon oil) to investigate the wear behavior of the composites compared to neat PA6,6 and demonstrated that significant increase in the operation life and 23% decrease in the wear rate is observed with the composite gear [62]. In a recent study, Bondy *et al.* investigated the fatigue performance of long CF/PA6,6 composite produced by direct/in-line compounding and compression molding and obtained peak stress of 105 MPa achieved over 10^6 cycles when the specimens were oriented in the flow direction [63]. However, the addition of GF and CF to the polymer matrix at such large amounts increases the overall weight of the polymer composite and limits the application areas where light-weighting is important.

The incorporation of micro and nanoscale additives into PAs to increase the mechanical properties while maintaining the overall weight became an important research subject [64–66]. Mainly; SiO₂ [67], clay [68], calcium carbonate [69, 70], and carbonaceous materials such as carbon nanotubes [30, 71], carbon fiber (CF) [72], carbon black (CB) [73], exfoliated graphite [74], and lately graphene [75] and graphene-related materials [76, 77] are being used to enhance the mechanical properties of polymers while maintaining the desired weight. Nevertheless, several challenges remain for the incorporation of such small-scale additives into the polymer matrix. Anisotropy, aggregation of particles, stacking problems, and brittleness introduced to structure restrict the application of these materials in the industry.

In the literature, several methods were reported to integrate nano-sized reinforcements to the PA matrix [32, 78]. In one of the studies, Mardlin *et al.* melt-compounded PA6,12 with flake graphite and GNP and revealed that at 40% loading ratio composites exhibited up to 240% increase in flexural modulus compared to the neat polymer, whereas the addition of GNPs at 20% resulted in a 300% increase in the impact strength. [74]. In another study, Kiziltas *et al.* fabricated PA6,10/GNP composites utilizing a twin-screw extruder up to 8 wt.% GNP loading ratios and investigated several key characteristics of the composites which demonstrated 95%, 16% and 9% improvement in tensile modulus, flexural modulus, and flexural strength at 8% GNP loading while thermal and rheological properties showed a percolation threshold around 2% loading [75]. However, addition of such high amounts of nanomaterials into polymer matrix is not economically feasible for certain industries such as automotive or household appliances.

Effective strengthening, weight-, and cost-reduction of polymers composites are recently accomplished by hybrid reinforcements of macro (GF, CF) and micro/nano (graphene, CNT) additives [31, 79]. The state of the art is inclined on the use virgin fibers and chemically modified nanomaterials as hybrid reinforcements to improve mechanical properties of composites. In one of the studies, Padhi *et al.* prepared hybrid composites with GF and micron sized blast furnace slag (BFS) to improve the impact strength and hardness polypropylene by 129% and 1317%, respectively, at 20 wt.% GF and 30 wt.% BFS loading [80]. Moreover, Zhang *et al.* modified surface of virgin carbon fibers with several modification agents including nano-SiO₂ and fabricated prepregs with PA6 to investigate the interfacial interactions between the fibers and the matrix and revealed that with the nano-SiO₂ modification, transverse fiber bundle strength of the composite increased 213% [67]. In a more recent study, Cho *et al.* coated CF with functionalized GO (graphene oxide) and CNT and prepared PA6,6/CF/CNT-GO composites by *in situ* polymerization with an objective to achieve better mechanical properties of the neat polymer [30]. The resulting composite exhibited 160% and 136% higher interfacial shear strength and tensile strength, respectively. Although hybrid reinforcements, especially with virgin CF and virgin graphene, provide significant weight reduction while increasing overall mechanical strength of the composite, suffer from major drawbacks such as high-cost and energy-intensive production techniques of virgin CF and non-scalable production of graphene related materials [81].

In the present study, the utilization of recycled carbon fibers and waste tire-derived GNP was favored due to economic and environmental benefits, contrary to the use of virgin fiber reinforcement, which is costly and requires energy-intensive production methods. Herein, recycled and upcycled reinforcements were blended in the PA6,6 matrix by melt compounding in a thermokinetic shear mixer with controlled GNP and recycled carbon fiber weight ratios. Additionally, the effect of the aspect ratio of the fillers on the mechanical properties and the interface of polymer/fiber is studied comparatively with high aspect ratio fibers and mixed aspect ratio GNP/recycled carbon fiber reinforcement. It is to be believed that this is the first study correlating the experimental work with the numerical data to investigate the thermokinetic mixing and injection molding of hybrid GNP/recycled carbon fiber reinforcement and their effect on the crystallinity, mechanical, thermal, and viscoelastic properties of PA6,6-based composites. Moreover, using waste tire-derived GNPs and recycled carbon fibers could introduce more environmentally friendly solutions for the composite industry with efficient processing design tools.

3.3. Materials and Method

3.3.1. Materials

Graphene nanoplatelets (GNP, Nanografen Co., Turkey), synthesized from the recycled carbon black received from the pyrolysis of waste tires by upcycling process, have 9 wt.% surface oxygen groups, 2.115 g/cm³ density, surface area of 120 m²/g, and an average platelet size of 50 nm confirmed by the Transmission Electron Microscope (TEM). Additional characterization spectra of GNP are given in Figure 2 in chapter 2. Recycled chopped carbon fiber bundles with 5 mm length and 2 mm diameter were supplied by DowAksa, Turkey. Polyamide 6,6 (PA6,6, EP 158, Ravago) is an engineering thermoplastic with applications in many areas due to its great toughness and impact properties. PA6,6 has a T_g around 55 °C as provided in the DSC curve with an extended temperature range in Figure 13.

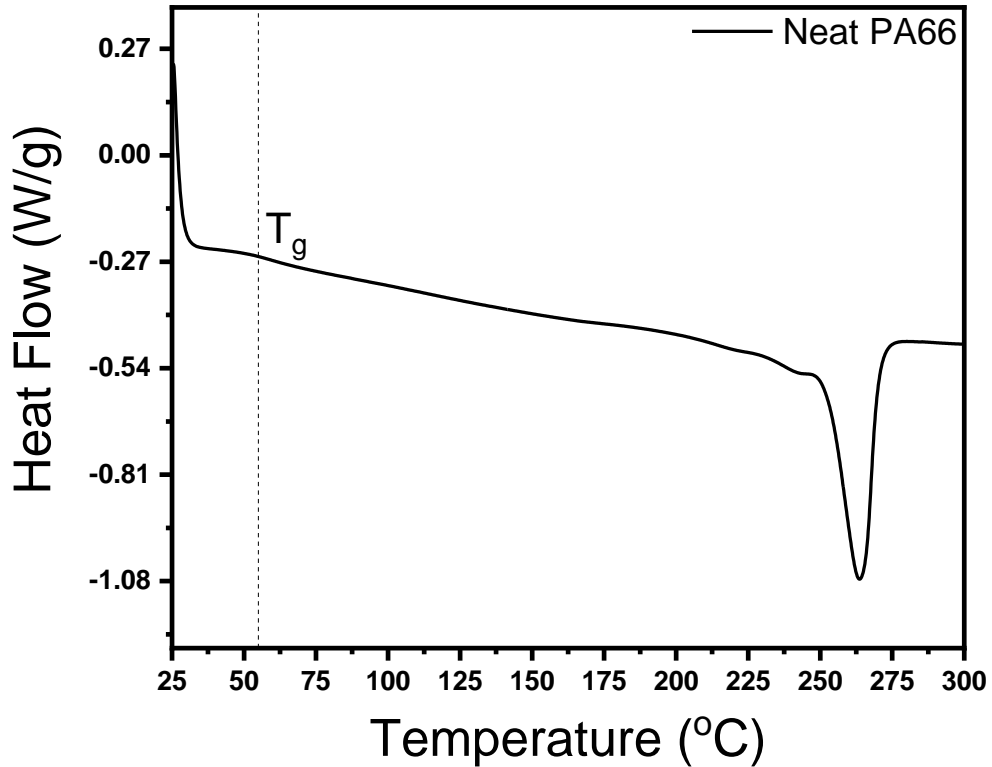


Figure 13. Heating cycle of the DSC analysis of neat PA6,6 with an extended temperature range

The average molecular weight of the PA6,6 is calculated using Merani's formula [82, 83]:

$$\overline{M}_n = 13870 \times (n_r - 1.4549) \quad (3.1)$$

Where \overline{M}_n is the average molecular weight and n_r is the relative viscosity. According to manufacturers technical datasheet, relative viscosity is provided as 2.67 ± 0.05 . Thus, average molecular weight of the PA6,6 is calculated to be around 16853 g mol^{-1} which is similar to the values reported in the literature [84, 85]. To be used in composite manufacturing, the moisture content of PA6,6 was removed by drying it in oven at $80 \text{ }^\circ\text{C}$ for 2 h even though the utilization of Gelimat thermokinetic mixer suggests circumventing the moisture removal step before the compounding process.

3.3.2. Fabrication of recycled carbon fiber reinforced PA6,6 and recycled carbon fiber-GNP reinforced PA66-based composites

A custom made Gelimat thermokinetic mixer (Dusatec Inc.) was used to prepare recycled carbon fiber reinforced PA6,6 composites for 5, 10, and 20 wt.% of recycled carbon fiber. To achieve homogenous dispersion, mixing was carried out at melt-phase at $280 \text{ }^\circ\text{C}$ with a rotation speed of $\sim 4500 \text{ rpm}$ for 5 s. Moreover, the hybrid composite with the highest loading of 20 wt.% recycled carbon fiber, and 0.3 wt.% GNP were melt-mixed to provide

a high degree of exfoliation of graphene and fibers through polymer chains and homogeneity. The compounds were then granulated by a crusher and molded by an Explore mini injection molding equipment with a melt temperature of 280 °C for 4 minutes, mold temperature of 50 °C, and injection pressure of 1 MPa (10 bar) for 23 s for mechanical tests. The compositions of the composite samples named according to recycled carbon fiber and GNP contents are listed in Table 1.

Table 7. Compositions of recycled carbon fiber and recycled carbon fiber-GNP reinforced hybrid composites

Sample	PA6,6 (wt.%)	Recycled carbon fiber (wt.%)	GNP (wt.%)
PA6,6-%5 Recycled carbon fiber	95	5	-
PA6,6-%10 Recycled carbon fiber	90	10	-
PA6,6-%20 Recycled carbon fiber	80	20	-
PA6,6-%20 Recycled carbon fiber-%0.3 GNP	79.7	20	0.3

Thermogravimetric analysis (TGA) results provided in Figure 14 indicate that the mixing ratio and the fiber/GNP content in the compounds are nominal and same as adjusted before the compounding process.

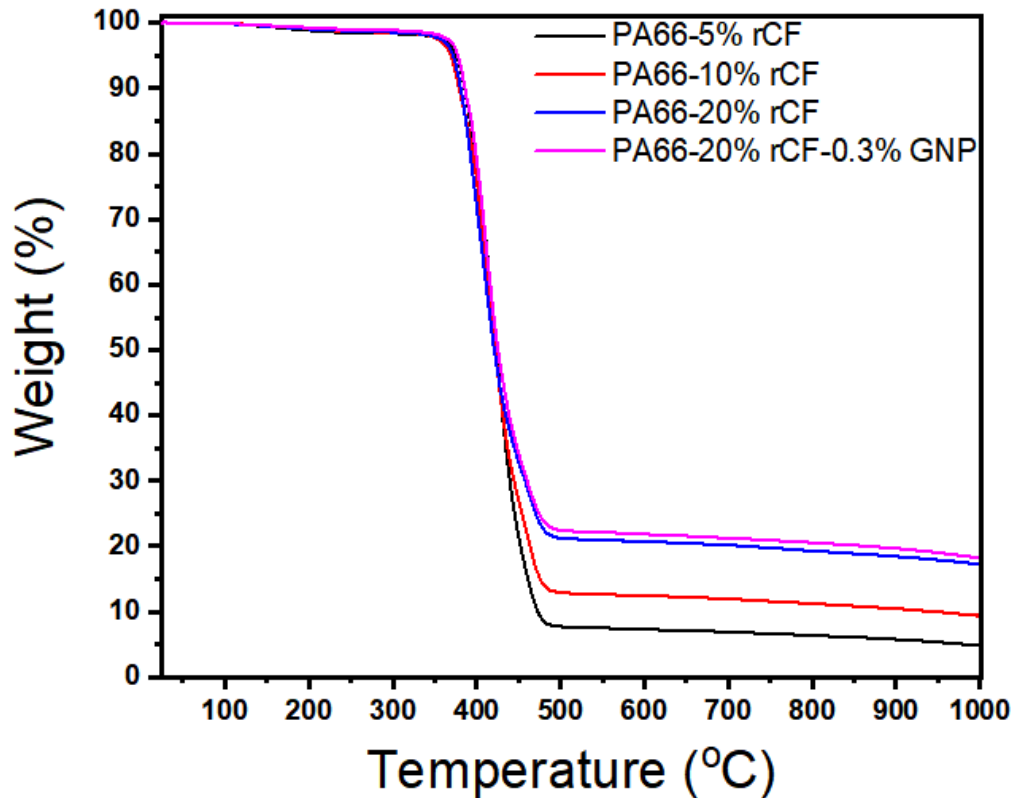


Figure 14. TGA analysis of PA6,6-based composites indicating the reinforcement amount in the compounds

3.3.3. Characterization

Different spectroscopic and macroscopic methods were used to examine the characteristics of graphene and its nanocomposites. In order to confirm the quality of the mixing and real fiber content in the compounds, thermogravimetric analysis (TGA) is performed under nitrogen atmosphere at $10\text{ }^{\circ}\text{C min}^{-1}$ heating rate from 25 to 1000 $^{\circ}\text{C}$ using a Mettler Toledo TGA/DSC 3⁺. The mechanical tests were conducted by using Instron 5982 Static Universal Test Machine (UTM) with a 5 kN load cell for ISO 527-2 tensile test using Type 1BA specimen and 2 mm/min test rate and ISO 178 three-point bending tests using the standard specimen and 2 mm/min test rate. Charpy notched impact tests were done using a CEAST 9050 impact test machine according to ISO 179 standard with a 2 mm notch, ISO 179-1/1eC method designation and 1 J hammer capacity. Thermal analyses of polymer composites were carried out by Differential Scanning Calorimetry (DSC) under a nitrogen atmosphere from 25 $^{\circ}\text{C}$ to 300 $^{\circ}\text{C}$ at $10\text{ }^{\circ}\text{C min}^{-1}$ rate [86, 87]. To examine the samples' thermal properties such as melting enthalpy (ΔH_m), melting temperature (T_m), crystallization enthalpy (ΔH_c), and crystallization temperature (T_c), a cooling cycle followed by another heating cycle were performed with same rate.

Rheological properties of the samples were investigated using Anton Paar MCR 702 TwinDrive Rheometer. To study the morphology of the fractured test specimens, samples were coated with a thin layer of Au/Pd alloy to provide conductivity. Fiber length, diameter, and morphology of the composites were investigated by carrying out the ash test in a chamber furnace under inert Ar atmosphere. Field Emission Scanning Electron Microscope (FESEM, Leo Supra 35VP) was used to investigate the surface topography and morphology of the fractured specimens, and also the residual ash from the ash test. X-ray Photoelectron Spectroscopy (XPS) was used to perform Elemental analysis for graphene samples.

3.4. Results & Discussion

3.4.1. Mechanical properties of PA6,6 composites reinforced with recycled carbon fiber and recycled carbon fiber-GNP

In the present study, recycled carbon fibers were utilized to improve the mechanical properties of the neat PA6,6 by adjusting the amount of carbon fibers in the composite from 5 wt.% to 20 wt.%. In our previous work, significant improvements were observed at 0.3 wt.% GNP loading in the PA6,6 matrix in terms of mechanical properties since GNP acted as both reinforcing and nucleating agent [86]. Therefore, 0.3 wt.% of GNP was kept constant in the compound formulations having recycled carbon fibers. Herein, to create a synergistic effect between recycled carbon fiber and GNP, a hybrid reinforcement with 20% recycled carbon fibers having 4 aspect ratio and 0.3% GNP with the aspect ratio of 1 was mixed in the PA6,6 using the thermokinetic shear mixer. As expected, mechanical properties of the composite improve with the increasing recycled carbon fiber amount in the composite. However, it is known that fiber fracture during the processing increases with the fiber content [88]. Since the mechanical properties of the composites are dominated by the fiber strength, and the fiber strength is mostly dependent on the length of the fibers, tensile properties of the composites did not show a linear improvement with the fiber loading.

Figure 15 shows the tensile test curves of the neat PA6,6, recycled carbon fiber-reinforced PA6,6, and recycled carbon fiber-GNP reinforced PA6,6 composites and Table 8 summarizes the change in tensile strength, modulus, and tensile strain at failure in comparison with the neat polymer. Introducing the recycled carbon fibers to the polymer matrix significantly increased the stiffness compared to the neat PA6,6. Moreover,

oxygen-containing surface groups in GNP contributed to the interfacial interactions between the fibers and the matrix, increasing the tensile strength further. Tensile test results indicate that the hybrid reinforced composite with 20% recycled carbon fiber and 0.3% GNP has the highest tensile strength improvement by 43.3% and reached 78.8 MPa compared to the neat PA6,6 with 54.9 MPa. Moreover, tensile modulus of the same composite improved by 94.8% and reached 4547 MPa, indicating a favorable interface interaction between the fibers and the matrix. Moreover, as the mechanical properties of the semicrystalline thermoplastic composites are highly dependent on the crystallinity of the polymer [40], the enhanced tensile properties are due to the increased crystallization, that is later confirmed by DSC analysis in the following section.

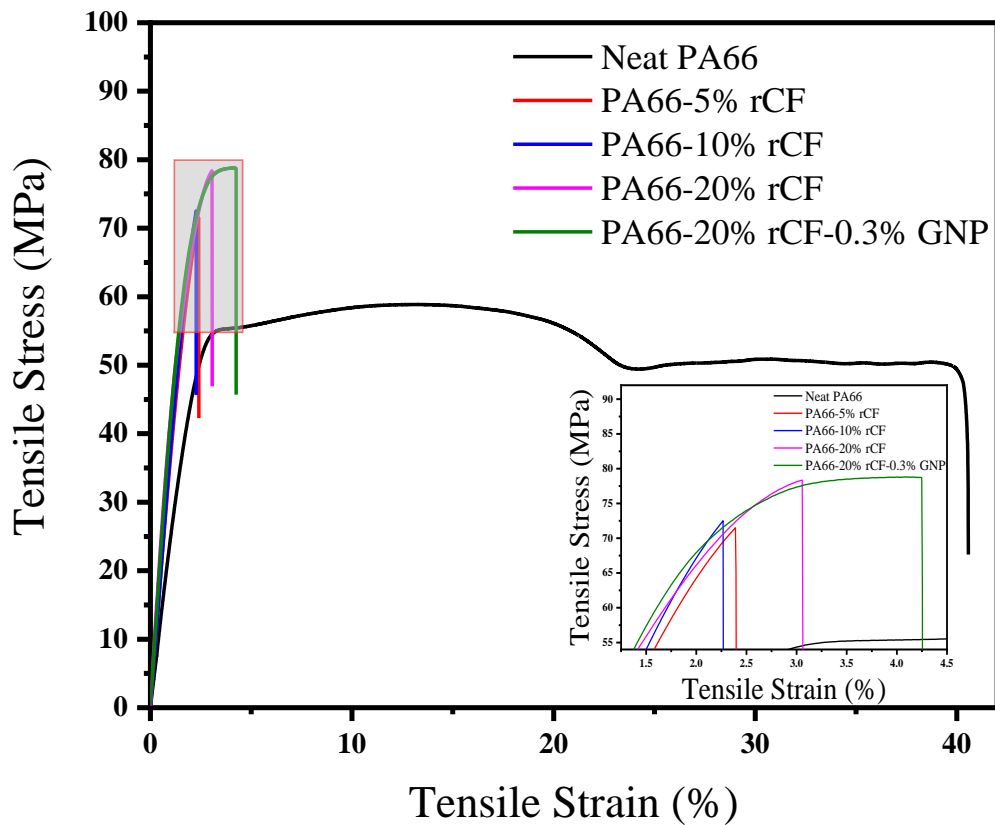


Figure 15. Tensile test curves of neat PA6,6, recycled carbon fiber-based PA6,6, and recycled carbon fiber-GNP reinforced composites

Table 8. Tensile properties of neat PA6,6, recycled carbon fiber-based PA6,6 and recycled carbon fiber/GNP-based composites

Sample	Maximum Tensile Strength (UTS, MPa)	Improvement (%)	Tensile Modulus (MPa)	Improvement (%)	Tensile Strain at Failure (%)
Neat PA6,6	54.9±6.0	-	2334±154	-	16.8±21

PA6,6-5% Recycled carbon fiber	71.9±4.5	30.9	3857±155	65.2	2.5±0.4
PA6,6-10% Recycled carbon fiber	72.5±8.3	32.0	3986±32	70.8	3.3±1.1
PA6,6-20% Recycled carbon fiber	77.9±2.5	41.8	4553±185	95.0	3.5±0.8
PA6,6-20% Recycled carbon fiber-0.3% GNP	78.8±5.0	43.53	4547±236	94.8	4.2±1.3

Figure 16 displays the flexural test curves of neat PA6,6, recycled carbon fiber reinforced PA6,6, and recycled carbon fiber-GNP reinforced PA6,6 composites after flexural tests and Table 9 summarizes flexural strength, strain, modulus, and corresponding improvements of the samples. It is known that the data obtained by three-point bending test, namely, flexural strength is an important parameter to understand the resistance of the material to be fractured, meanwhile, the flexural modulus gives an insight into a material's tendency to deflect and bend under this loading condition [89]. Similar to the tensile properties, flexural strength and flexural modulus improve with the increased recycled carbon fiber concentration. Moreover, due to improved interfacial interactions between fibers and the matrix due to the incorporation of GNP [79], the composite's resistance to shear forces during bending is also improved, as shown by the further improvement in the flexural strength and modulus values. The maximum flexural strength was achieved by incorporating hybrid reinforcement with 20% recycled carbon fiber and 0.3% GNP as 126 MPa, which resulted in a 35.4% improvement compared to neat polymer. Furthermore, drastic improvements were observed in the flexural modulus of the composites by up to 86.6% increase compared to the neat PA6,6.

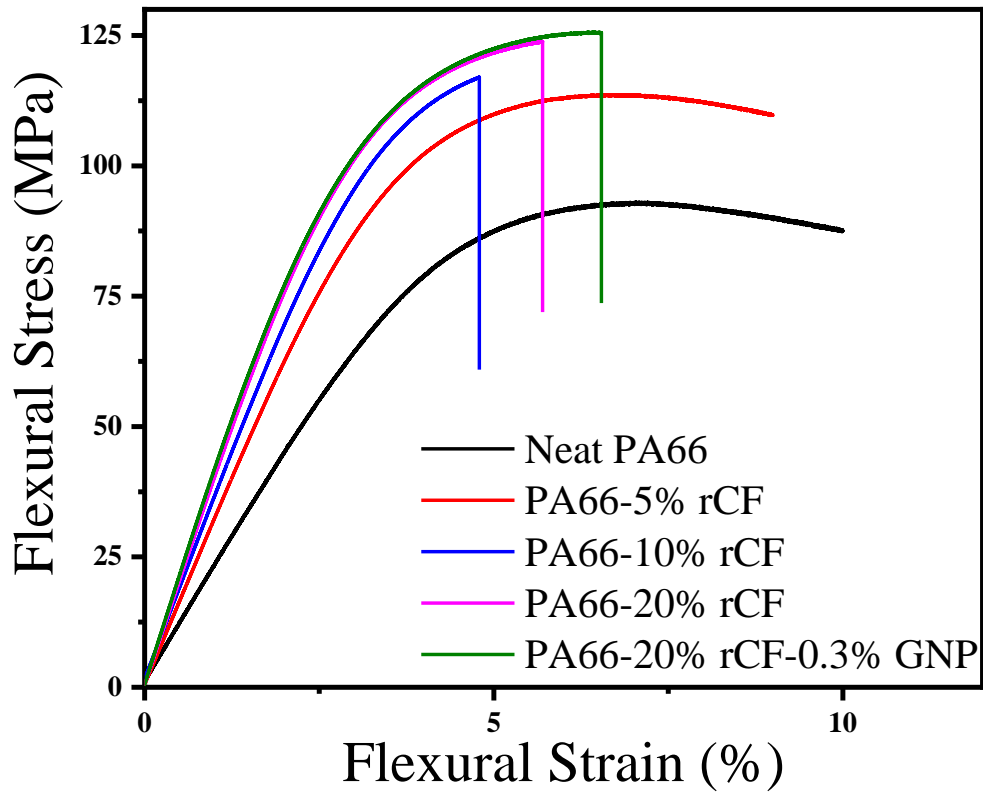


Figure 16. Flexural test curves of neat PA6,6, recycled carbon fiber-based PA6,6, and recycled carbon fiber-GNP reinforced composites

Table 9. Flexural properties of neat PA6,6, recycled carbon fiber-based PA6,6 composites, and recycled carbon fiber/GNP-based PA6,6 composites

Sample	Flexural Strength (MPa)	Improvement (%)	Flexural Modulus (MPa)	Improvement (%)	Flexural Strain (%)
Neat PA6,6	93±2.3	-	2250±68	-	7.05±0.1
PA6,6-5% Recycled carbon fiber	113±16.2	21.5	3250±70	44.4	6.06±2.8
PA6,6-10% Recycled carbon fiber	116±16.2	24.7	3650±200	62.2	5.05±2.0
PA6,6-20% Recycled carbon fiber	124±3.2	33.3	4010±157	78.2	5.7±0.5
PA6,6-20% Recycled carbon fiber-0.3% GNP	126±4.2	35.4	4200±98	86.6	6.45±1.1

Furthermore, the interactions between PA6,6 matrix and reinforcing materials are evaluated under impact loadings. The Charpy notched impact strength of 20% recycled carbon fiber reinforced composites with and without GNP as co-reinforcement are given in Table 10. The addition of both recycled carbon fiber and recycled carbon fiber-GNP led to slight decrease in impact strength compared to the neat PA6,6, which can be attributed to the formation of stress concentration zones at the end of fibers and other

kinds of reinforcements leading to decrease in the energy absorption capability of the thermoplastic matrix [38]. However, the recycled carbon fiber-GNP reinforced composite showed better performance and increased the impact energy by 7.7% compared to the one reinforced only by fiber due to the enhanced fiber/matrix interface by GNP addition, as confirmed by SEM analysis in the following sections.

Table 10. Charpy notched impact test results of neat PA6,6, recycled carbon fiber and recycled carbon fiber-GNP reinforced composites

Sample	Charpy Notched Impact Energy (kJ m ⁻²)
Neat PA6,6	5.51±1.81
PA6,6-20% Recycled carbon fiber	2.98±0.78
PA6,6-20% Recycled carbon fiber-0.3% GNP	3.21±0.41

3.4.2. Thermal and crystallinity properties of recycled carbon fiber reinforced PA6,6 and recycled carbon fiber-GNP reinforced PA6,6 composites

DSC technique is used to understand thermal behavior of materials; therefore, this technique is used in this study to gain insight on the melting and crystallization properties of neat PA6,6, recycled carbon fiber-based, and recycled carbon fiber-GNP reinforced composites using a sample weight range of 8.6 mg to 15 mg. The crystallization curve obtained from the first cooling, and the melting curve from the second heating of neat PA6,6, PA6,6-recycled carbon fiber composites, and PA6,6-recycled carbon fiber-GNP composite have been shown in Figure 17a and Figure 17b, respectively. Thermal parameters of neat PA6,6, PA6,6-recycled carbon fiber and PA6,6-recycled carbon fiber-GNP composites have been summarized in Table 11. No considerable change for the melting behavior of neat PA6,6 and recycled carbon fiber-based composites is observed during the DSC analysis, indicating a thermally stable composite production; however, the crystallization temperatures increase significantly with the addition of recycled carbon fiber and GNP indicating that the carbon-based reinforcements in the polymer initiated early crystallization. Crystallinity degrees of the samples can be quantitatively analyzed using the melting parameters of the polymer using the equation below [90]:

$$X_C = \left(\frac{\Delta H_M}{\Delta H_M^{100\%}(1 - W_f)} \right) \times 100 \quad (3.2)$$

where X_C is the degree of crystallization, ΔH_M is the melting enthalpy, $\Delta H_M^{100\%}$ is the melting enthalpy of 100% crystalline PA6,6, and W_f is the fiber weight fraction. The melting enthalpy of 100% crystalline PA6,6 is 188.4 J g⁻¹ according to the literature [42].

Equation 3.2 is used to calculate the degree of crystallization of the samples, which are given in Table 11. The increase in overall crystallinity is a consequence of early start of crystallization which leads crystals to have more time to grow. Moreover, the nucleating agent behavior of GNP has led to a further increase in the crystallinity of the composite. The improvement in crystallinity confirmed the increase in mechanical properties of recycled carbon fiber-based PA6,6 composites.

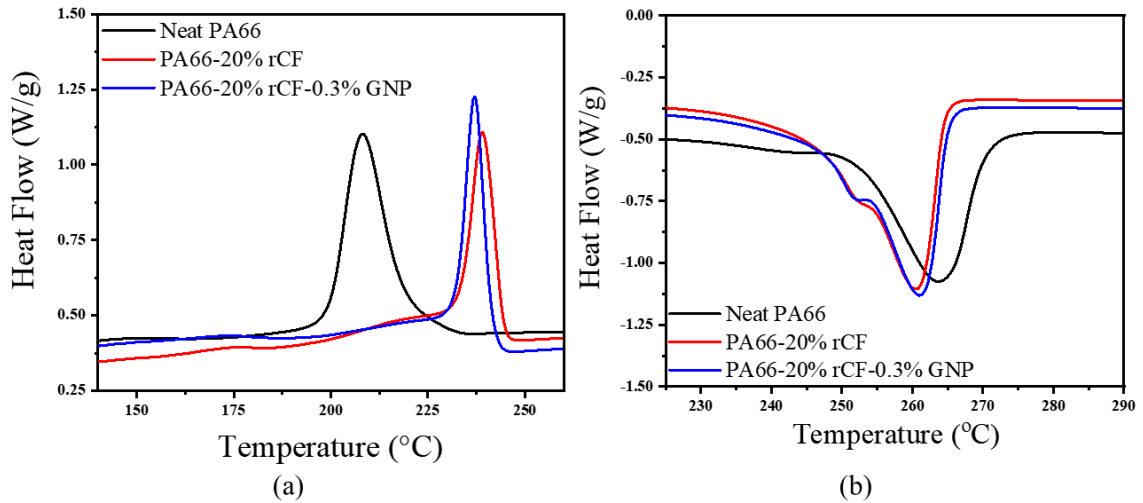


Figure 17. First cooling (a) and second heating (b) cycle DSC curves of the neat PA6,6, PA6,6-recycled carbon fiber, and PA6,6-recycled carbon fiber-GNP composites

Table 11. Thermal parameters and crystallinity degrees of neat PA6,6, and reinforced composites

Sample	Melting Peak Temperature (°C)	Melting Integral, ΔH_M (J g ⁻¹)	Crystallization Peak Temperature (°C)	Crystallization Integral, ΔH_C (J g ⁻¹)	Crystallinity (%)
Neat PA6,6	262	-64.18	209	56.56	34.06
PA6,6-20% Recycled carbon fiber	259	-60.07	239	50.19	39.85
PA6,6-20% Recycled carbon fiber-0.3% GNP	260	-60.55	237	54.12	40.32

3.4.3. The effect of recycled carbon fiber and recycled carbon fiber-GNP hybrid reinforcement on the rheological behavior of PA6,6 composites

Rheological behavior of the thermoplastics and reinforced compounds of importance for the melt blending and molding applications. In this regard, the complex viscosity of the thermoplastics is an important parameter to estimate the processability of the produced compounds [47]. As the temperature increases and is around the melting point of the

thermoplastics, complex viscosity drops. This behavior is observed for both neat PA6,6 and reinforced composites in Figure 18a obtained by temperature sweep method with constant frequency. This drop is rather prominent in 20% recycled carbon fiber reinforced compound and accompanied by the drop in storage moduli, as shown in Figure 18b. The decrease in the storage modulus at high temperatures indicates a poor thermal stability of the compound, as opposed to the usually limited long-distance chain movement observed by the stable viscosities at high temperatures [48]. Since the storage modulus is related to the elastic part of the viscoelasticity of the material and gives information about the stored energy before plastic deformation, decrease in storage modulus indicates that the polymer is unable to store energy. The addition of reinforcements such as recycled carbon fiber and recycled carbon fiber-GNP to the polymer affects the composites' viscosity and has a significant effect on the storage modulus [49]. Moreover, adding GNP recovers the thermal stability otherwise lost at the 20% recycled carbon fiber compound by distributing energy more efficiently throughout the system.

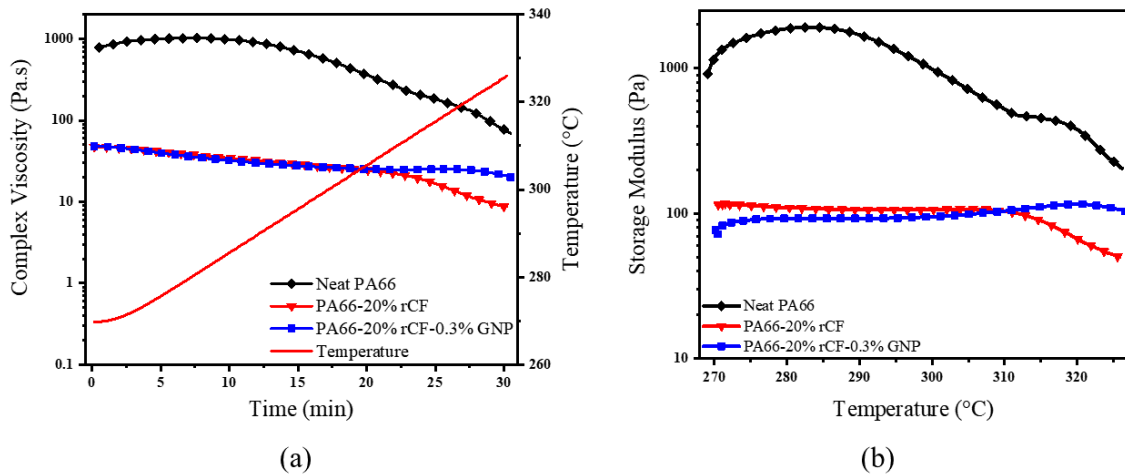


Figure 18. Changes in complex viscosity (a) and storage moduli (b) with the addition of recycled carbon fiber and recycled carbon fiber-GNP to PA6,6 as a function of time and temperature

3.4.4. Cross-sectional fracture surface analysis of recycled carbon fiber and recycled carbon fiber-GNP reinforced PA6,6 composites

Fracture surface analysis of the tensile test specimens provides an important insight on the distribution of reinforcing materials in the composite, failure mode, and fiber morphology before and after the processing [91, 92]. Surface morphology of the recycled carbon fiber bundle and GNP, and fracture surfaces of neat PA6,6, recycled carbon fiber, and recycled carbon fiber-GNP reinforced composites, were investigated using a

scanning electron microscope (SEM) to understand the distribution and interface interactions between the fibers and the PA6,6 matrix. Figure 19a displays the recycled carbon fiber bundle structure formed by several microfibers connected with a sizing material remaining from a previous application as also seen in the literature [93]. GNP morphology in Figure 19b clearly shows the platelet structure which can easily be exfoliated during the shear mixing process. Figure 19c displays that the average layer size of GNPs around 50 nm with an aspect ratio around 1. The fracture surfaces of neat PA6,6 (Figure 19d), and 20% recycled carbon fiber reinforced composites (Figure 19e) display several fibers and fiber imprints with increasing density as expected with the increasing recycled carbon fiber loading [94]. SEM images indicate that the dominant failure mechanism is interface failure due to pull-out because of the weak bonding between the fibers and the matrix [95]. Moreover, although similar case is observed with the recycled carbon fiber-GNP reinforced composite in Figure 19f, a high magnification image of the fiber in Figure 19g reveals that the fiber/matrix interface contains a film-like GNP structure which slightly improves the interface strength as confirmed by the mechanical test results, resembling a similar behavior observed in a previous study [86].

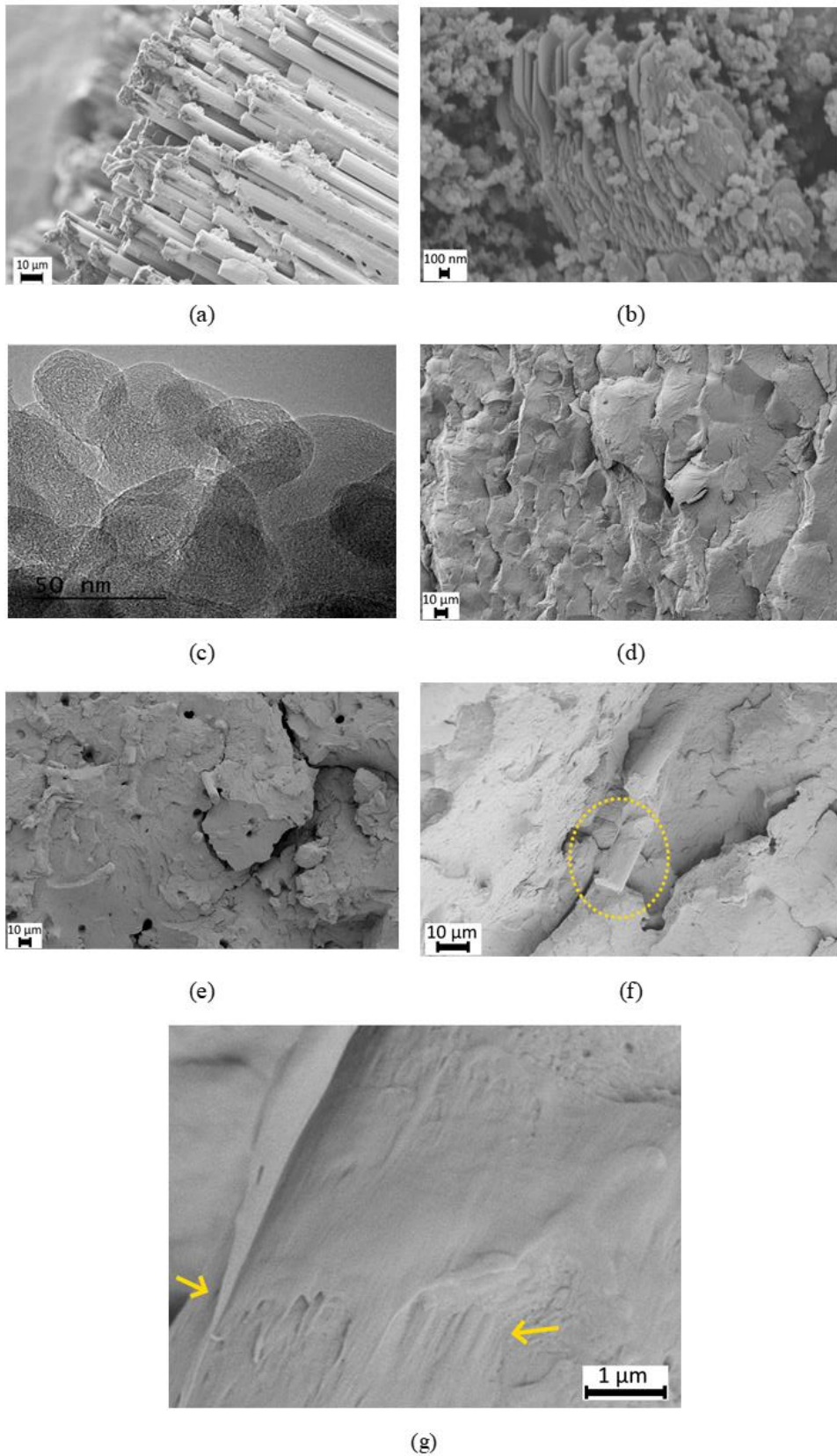


Figure 19. SEM micrographs of recycled carbon fiber bundle at 1.75kx (a), GNP at 75kx, (b), TEM image of GNP at 500kx (c), fracture surface cross sections of neat PA6,6 at 1kx (d), 20% recycled carbon fiber at 1kx (e), and 20% recycled carbon fiber-0.3% GNP at 2.5kx and 50kx (f, g) reinforced composites

Ash test is done under inert atmosphere to determine the fiber morphology in the composites after compounding process. Furthermore, consequent SEM analysis done on the ash residues can give fiber length, diameter, and aspect ratio distribution of the reinforcing fibers in the final composite. The SEM images in Figure 20 indicate that compared to the relatively large size of the bundles, single fibers are significantly shortened and narrowed due to the high shear thermokinetic mixing. This results in a better distribution of the fibers in the matrix, however, decreases the overall expected mechanical properties of the composites due to reduction in critical fiber length.

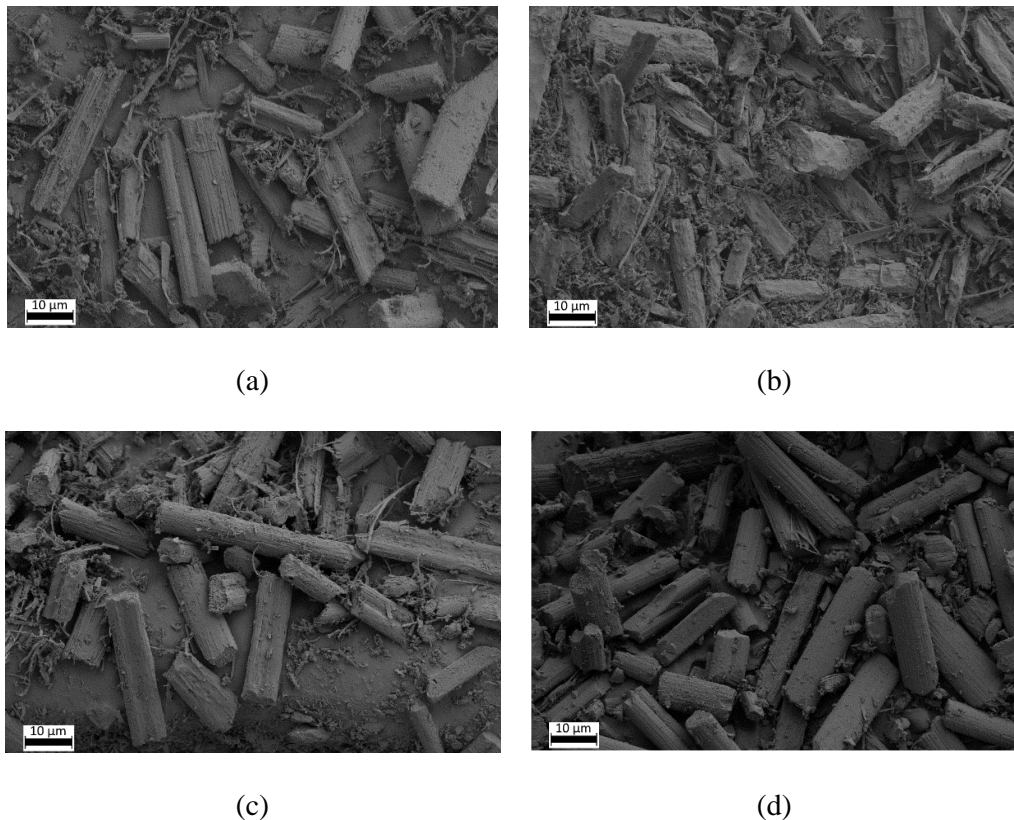
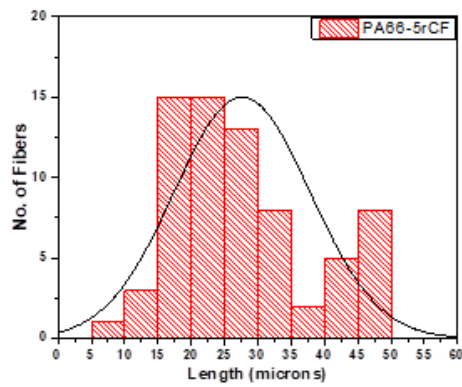
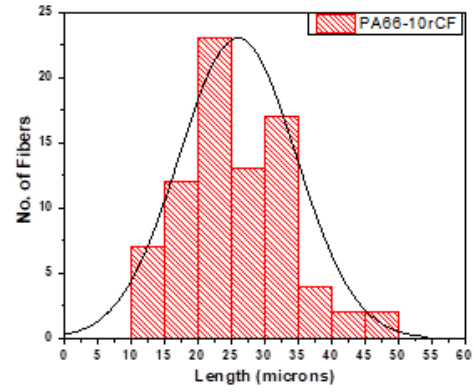


Figure 20. SEM images of 5% (a), 10% (b), 20% rCF (c), 20% rCF-0.3% GNP (d) reinforced composite ashes

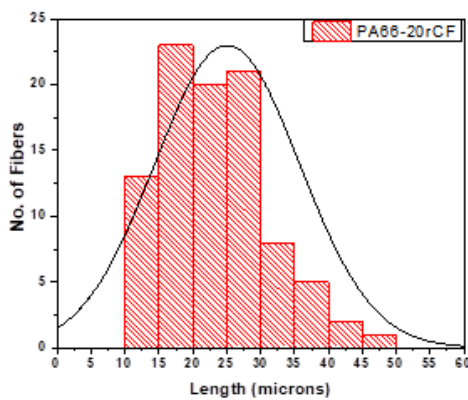
From the SEM images obtained after the ash test, it was observed that during the processing (shear mixing and/or injection) of the composites, fibers were fractured where the initial rCF bundle lengths and diameters are 5 mm and 2 mm, respectively, decreases to μm scales as given in Figure 21. Furthermore, aspect ratios of the fibers show a wide distribution from 2 to 7 compared to 2.5 of the bundles and 1 of the GNP.



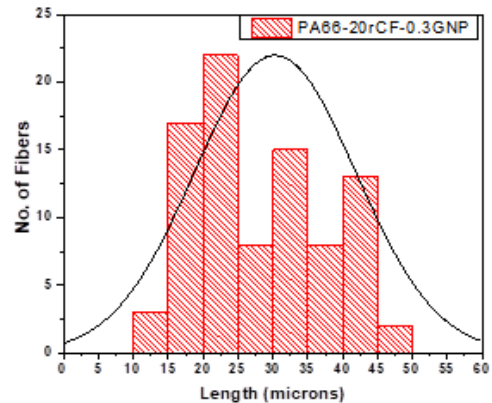
(a)



(b)



(c)



(d)

Figure 21. Length distribution of fibers in 5% (a), 10% (b), 20% rCF (c), 20% rCF-0.3% GNP (d) reinforced composite ashes

3.5. Conclusions

In conclusion, this study successfully incorporated recycled carbon fibers and waste tire-derived graphene nanoplatelets (GNP) into the PA6,6 polymer matrix, resulting in significant improvements in mechanical properties. The synergistic effect of integrating 20 wt.% recycled carbon fibers and 0.3 wt.% GNP led to an increase in flexural modulus and strength by 86.6% and 35.4%, respectively, compared to the neat polymer. Tensile strength and modulus values were also improved by 43.3% and 94.8%, respectively. Moreover, the addition of 0.3% GNP increased Charpy notched impact energy by 7.7% compared to the composite with 20% recycled carbon fiber.

Consequently, this study provides a platform by bringing industrial insight and offering a sustainable approach to the use of multi-scale recycled reinforcements by establishing relations based on the aspect ratio and dimension of carbon materials. With this work, it

will be possible to integrate the recycled additives in compound formulations by supporting sustainability approaches and enhancing injection molding process by providing lightweight and circular economy-based solutions, especially in the commodity level applications such as automotive, sports and leisure, and plastics sector.

Future research can expand on this work by further exploring the characterization techniques and optimization strategies for composite performance. Additionally, investigations into the long-term durability and environmental impact of these composites will be crucial. By embracing these future directions, this study lays the foundation for the integration of recycled additives in compound formulations, supporting sustainability and enhancing the injection molding process for broader applications.

CHAPTER 4: A Comprehensive Dimensional Analysis of Waste-Derived Reinforcements in Interface Interactions with Semi-Bio-Based PA6,10 Composites

4.1. Abstract

This study achieves interface sensitivity in semi-synthetic polyamides by applying dimensional analysis to graphene derived from waste sources like coffee, tires, and chopped carbon fiber resulting in lightweight and high-performance composites. Graphene from tires in platelet form (GNP) and graphene from coffee in spherical form (CWC) and carbon fibers in bundle form (CF) were incorporated into Polyamide 6,10 (PA6,10) with high-shear mixer by examining optimum loading ratio for each reinforcement by supporting interface characterization. Regarding the performance results by keeping loading ratio same, specific flexural properties are significantly enhanced when employing high aspect ratio CF reinforcement, while the platelet structure of GNP is more effective in improving specific tensile properties. Additionally, the spherical graphene of CWC exhibited the highest crystallinity, along with CF. These insights offer valuable guidance for selecting the most suitable reinforcement based on specific compound requirements. In addition, sustainable PA6,10-based compounds reinforced with waste-derived materials were compared to commercial synthetic PA6-based compounds with similar thermal characteristics but superior mechanical performance. The research revealed that the addition of 20 wt.% CWC to the PA6,10 matrix outperforms commercial synthetic compounds in terms of specific tensile modulus, demonstrating the potential of tailored waste-derived reinforcement to replace synthetic products while improving tensile properties. The findings of this study demonstrate that effectively incorporating waste-derived reinforcing materials into semi-bio-based composites presents a promising strategy to improve performance and serve as viable alternatives to commercial products, particularly in applications that require lightweighting and robust load-bearing capabilities.

4.2. Introduction

The emerging trends in leading transport industries regulated by intergovernmental organizations such as European Union and United Nations are shifting towards lifestyle of health and sustainability which allows materials with specific set of properties to enter the market and enable the bio-sourcing and ecological aspects to become the performance factors for these application segments [96]. Considering this point of view, the use of semi-bio-based polyamides (PA) such as PA6,10 can replace its synthetic counterparts such as PA6 and PA6,6 even though the latter is still economically more feasible [97]. Bio-based PAs such as PA10,10 and PA11 offer low humidity absorption and high chemical resistance due to relatively low density of amide linkage sites, as a result, synthetic PAs with shorter chains outperform them in terms of mechanical properties and thermal resistance due to latter having stronger hydrogen bonding with increased number of amide linkage sites [75]. Consequently, semi-bio-based PA6,10 with a mid-range chain length offers low humidity absorption compared to the synthetic PAs and higher mechanical strength compared to long chain bio-based PAs.

Incorporation of reinforcing materials in order to surmount the shortcomings in mechanical properties of bio-based PAs has recently attracted attention [98, 99]. One approach is to incorporate nanoscale fillers such as graphene or carbon nanotubes (CNT) which drastically enhances certain properties such as mechanical and flame retardancy while reducing permeability allowing sealant applications. In one of the studies, Lee *et al.* reported acyl chloride-functionalized graphene oxide reinforced PA6,10 nanocomposite by *in situ* polymerization technique with 36.9% increased thermal conductivity at 0.95% GO loading [100]. In another study, Maset *et al.* extruded halloysite nanotube (HNT) with PA6,10 and reached 122% improvement in the tensile modulus, however, the tensile strength reduced by 10% at 30% HNT loading [101]. Moreover, Kang *et al.* fabricated multi-walled CNT-PA6,10 films by *in situ* polymerization with a 170% improved tensile modulus at 1.5% CNT loading [102]. Nevertheless, the scalability aspect of *in situ* polymerization and the agglomeration of nanoscale additives during the extrusion process leading to a reduction in composite strength restrict the use of these additives in the industry.

The use of microscale fillers is another way to compensate for the mechanical downsides of the bio-based and semi-bio-based PAs. Previous studies suggest that melt blending is suitable for integrating these reinforcements to the matrix to be used in large-scale applications such as automotive industry [103, 104]. In one of these studies, Tian *et al.*

investigated the tensile and damping properties of micro cellulose reinforced PA6,10 composites and concluded that at 10% loading, tensile modulus improved by 22% while the damping ratio increased by 67% [103]. In another study, Ogunsona *et al.* utilized pyrolyzed *mischantus* fibers to reinforce PA6,10 and improved the tensile and the flexural moduli by 50% and 87%, respectively, at 20% loading with <500 μm long microfibers [105]. Moreover, Battezzore *et al.* studied the effects of rice husk ash on PA6,10 composites and obtained 45% increased tensile modulus accompanied with 1% increase in yield strength at 20% loading [106]. However, the use of such high loadings may increase the density of fabricated composite and deter its use in applications where light weighting is important.

One of the most efficient methods to improve the mechanical properties of thermoplastics is blending with macroscale reinforcements such as natural, glass, or carbon fibers [60, 107, 108]. In one of the studies, Kuciel *et al.* utilized flax fibers (FF), glass fibers (GF), and carbon fibers (CF) at 10% loadings to fabricate bio-based PA composites with 107%, 488%, and 1042% increased tensile moduli, respectively [109]. In a recent study, Artykbaeva *et al.* used PA6-PA6,10 blend matrix with 40% GF reinforcement for improving the tensile modulus and strength by 5 times and 57%, respectively [110]. Similarly, Nikiforov *et al.* investigated the effect of several fiber reinforcements in PA10,10 and reported that, at 40% GF loading, tensile modulus and yield strength improved by 455% and 184%, respectively [111]. In another study, Quiles-Carrillo *et al.* reported the effects of silane treatment on the waste derived slate fiber reinforced PA10,10 composite parts and concluded that glycidyl-silane treated fibers improved tensile modulus by 241% while the tensile strength improved by 96% [99]. In a more recent study, Caltagirone *et al.* proposed a commercially available recycled carbon fibers to substitute virgin carbon fiber for reinforcing automotive grade synthetic PA6,6 composites by achieving comparable mechanical properties [112]. Lastly, Dericiler *et al.* incorporated multi aspect ratio hybrid reinforcement of 20 wt.% recycled carbon fiber and 0.3 wt.% GNP into PA6,6 which resulted in 94% increase in tensile properties and 86% increase in flexural modulus [113]. Nevertheless, a comprehensive study correlating the mechanical properties with thermal and morphological properties of bio-based or semi-bio-based PAs reinforced with different aspect ratio reinforcements is missing from the literature.

In this study, the utilization of waste-derived reinforcing materials, including GNP derived from waste tires, carbonized waste coffee, and waste carbon fibers were favored, in combination with a semi-bio-based PA6,10 matrix. This choice was driven by the economic and environmental advantages offered by these waste-derived materials, as opposed to using a synthetic PA matrix with virgin reinforcements, which are expensive and require energy-intensive production techniques. Therefore, recycled and upcycled reinforcements melt-blended with the PA6,10 matrix with a controlled GNP, CWC, and CF weight ratios using a thermokinetic shear mixer. The interactions between the interfaces of waste-derived reinforcements and PA6,10 matrix as well as the effect of the aspect ratio, size, and morphology of the reinforcing materials on the mechanical and thermal properties is studied comparatively. This is the first study in the literature encompassing wide range of multiscale waste-derived reinforcing materials with different morphological properties in combination with semi-bio-based PA6,10 matrix where mechanical and thermal properties together with interfacial interactions is investigated. Subsequently, a benchmarking study is also carried out to determine the lightweighting potential of developed sustainable compounds with selected automotive grade commercial synthetic compounds in terms of specific strength and specific modulus. This work reveals that fabricated sustainable compounds can replace several products in the market for automotive industry by supporting sustainability initiatives and offering lightweight, circular economy-driven solutions.

4.3. Materials and Methods

4.3.1. Materials

The effects of reinforcements size and morphology was investigated by utilizing graphene nanoplatelets (GNP) as the nanoscale reinforcement, carbonized waste coffee (CWC) as the microscale reinforcement, and waste carbon fiber (CF) as the macroscale reinforcement. Graphene nanoplatelets (GNP) synthesized from the recycled carbon black received from the pyrolysis of waste tires by upcycling process were obtained from Nanografen Co., Turkey. The density of the waste tire-derived GNPs is calculated as 2.115 g/cm^3 . GNPs have 9 wt.% surface oxygen groups with a surface area of $120 \text{ m}^2/\text{g}$ and an average platelet size of 50 nm from Transmission Electron Microscope (TEM) given in Figure 22a. For the synthesis process of CWC, waste coffee was collected daily after each consumption and dried in the oven at $80 \text{ }^\circ\text{C}$ overnight before the pyrolysis

process. Upcycled graphene was produced using dried waste coffee and applying direct and flash pyrolysis using a rotating furnace. For this process, a custom-made Protherm rotary furnace was used to perform the pyrolysis process in a short time. Pyrolysis was performed at 1000 °C for 5 sec under argon atmosphere with a yield of 15%. The furnace has an angle and rotation control panel, and the speed of material fed into the furnace was adjusted by changing the parameters in a speed and temperature-controlled feed zone. The continuous process was maintained by constantly feeding waste coffee into the rotary furnace and collecting the upcycled graphene at the discharge zone. The temperature was kept constant at 1000 °C at all three furnace zones to provide thermal stability. TEM image of CWC is given in Figure 22b. Waste CF bundles were supplied by DowAksa, Turkey. Polyamide 6,10 (PA6,10, Tecomid NI, Eurotec) is a semi bio-based polyamide with low moisture absorption, high salt, hydrolysis, and pressure resistance and is used as the matrix material for composite production. PA6,10 was dried in the oven at 80 °C for 2 h before each usage to remove the moisture.

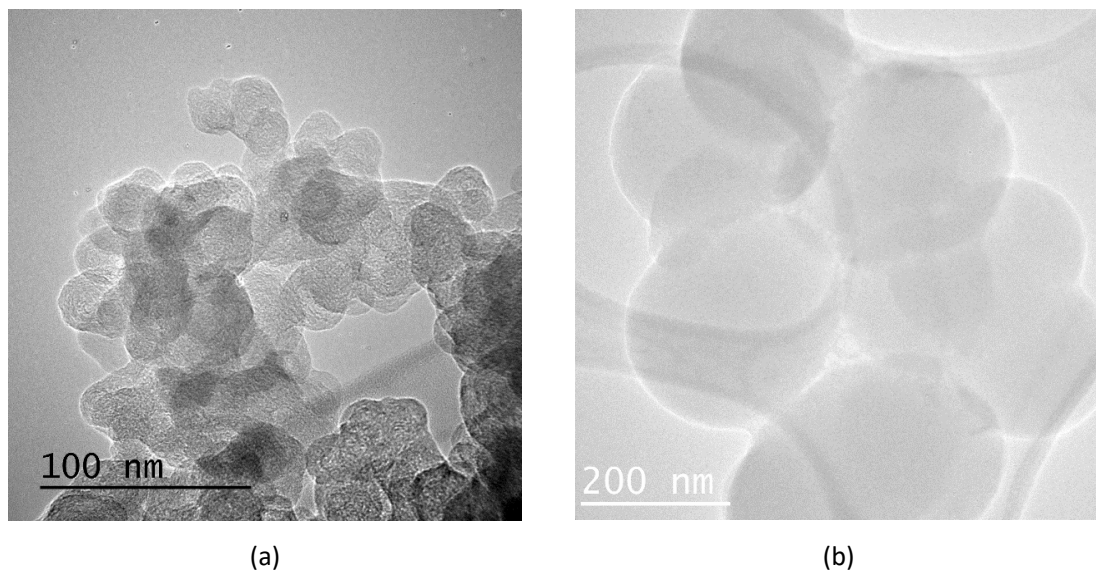


Figure 22. TEM images of GNP (a) and CWC (b)

4.3.2. Fabrication of PA6,10-based composites with different scale reinforcements

PA6,10-based composites were prepared by a custom made Gelimat thermokinetic shear mixer (Dusatec Inc.) at a rotation speed of ~ 4000 rpm at 230 °C for 5 s. Loading ratios of 0.3, 0.4, 0.5, and 1 wt.% for the nanoscale reinforcement were adjusted and mixed with PA6,10 at the melt-phase to prevent agglomeration and attain a homogenous dispersion while microscale and macroscale reinforced composite loading ratios of 1, 5, 10, and 20 wt.% were similarly adjusted and mixed at the melt-phase. The obtained products were

then crushed into granules and injection molded by an Explore mini-injection molding machine for mechanical tests. The schematic representation of the fabrication process is given in Figure 23.

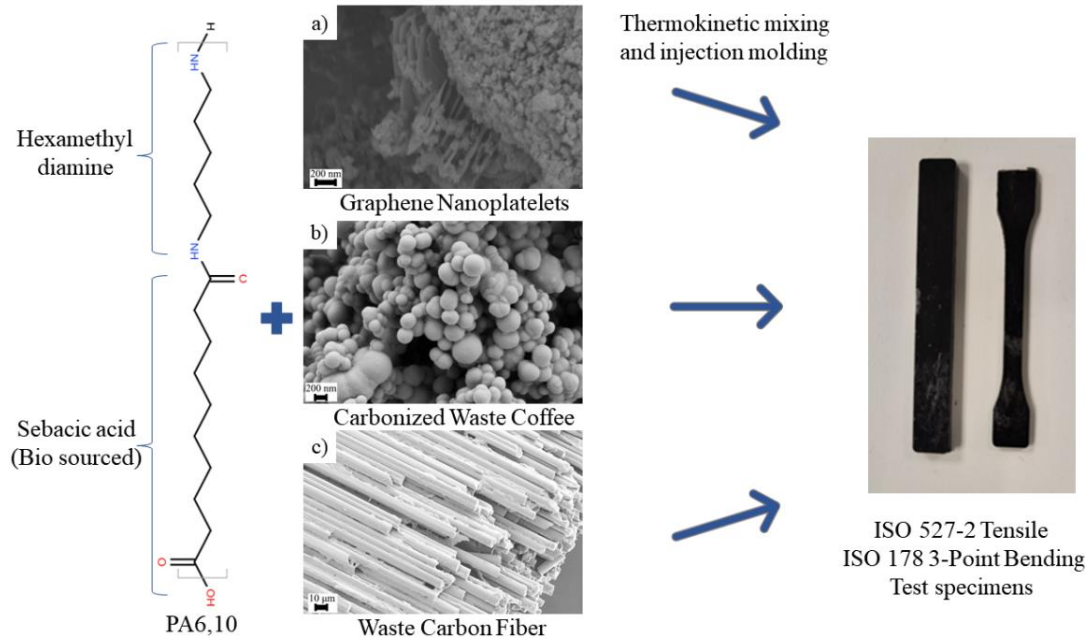


Figure 23. Schematic representation of the fabrication process of PA6,10-based composites

4.3.3. Characterization

The characteristics of reinforcing materials (GNP, CWC, CF), the matrix material (PA6,10) and the composites were examined using various spectroscopic and macroscopic techniques. Elemental analysis has been carried out using X-ray Photoelectron Spectroscopy (XPS) for GNP and CWC samples. Raman spectroscopy and X-ray Diffraction techniques were used to confirm the characteristic peaks and examine the microstructure of GNP and CWC. The mechanical tests were conducted by using Instron 5982 Static Universal Test Machine (UTM) with a 5 kN load cell for ISO 527-2 tensile and ISO 178 three-point bending tests. Thermal analyses of polymer composite samples were carried out by Differential Scanning Calorimetry (DSC) technique using Mettler Toledo DSC 3+ 700 under a nitrogen atmosphere between 25 °C and 300 °C. Firstly, samples were heated and held at 300 °C for 5 min to eliminate the thermal history. A cooling cycle followed by an additional heating cycle were performed at the rate of 10 °C/min to investigate the samples' thermal behavior. STARE software from Mettler Toledo was used in order to obtain the melting enthalpy (ΔH_m), crystallization enthalpy (ΔH_c), as well as melting (T_m), and crystallization temperatures (T_c). Anton Paar MCR

702 TwinDrive Rheometer with a parallel plate configuration was used for the rheological characterization of the specimens. In order to carry out the morphological studies, fractured test specimens were sputter-coated with a thin layer of Au/Pd alloy to provide conductivity. Surface topography and morphology of reinforcing materials and the fractured composite specimens were investigated using a Leo Supra 35VP Field Emission Scanning Electron Microscope (FESEM).

4.4. Results and Discussion

4.4.1. Structural transformation of waste coffee into upcycled graphene (CWC)

Herein, upcycled graphene with a misaligned turbostratic structure is obtained by flash pyrolysis of waste coffee in a rotary furnace. One of the leading indicators of graphene formation is the characteristic peaks seen in the Raman spectroscopy. Raman spectra of graphene constitute distinct peaks that correspond to specific structural vibrations [114]. The D peak is generally located at around $\sim 1350\text{ cm}^{-1}$ and appears due to the point defects in the planar structure. The G band corresponds to the in-plane stretching vibration of sp^2 hybridized C atoms and appears around $\sim 1580\text{ cm}^{-1}$ [115]. The intensity ratio of G and D peaks (I_G/I_D) gives insight into graphene's structural order and quality [116]. Figure 24 displays the Raman spectra of waste coffee, upcycled graphene, and their respective I_G/I_D values. It can be seen that the flash pyrolysis process has led to the formation of graphene-like structures with the I_G/I_D ratio of 1.08, which is comparable to the chemical reduction [117] or electrochemistry-based [118] graphene synthesis methods, while waste coffee did not show any characteristic peaks. In the literature, especially in the field of electrochemical applications, carbonized biomass-derived materials having significant structural defects are generally named as turbostratic carbon or hard carbon [119]. This hard carbon structure usually contains curved graphene layers in contrast to flat layers in graphite [120]. However, this curved and defective structure causes an increase in D peak indicating an increase in defects [119, 121]. In our work, G peak intensity is higher which confirms a relative order on the hexagonal sp^2 bond structure [115]. On the other hand, XRD indicates the formation of turbostratic structures partially with the peaks assigned as seen in Figure 25. In other words, flash pyrolysis process led to the formation of graphene like structures due to the occurrence of (002) belonging to main characteristic peak of graphene.

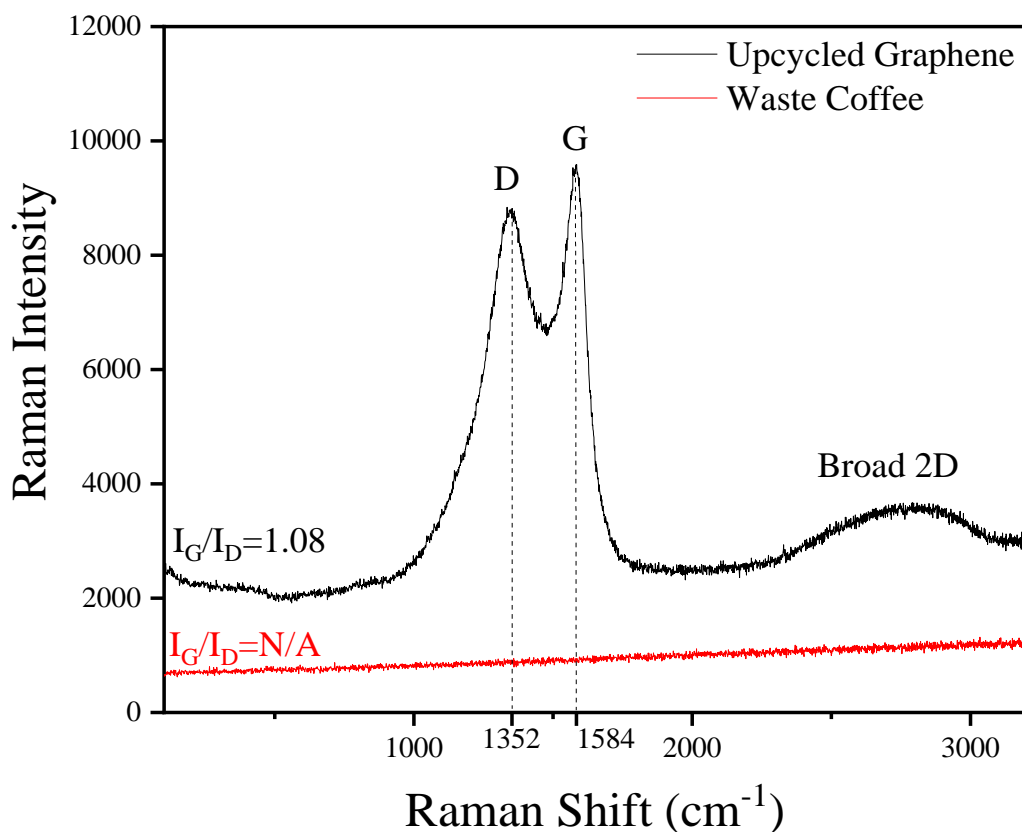


Figure 24. Raman spectra of waste coffee and upcycled graphene from coffee

Changes in the crystalline structure from the waste coffee to upcycled graphene also play a significant role in the electronic properties of the end-product [122]. XRD patterns of the waste coffee and upcycled graphene were investigated to obtain information on the crystalline structures of the samples. Figure 25 shows the XRD patterns of waste coffee and upcycled graphene. Relatively high carbon content in the waste coffee results in the formation of a distinct (002) peak at $2\theta=20^\circ$ diffraction angle, which is slightly shifted to $2\theta=24^\circ$ in the upcycled graphene, indicating a wrinkled plane resulting in a turbostratic structure [123]. Moreover, upcycled graphene displays a weak (100) peak at $2\theta=42^\circ$, typically observed in turbostratic graphene structures [124]. Furthermore, a less pronounced (002) peak in upcycled graphene suggests a smaller crystalline size in the z-direction [125]. Table 12 summarizes the crystallinities of the waste coffee and upcycled graphene.

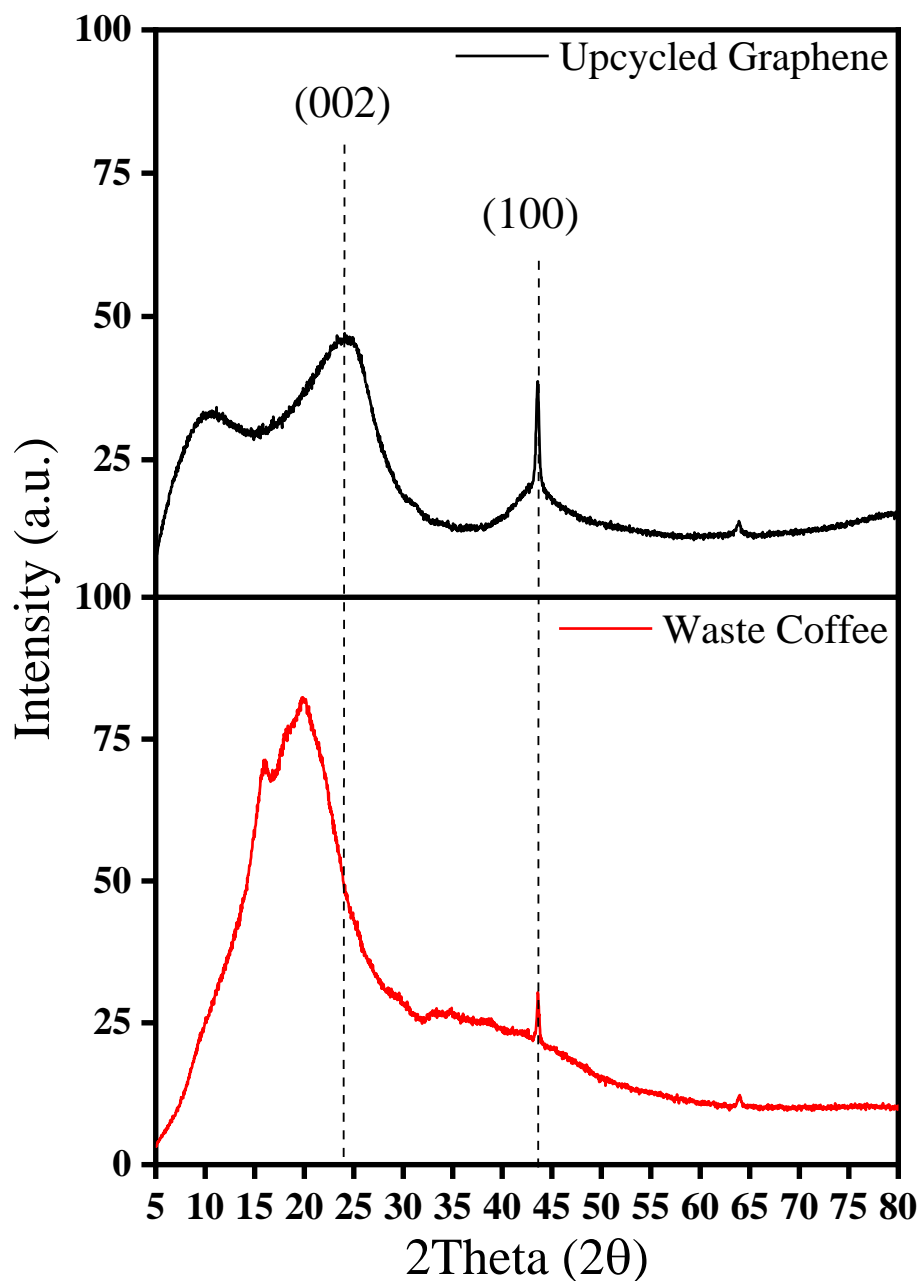


Figure 25. XRD patterns of the waste coffee and upcycled graphene

Table 12. Crystallinities of waste coffee and upcycled graphene

Sample	Crystallinity (%)	Amorphous (%)
Waste Coffee	37.8	62.2
Upcycled Graphene	49.4	50.6

Determination of the surface functional groups on the waste coffee and upcycled graphene is important due to their role in the capacitive behavior and charge transfer mechanisms for supercapacitor applications. Moreover, transformation from waste coffee to upcycled graphene can be observed by the removal of functional groups on the surface

due to flash pyrolysis. FT-IR technique is utilized to probe the functional groups present in the waste coffee and upcycled graphene, and FT-IR spectra of the samples are given in Figure 26. Waste coffee displays various molecular vibrations regarding the caffeine and other molecular complexes in the structure, however, after the flash pyrolysis process, it can be seen that the transmission ability of the sample is decreased, and other molecular complexes are removed from the structure. The waste coffee displays several peaks such as a small band at 3367 cm^{-1} due to the presence of the OH group [126], while the peaks at 2919 cm^{-1} and 2851 cm^{-1} are related to the CH, CH₃ (methyl), and CH₂ bonds in aliphatic organic compounds. Carbonyl and N-H vibration peaks also appear around 1747 cm^{-1} , 1451 cm^{-1} and 813 cm^{-1} due to caffeine content in the waste coffee [127]. Additionally, molecular vibrations of aromatic acids, aliphatic acids, lipids, and R-OH groups are visible at around 1680 cm^{-1} , 1700 cm^{-1} , 1350 cm^{-1} , and 1030 cm^{-1} , respectively [128]. After flash pyrolysis, only two major peaks remained in the structure as the peak around 1580 cm^{-1} identifies the aromatic C=C hexagonal structure and rises due to graphitic backbone vibration while the peak around 883 cm^{-1} corresponds to the C-O-C epoxide group with an out-of-plane O atom [129]. As the high-temperature flash pyrolysis process decomposes the organic bonds in the structure, which is known as the reverse Boudouard process, only micro sized carbonaceous residue remains [130].

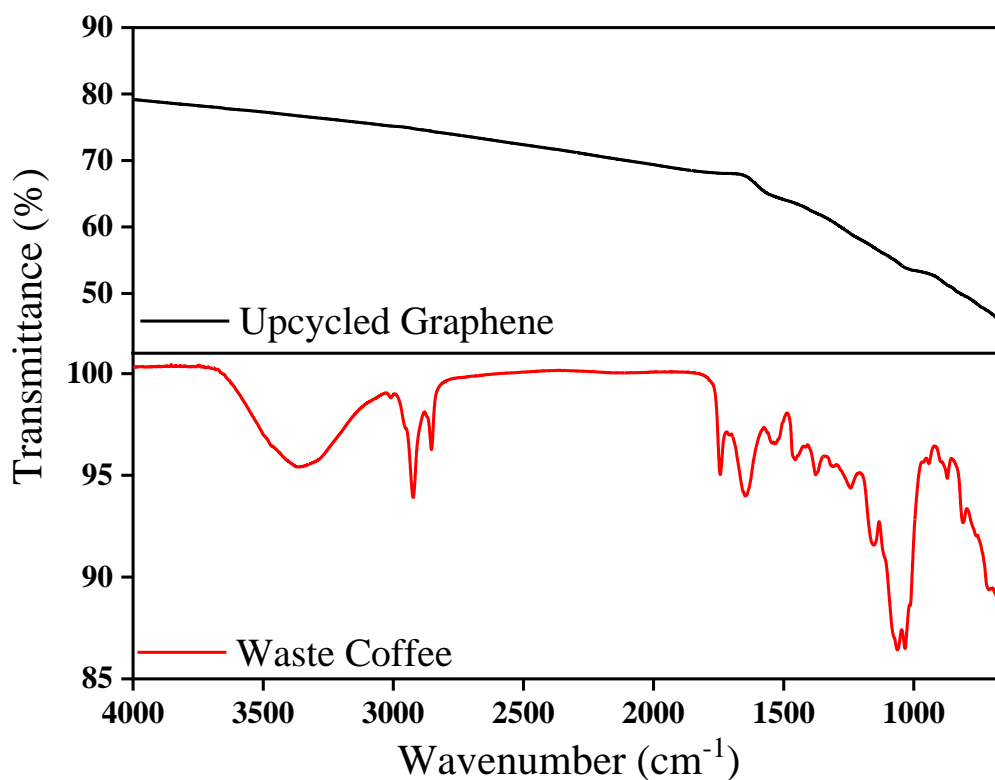


Figure 26. FT-IR spectra of waste coffee and upcycled graphene

X-Ray Photoelectron Spectroscopy (XPS) is a widely used surface chemistry analysis technique to investigate the samples' elemental composition and molecular structure. As the performance of supercapacitors greatly depends on the surface features of electrode materials and their elemental composition, the determination of these properties using XPS provides beneficial insight into the supercapacitor application. Figure 27 displays the XPS survey spectra of waste coffee and upcycled graphene. It is shown that the C/O ratio of the sample has increased due to the flash pyrolysis process. Figure 28a shows the deconvoluted C1s spectrum of the waste coffee, while Figure 28b displays the same spectrum for the upcycled graphene. Although most of the C1s peak constitutes of sp^2 C-C group at around 284.2 eV, weak C-O peak at around 285.7 eV and C=O peak at around 288.2 eV may suggest an incomplete transformation or slight oxidization by the atmospheric oxygen [131, 132]. Figure 28 also displays the deconvoluted O1s spectrum of the waste coffee (c) and upcycled graphene (d). It can be seen that the majority of the oxygen is present in a C-O formation indicated by the peak around 532 eV. Additionally, C=O groups with the binding energy at around 533.5 eV for both samples are also present in the structure [133–135]. Elemental and molecular analyses of waste coffee and upcycled graphene from coffee are summarized in Table 13. XPS analysis results showed

that the significant increase in the C/O ratio after the flash pyrolysis confirmed the formation of highly carbonaceous material suitable for supercapacitor electrode application.

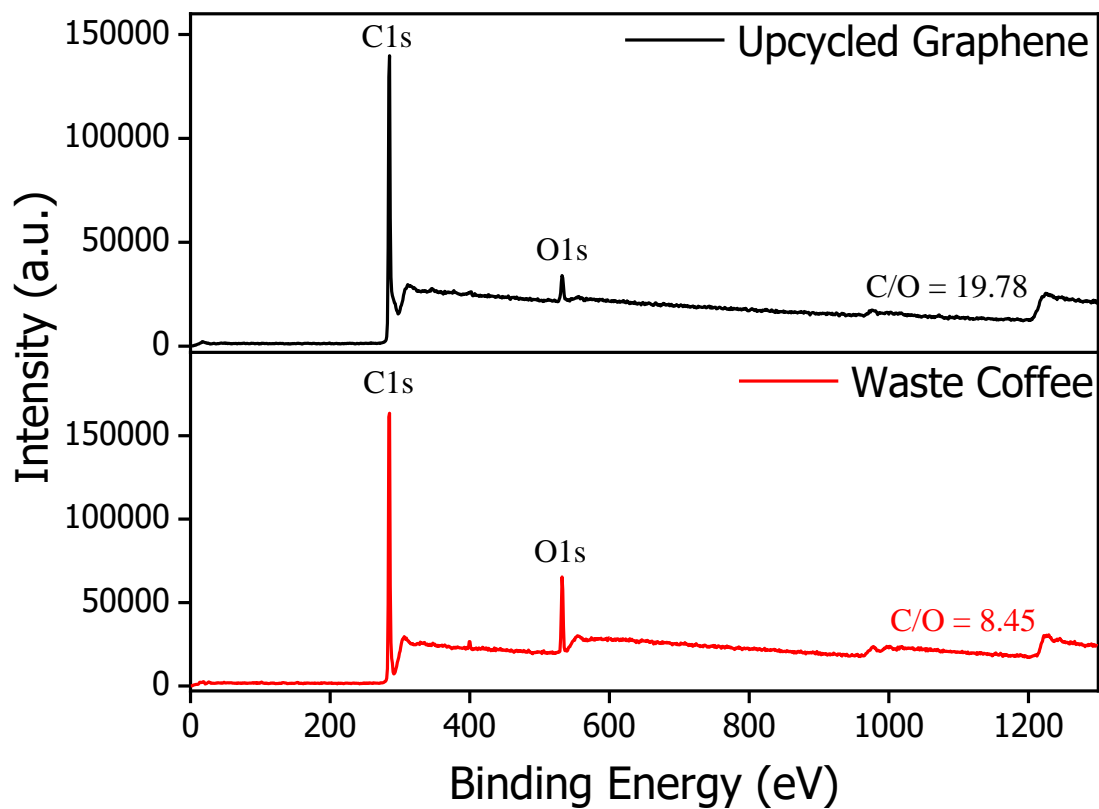


Figure 27. XPS survey scans of waste coffee and upcycled graphene

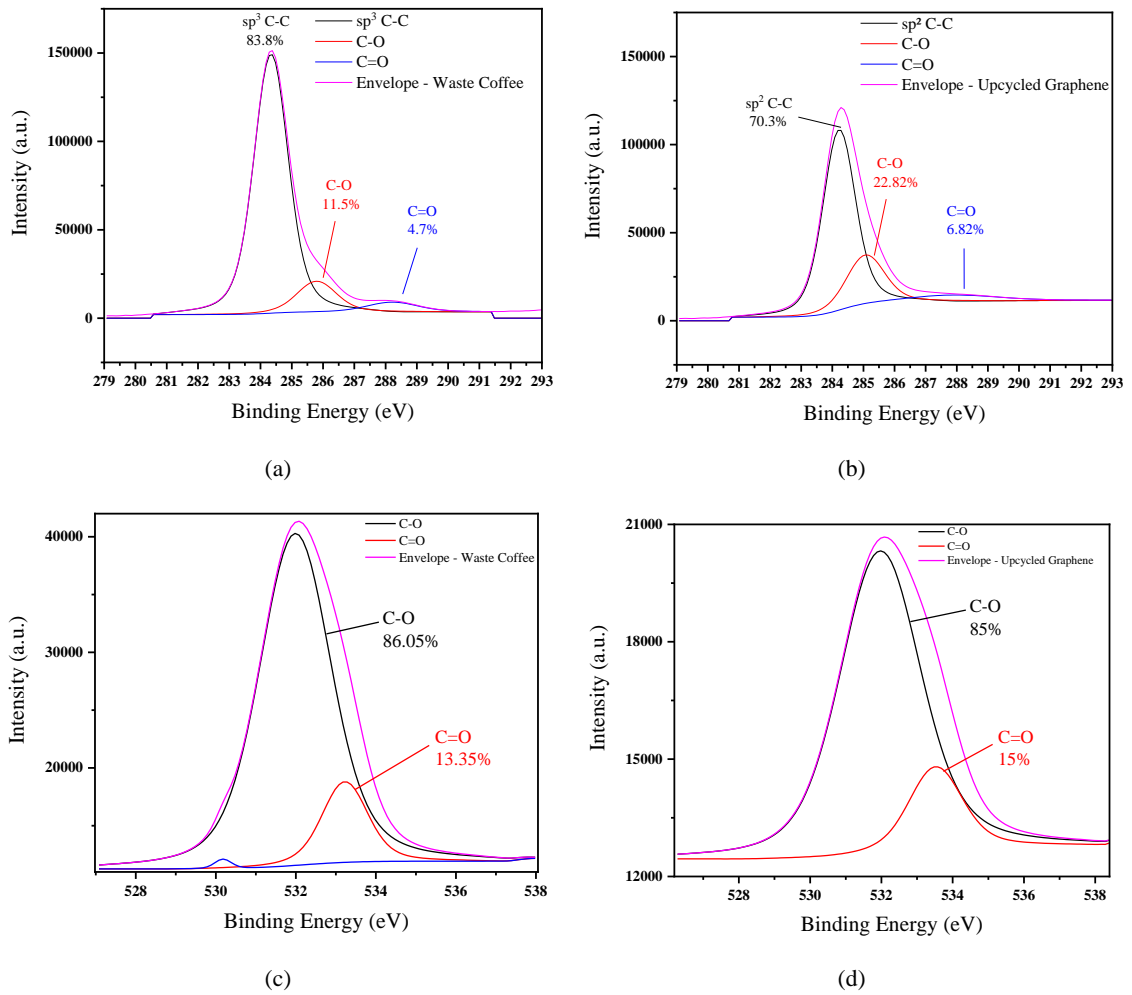


Figure 28. Deconvoluted C1s scans of waste coffee (a) and upcycled graphene (b) and deconvoluted O1s scans of waste coffee (c) and upcycled graphene (d)

Table 13. A summary of the elemental composition of waste coffee and upcycled coffee and their molecular bonds

Sample	Element Composition			Functional Group Composition of C1s				Functional Group Composition of O1s		
	C (at%)	O (at%)	Others (at%)	sp ² C-C (at%)	sp ³ C-C (at%)	C-O (at%)	C=O (at%)	C-O (at%)	C=O (at%)	Other (at%)
Waste Coffee	88.28	10.44	1.28	-	83.80	11.50	4.70	86.05	13.35	0.60
Upcycled Graphene	93.21	4.71	2.08	70.36	-	22.82	6.82	85.00	15.00	-

Surface properties of electrode materials play a crucial role in the charge transfer, and it is essential to investigate their surface topography by microscopic techniques. SEM analysis provides to monitor the effect of flash pyrolysis and fast spinning at high temperatures on the waste coffee particles. Figure 29 displays the surface morphology of waste coffee before (a, b) and after the flash pyrolysis in the rotary furnace (c, d),

respectively, at different magnifications. As seen in SEM images, flash pyrolysis leads to the sphericalization and size reduction of the particles, and thus the formation of spherical graphene structures with various sizes and conjugation degrees is observed. To date, there are several developed theories on the sphericalization mechanism of carbonaceous materials at high temperatures [136–139]. The general consensus is that as the temperature increases, aromatic compounds undergo dehydration, polymerization through cross-linking, and carbonization by intermolecular dehydration, respectively, leading to spherical shapes with the lowest surface energy [140].

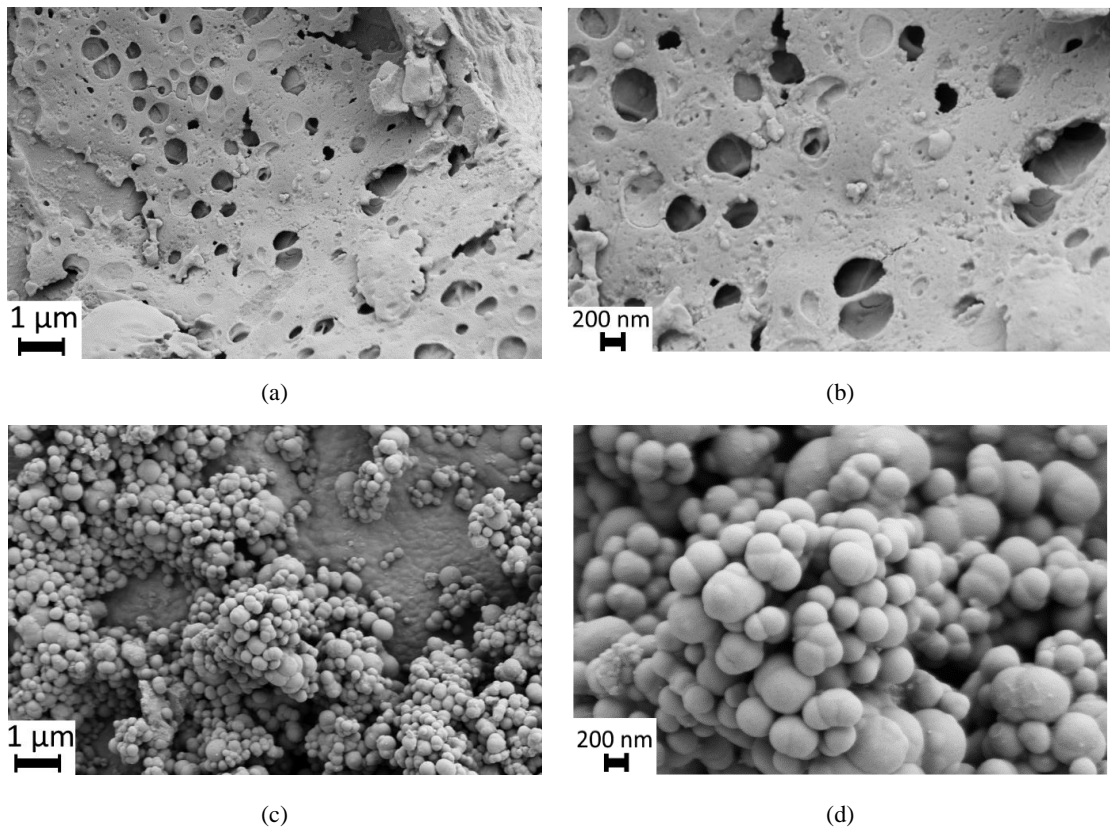


Figure 29. SEM images of waste coffee before (a, b) and after (c, d) flash pyrolysis at 25,000X (a, c) and 75,000X (b, d) magnifications.

4.4.2. The characteristics of waste-driven reinforcements

The effective reinforcement in composite materials is mainly dependent on aspect ratio [141, 142], morphology [143], and size [144] of the reinforcing material. Thus, characteristic properties of waste-driven reinforcing materials including their source, morphology, aspect ratio, and size are given in Table 14. Moreover, microstructural characterizations in terms of X-ray diffraction (XRD) pattern and Raman spectra are given in Figure 30 and Figure 31, respectively. Detailed analysis of the XRD patterns and

Raman spectra of GNP and CWC are already carried out in our previous studies [86, 145] and in section 2.3.1 and in section 4.4.1. Furthermore, CF displays an XRD peak around $2\theta=25^\circ$ similar to a virgin carbon fiber [146] due to hexagonal carbon backbone. In addition, Raman spectrum of CF shows characteristic D and G peaks at 1358 and 1595 cm^{-1} corresponding to ordered and disordered graphitic backbone of CF [147] arising from first order Raman scattering and the absence of 2D peak is due to lack of second order double resonance Raman process which is similarly observed in CF structures [148]. In addition, elemental analysis of CF surface is carried out using energy dispersive X-ray (EDX) and given in Figure 32 to further analyze the surface of the waste derived reinforcement.

Table 14. Characteristic properties of waste-driven reinforcing materials.

Characteristic	GNP	CWC	CF
Source	Waste Tire	Waste Coffee	Waste Carbon Fiber
Morphology	Platelet	Spherical	Fiber Bundle
Aspect Ratio	1	1	4
Size	~50 nm	~250 nm	~5 mm

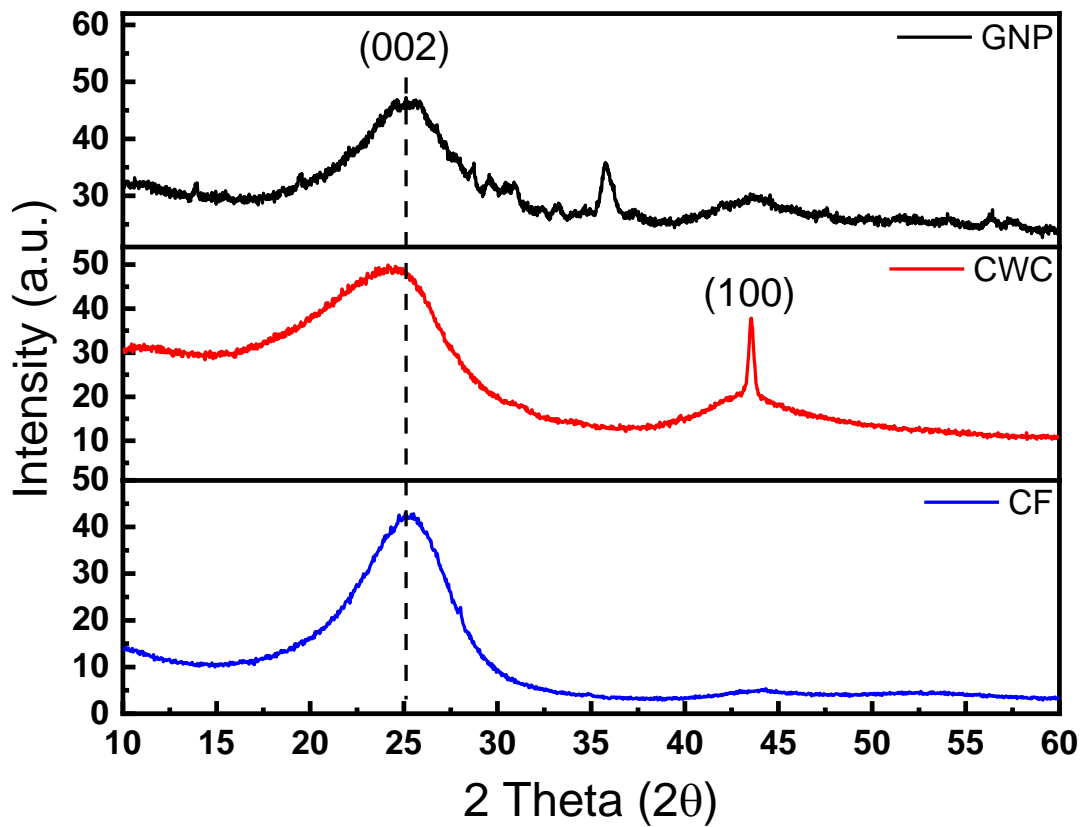


Figure 30. XRD patterns of waste-driven reinforcing materials

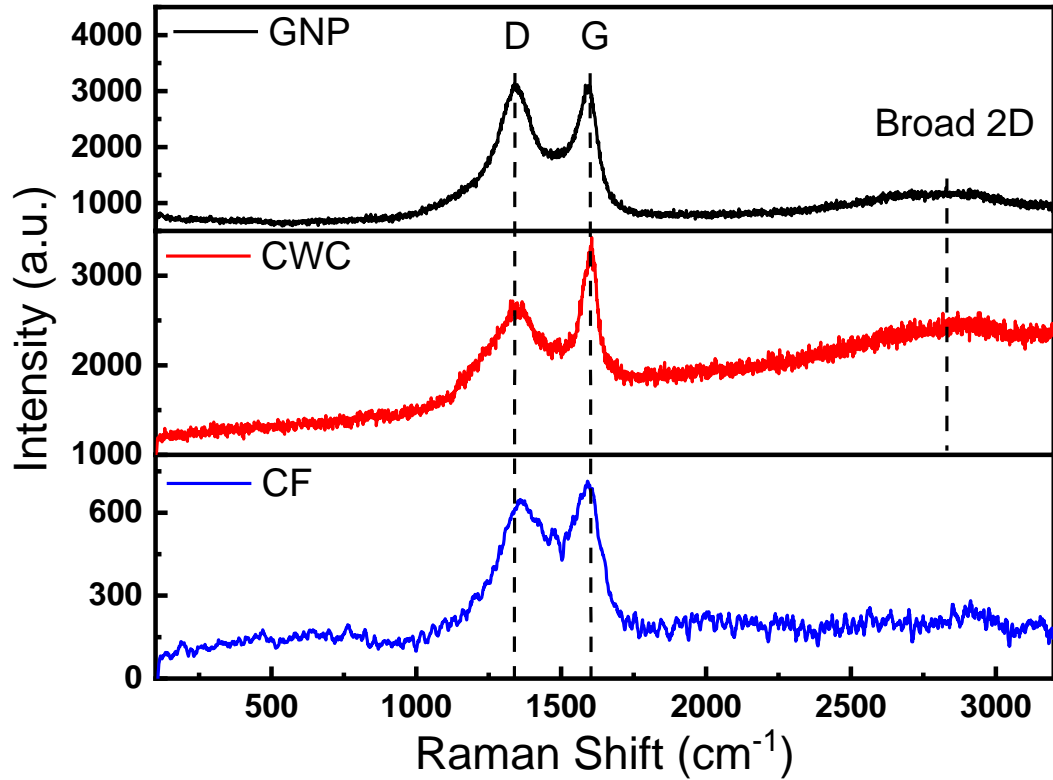
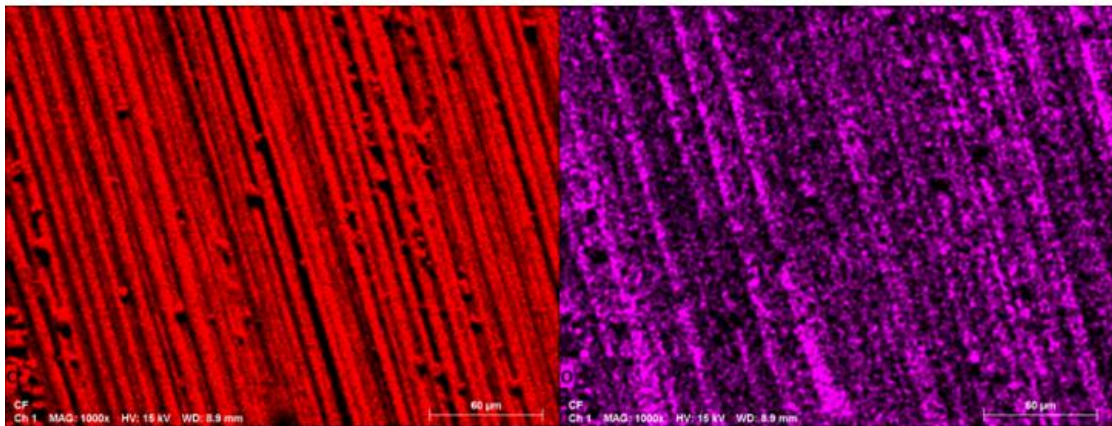
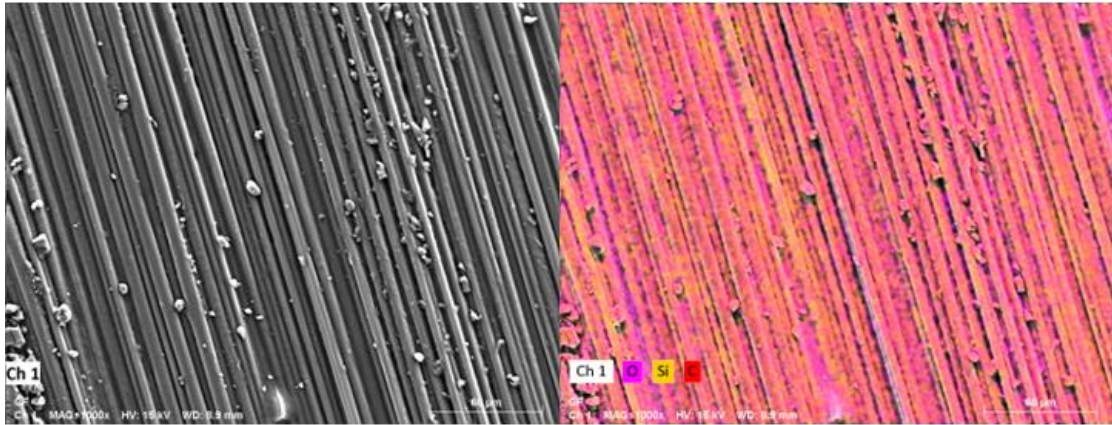


Figure 31. Raman spectra of waste-driven reinforcing materials



Element	At. No.	Mass [%]	Mass Norm. [%]	Atom [%]
Silicon	14	0.540635	0.540635	0.235768
Oxygen	8	6.519626	6.519626	4.990943
Carbon	6	92.93974	92.93974	94.77329

Figure 32. EDX Mapping and elemental analysis of CF

4.4.3. Mechanical performance of sustainable PA6,10-based composites

In the present study, different reinforcement types and loading ratios were utilized to improve the mechanical performance of PA6,10-based composites. For microscale and macroscale reinforcements, a loading ratio range between 1 wt.% and 20 wt.% was selected which are the common loading ratios for thermoplastic composites in the industry. For GNP, loading ratio range from 0.3 wt.% to 1 wt.% were selected according to our previous study indicating that for PA6,6 optimal mechanical properties obtained at 0.3 wt.% loading [86]. Even though at high loading ratios nanomaterials tend to

agglomerate and result in non-efficient reinforcing potential, maximum loading ratio of 1 wt.% is selected to enable a comparison with microscale and macroscale reinforcing materials. Herein, several waste-driven reinforcing materials at various morphologies, sizes and aspect ratios were compounded with semi-bio-based PA6,10 to create lightweight sustainable composites using a thermokinetic shear mixer and effect of reinforcement characteristics is investigated through tensile and flexural properties of the composites.

Figure 33 shows the tensile properties of PA6,10-based composites with varying reinforcement material and loading ratio and Table 15 summarizes the change in tensile strength, modulus, and tensile strain at failure in comparison with the neat polymer. Tensile stress-strain curves of neat PA6,10 and PA6,10-based composites are provided in Figure 34a-c. Tensile test results indicate that with the addition of any amount of reinforcing material to the PA6,10 matrix, yield strength and modulus improves, as expected, due to load transfer from matrix to the reinforcing material. Optimum loading ratio for GNP reinforcement is reached at 0.5 wt.% loading by 38% and 50% improvements in yield strength and tensile modulus indicating to an agglomeration limit whereas at 1 wt.% a drop in tensile modulus is observed which could be due slight agglomeration of the nanomaterials. Nevertheless, this increase in optimum loading ratio of 0.5 wt.% GNP in PA6,10 compared to 0.3 wt.% GNP in PA6,6 as seen in our previous work [86], can indicate to a relation between the optimum loading ratio and the chain length of the matrix material. Moreover, at the same loading ratio (1 wt.%), effective interfacial interactions between the surface oxygen groups on GNP and amide linkage groups in PA6,10 chain resulted in a more efficient reinforcing in terms of tensile properties. However, maximum yield strength of 59.03 MPa is obtained at 20 wt.% CF loading and maximum tensile modulus of 2921 MPa is reached at 20 wt.% CWC loading, by improving the tensile properties of neat polymer by 40% and 87%, respectively.

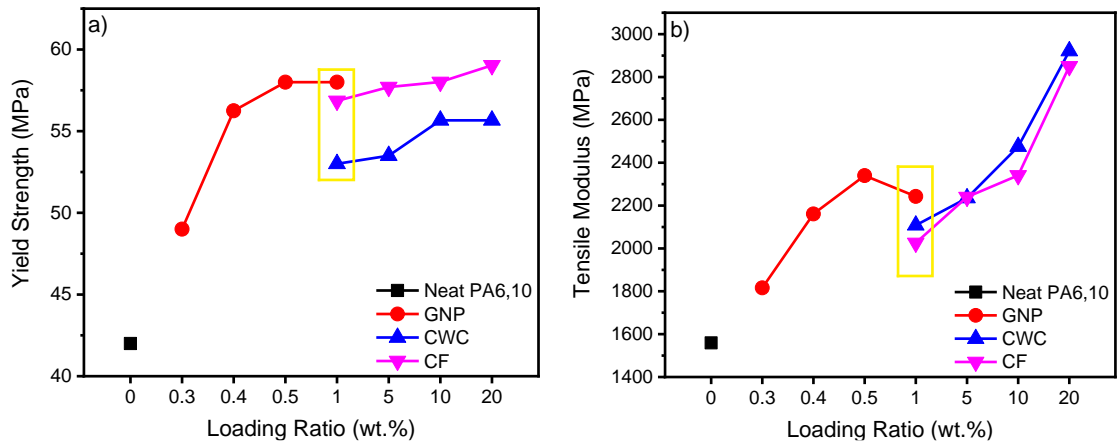


Figure 33. Yield strength (a) and tensile modulus (b) of PA6,10-based composites with respect to reinforcement loading ratios

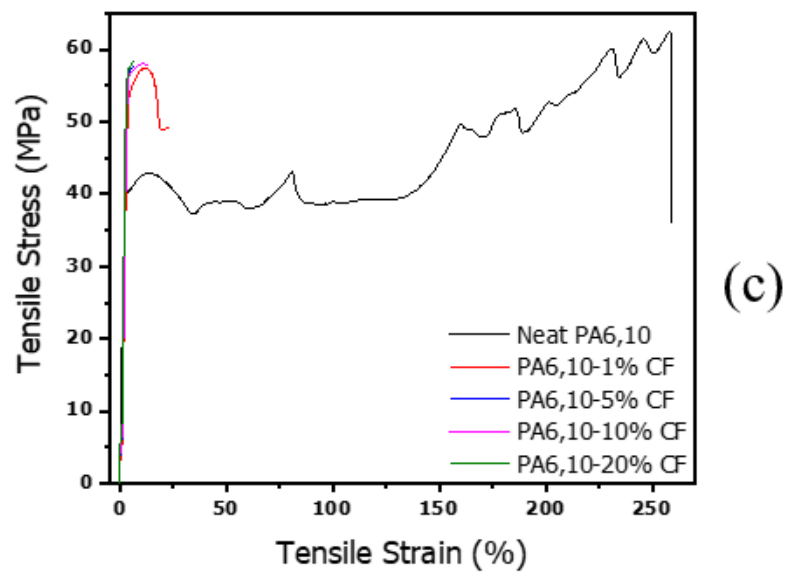
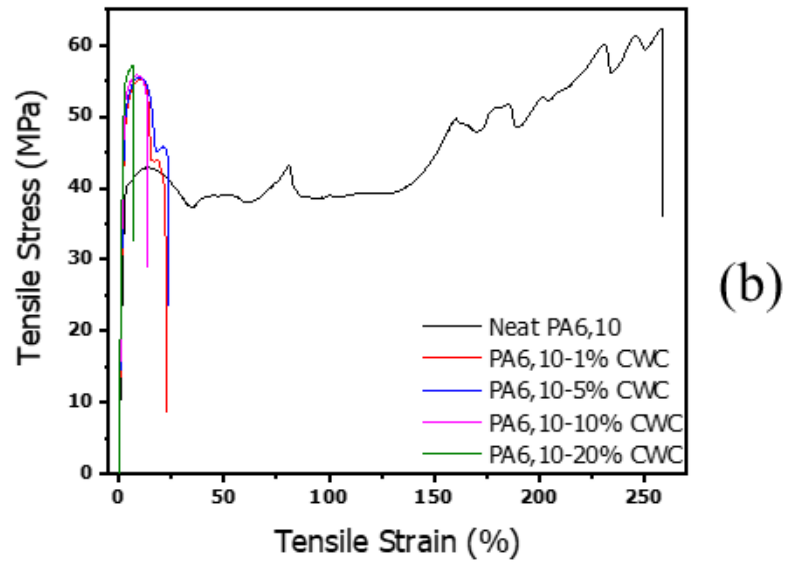
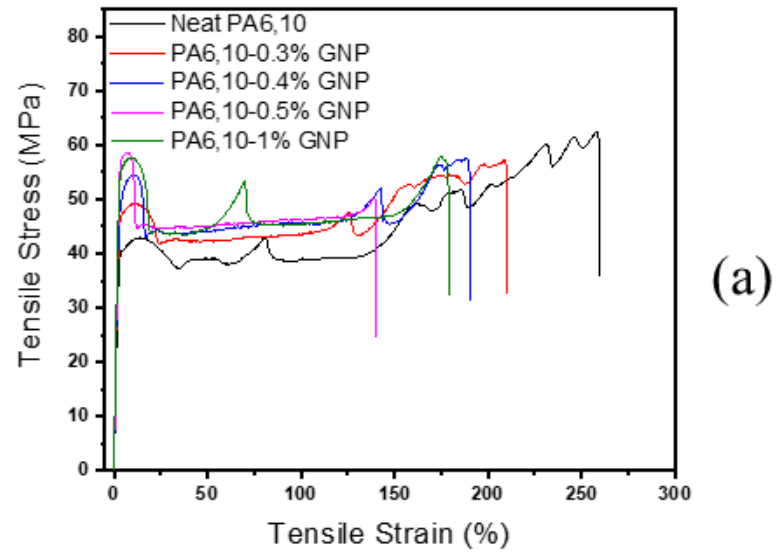


Figure 34. Tensile stress-strain curves of GNP-reinforced (a), CWC-reinforced (b), and CF-reinforced (c) composites

Table 15. Tensile properties of PA6,10-based composites and improvements compared to the neat polymer

Sample	Yield Strength (Zero Slope, MPa)	Improvement (%)	Tensile Modulus (MPa)	Improvement (%)	Tensile Strain at Yield Strength (%)
Neat PA6,10	42.00±1.1	-	1559±55	-	13.5±0.5
PA6,10-0.3% GNP	49.00±0.8	16.67	1816±94	16.48	10.4±0.6
PA6,10-0.4% GNP	56.25±1.7	33.92	2161±68	38.61	9.1±0.6
PA6,10-0.5% GNP	58.00±1.1	38.09	2340±228	50.09	8.1±1.0
PA6,10-1% GNP	58.00±0.8	38.09	2243±112	43.87	8.6±0.5
PA6,10-1% CWC	53.00±4.6	26.19	2108±96	35.21	7.8±3.4
PA6,10-5% CWC	53.50±3.3	27.38	2235±64	43.36	7.2±3.4
PA6,10-10% CWC	55.66±0.5	32.52	2475±127	58.75	9.8±0.6
PA6,10-20% CWC	55.66±1.5	32.52	2921±360	87.36	7.7±1.9
PA6,10-1% CF	56.85±3.4	35.35	2026±97	29.95	10.4±2.0
PA6,10-5% CF	57.70±2.5	37.38	2240±207	43.68	8.0±4.0
PA6,10-10% CF	58.01±0.1	38.11	2341±12	50.16	9.8±0.2
PA6,10-20% CF	59.03±0.5	40.54	2850±70	82.80	10.8±0.8

Figure 35 displays the flexural properties of neat PA6,10 and PA6,10-based composites and Table 16 summarizes flexural strength, strain, modulus, and corresponding improvements of the samples. Flexural stress-strain curves of neat PA6,10 and PA6,10-based composites are provided in Figure 36a-c. Three-point bending flexural tests provide important insight into material properties and reinforcement dispersion due to complex loading system creating maximum compression stress and maximum tensile stress zones at opposite edges of the specimen [149]. Flexural strength data obtained from the three-point bending test indicates the materials resistance to fracture, while the flexural modulus is related with the composites' ability to deflect and bend under this loading condition [89]. Similarly, flexural strength and flexural modulus improve with the addition of waste-derived reinforcing materials. Moreover, GNP-based composites display the same trend showing the optimum properties at 0.5 wt.% loading by improving the flexural strength and modulus by 12% and 13%, respectively, compared to the neat polymer. However, CF-based composites performed better compared to other reinforcing materials in this complex loading situation, due to fiber morphology distributing the loads

through fibers thickness and providing overall better load transfers whereas the spherical and platelet structure of CWC and GNP is not as efficient as CF in this load system. The maximum improvements in flexural strength and modulus were achieved by incorporating 20 wt.% CF to the matrix by 24% and 48%, and reached 90 MPa and 2887 MPa, respectively.

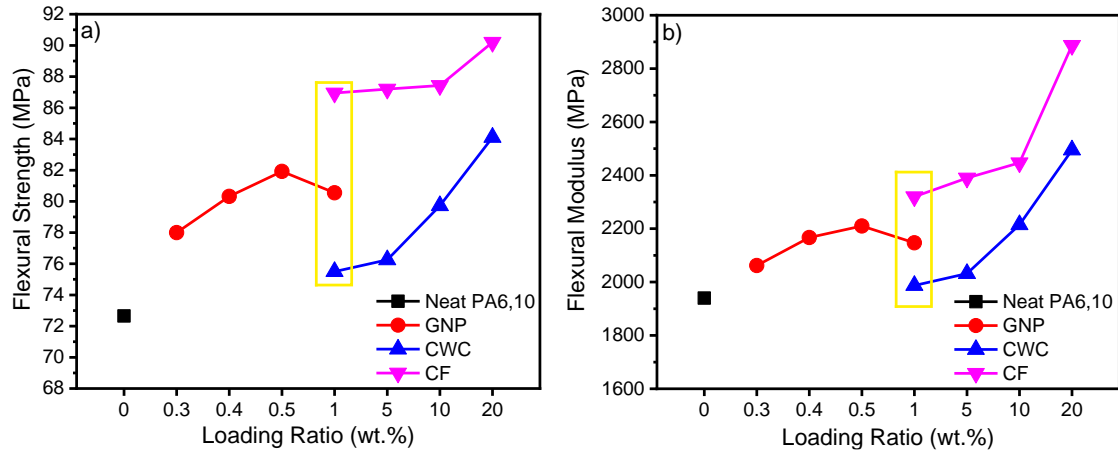


Figure 35. Flexural strength (a) and modulus (b) of PA6,10-based composites with respect to reinforcement loading ratios

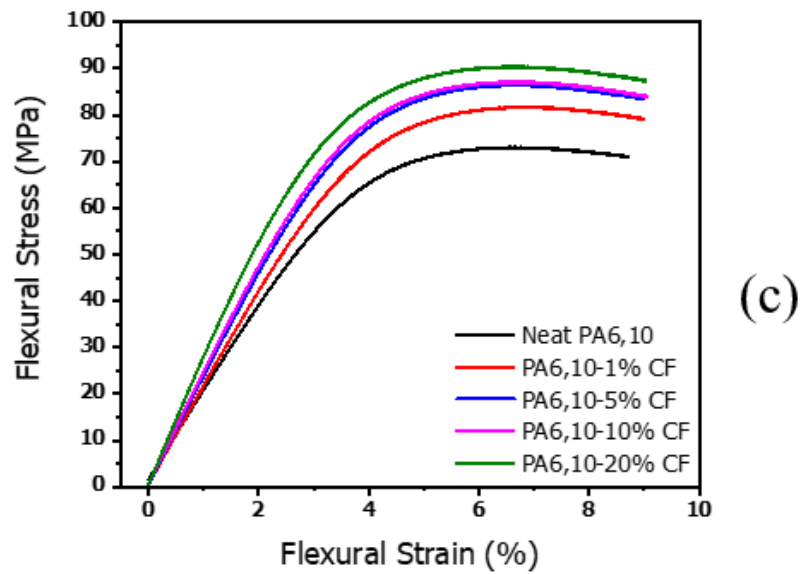
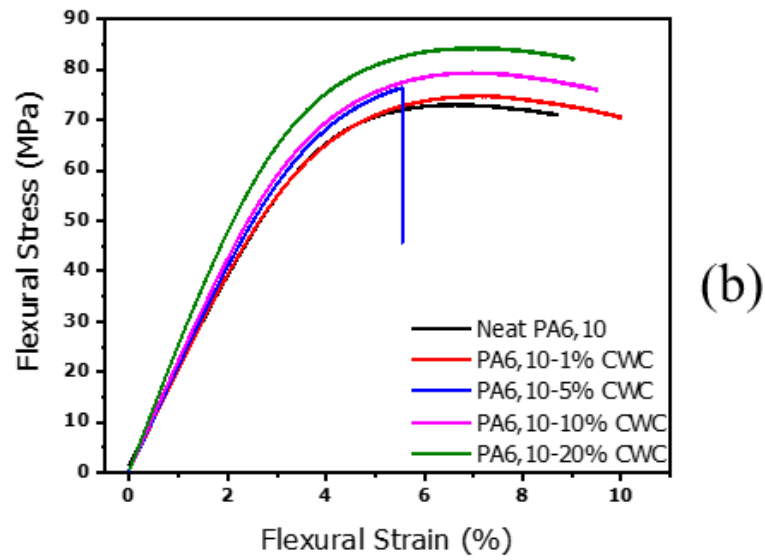
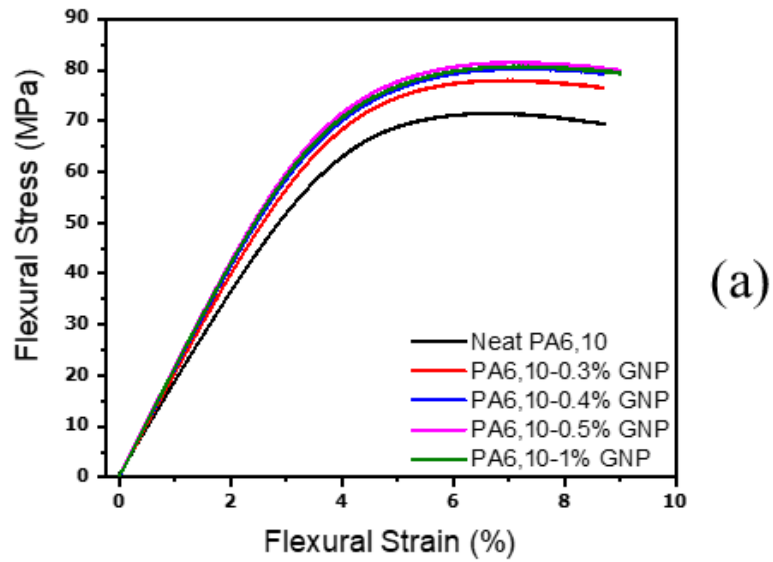


Figure 36. Flexural stress-strain curves of GNP-reinforced (a), CWC-reinforced (b), and CF-reinforced (c) composites

Table 16. Flexural properties of PA6,10-based composites

Sample	Flexural Strength (MPa)	Improvement (%)	Flexural Modulus (MPa)	Improvement (%)	Flexural Strain (%)
Neat PA6,10	72.65±1.5	-	1940±49	-	6.62±0.1
PA6,10-0.3% GNP	78.00±0.4	7.36	2062±75	6.31	6.67±0.7
PA6,10-0.4% GNP	80.32±0.4	10.56	2167±22	11.73	7.18±0.1
PA6,10-0.5% GNP	81.92±2.1	12.77	2210±82	13.92	7.00±0.1
PA6,10-1% GNP	80.55±0.6	10.87	2147±29	10.70	7.20±0.1
PA6,10-1% CWC	75.50±2.4	3.92	1987±79	2.58	7.4±0.2
PA6,10-5% CWC	76.25±1.7	4.89	2032±50	4.64	6.83±0.8
PA6,10-10% CWC	79.72±0.4	9.70	2215±23	14.43	7.1±0.1
PA6,10-20% CWC	84.10±0.5	15.76	2495±33	28.35	6.8±0.1
PA6,10-1% CF	86.95±7.4	19.68	2320±240	19.59	6.77±0.1
PA6,10-5% CF	87.20±0.6	20.03	2390±43	23.20	6.63±0.1
PA6,10-10% CF	87.43±0.3	20.23	2447±9.5	26.16	6.61±0.1
PA6,10-20% CF	90.2±0.6	24.16	2887±55	48.81	6.56±0.1

The lightweighting concept plays a critical role in the automotive industry in overcoming several challenges such as the low range of electric vehicles and reducing the carbon emission of internal combustion engine vehicles by providing more efficient fuel consumption. Fabrication of lightweight sustainable parts that could replace their synthetic commercial counterparts depend on many factors such as mechanical requirements, weight requirements, thermal requirements, and economical requirements. One of the most effective measures to investigate the lightweighting effect of the compounds is the specific mechanical properties such as specific modulus and specific strength. Therefore, commercial synthetic PA6-based compounds reinforced with virgin materials such as glass fibers, glass beads, and/or mineral fillings were compared with PA6,10-based sustainable compounds reinforced with waste-derived materials in terms of lightweighting potential due to both polymers having very similar thermal characteristics and the synthetic one having even better mechanical performance [150–152]. Several commercial synthetic compounds and sustainable compounds in terms of

key lightweighting parameters are summarized in Table 17. For calculating specific tensile properties, tensile property, either obtained from the manufacturer’s website or experimentally tested in this work, is divided by the density value (obtained or measured). The synergistic effect of combining semi-bio-based matrix and waste-driven reinforcements is seen by significant improvements in terms of specific tensile modulus and specific tensile strength. The addition of 20 wt.% CWC to the PA6,10 matrix improved the specific tensile modulus above all the selected commercial synthetic compounds, most notably the compound reinforced with 15 wt.% virgin GF and the compound reinforced with 10 wt.% virgin GF and 30 wt.% mineral filling. Consequently, this investigation confirms that using tailored selection of waste-derived reinforcing material, sustainable compounds can replace several synthetic products in the market in terms of both tensile properties, lightweighting, and environmental impact.

Table 17. Densities and specific properties of commercial PA6-based compounds and fabricated PA6,10-based composites

Sample	Density (ρ, g/cm³)	Specific Tensile Modulus (E/ρ, MPa.cm³/g)	Specific Tensile (Yield) Strength (σ/ρ, MPa.cm³/g)*
Akromid® B28 GM 10/20 LA Black [153]	1.35	2222.22	44.44
Akromid® B3 GF10 1 Black [154]	1.20	2250.00	45.83
Akromid® B28 GFM 10/30 7 Black [155]	1.57	2356.68	28.66
Akromid® B3 GF 15 S3 Black [156]	1.21	2479.33	61.98
Neat PA6,10	1.11	1408.14	37.93
PA6,10-0.5% GNP	1.11	2113.58	52.38
PA6,10-20% CWC	1.16	2522.86	48.07
PA6,10-20% CF	1.18	2415.39	50.02

* Tensile strength and density data (obtained from the manufacturer’s website) were used to calculate specific properties of the commercial compounds and compare with the yield strength data of the fabricated composites due to the fact that fabricated reinforced compounds have the equivalent values for yield and tensile strength.

4.4.4. Thermal and crystallinity characteristics of sustainable PA6,10-based composites

Thermal properties of neat PA6,10 and PA6,10-based composites were investigated using the DSC method, which gives insight into the crystallization and melting behavior of the composites. The first cooling cycle for crystallization behavior and the second heating cycle melting curves of neat PA6,10, PA6,10-0.5 wt.% GNP, PA6,10-20 wt.% CWC, and PA6,10-20 wt.% CF composites have been shown in Figure 37a and Figure 37b, respectively. Thermal parameters of neat PA6,10 and PA6,10-based composites have been summarized in Table 18. Figure 37a displays that the addition of reinforcing materials lead to an early crystallization by creating nucleation sites in the polymer melt. This effect was more pronounced in our previous study where the addition of GNP to the short chain PA6,6 led to an increase in T_c by 30 °C [86]. However, the maximum increase in T_c is observed in CF-based reinforcements by 16 °C while GNP and CWC increased the T_c by around 7 °C which is similar with the previous studies [75, 104]. These results indicates that the dynamics of crystallization depends highly on the combination of aspect ratio and chain length of the polymer where high aspect ratio CF is more effective in initiating nucleation and for short chain length polymers, low aspect ratio addition is even more effective. Figure 37b displays that the second heating DSC traces of neat PA6,10 as well as GNP- and CWC-reinforced composites contain two melting peaks with similar sizes. Similar behavior was also reported for neat PA10,10 and its composites and is attributed as to former peak resulting from the melt of the crystal formed previously, whereas the melting peak appearing at the higher temperature results from the melting of the melt-recrystallized sections [97, 157]. Neat PA6,10 shows a larger peak at 199 °C and a slightly smaller peak at 210 °C, whereas the reinforced composites show a smaller peak at around 202 °C and a larger peak around 215 °C. However, with the addition of high aspect ratio CF to the matrix, this behavior related to recrystallization and its melting is not observed. This can be linked to earlier nucleation with CF leading to the prevention of melt-recrystallization behavior whereas with GNP and CWC reinforcements recrystallization can occur due to crystallization starting at lower temperatures. Moreover, Figure 37b shows that the melting peak temperatures of the neat PA6,10 shifted upwards by 15 °C with the addition of all types of reinforcements. This change indicates that the thermal stability of the composites increased by these additions allowing a higher operation temperature.

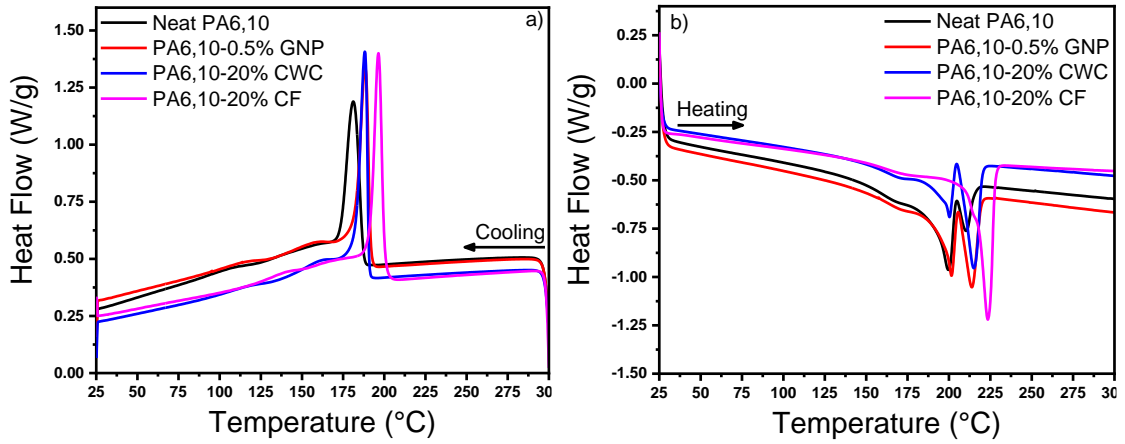


Figure 37. Cooling (a) and second heating (b) DSC traces of neat PA6,10 and PA6,10-based composites

Crystallinity degrees of the samples can be quantitatively analyzed using the melting parameters of the polymer using the equation below [90]:

$$X_C = \left(\frac{\Delta H_M}{\Delta H_M^{100\%}(1 - W_r)} \right) \times 100 \quad (4.1)$$

where X_C is the degree of crystallization, ΔH_M is the melting enthalpy, $\Delta H_M^{100\%}$ is the melting enthalpy of 100% crystalline PA6,10, and W_r is the reinforcement weight fraction. In the literature, several melting enthalpy values for the 100% crystalline PA6,10 is given ranging from 197 J/g to 299 J/g [75, 158–161]. In this study, melting enthalpy of 100% crystalline neat PA6,10 is selected as 200 J/g [158]. Table 18 indicates that with the addition every kind of waste-derived reinforcing materials to the matrix, crystallinity of the samples increase due to presence of these materials initiating nucleation of crystalline phases due to increased surface energy at the reinforcement-melt interface [162, 163]. Herein, the addition of GNP, CWC, and CF led to the increase in crystallinity up to 8%, 13%, and 12%, respectively. It should be noted that increased crystallinity also plays role in the mechanical properties of semi-crystalline polymers such as PAs and supports the improved properties observed in mechanical tests [40].

Table 18. Thermal parameters and crystallinity degrees of neat PA6,10 and reinforced composites

Sample	Melting Peak Temperature (°C)	Melting Integral, ΔH_M (J/g)	Crystallization Peak Temperature (°C)	Crystallization Integral, ΔH_c (J/g)	Crystallinity (%)
Neat PA6,10	199	-35.76	181	36.98	17.88
PA6,10-0.3% GNP	213	-40.35	187	37.23	20.24
PA6,10-0.4% GNP	214	-43.39	188	38.52	21.78
PA6,10-0.5% GNP	213	-44.30	188	37.86	22.26
PA6,10-1% GNP	215	-51.11	188	58.00	25.66
PA6,10-1% CWC	215	-54.60	189	39.29	27.58
PA6,10-5% CWC	216	-57.48	189	36.92	30.25
PA6,10-10% CWC	215	-49.08	188	36.61	27.27
PA6,10-20% CWC	215	-39.33	188	34.55	24.58
PA6,10-1% CF	222	-54.31	196	41.58	27.42
PA6,10-5% CF	223	-56.81	196	58.13	29.90
PA6,10-10% CF	223	-48.84	197	49.26	27.13
PA6,10-20% CF	223	-45.77	197	46.60	28.60

4.4.5. The effect of reinforcement aspect ratio and morphology on the rheological properties of PA6,10-based composites

Rheological behavior of the thermoplastics and reinforced compounds of importance for the melt blending and molding applications. In this regard, the complex viscosity of the thermoplastics is an important parameter to estimate the processability of the produced compounds [47]. The dynamics of polymer processing such as injection molding is an important area to investigate due to the complex behavior of melt polymer and the dispersed reinforcements and forces acting on this system. This behavior can be estimated by frequency sweep method at the melt temperature of the polymer matrix (230 °C). Due to the polymer flow behavior creating a velocity difference between the inner and outer

areas of the mold during the injection molding process, shear stresses arise. These shear stresses can be detrimental to the overall properties of the final product due to breakage of the bonds between the polymer chains. Figure 38a displays the shear stresses of neat PA6,10 and 1 wt.% reinforced composites. Initially, at lower frequencies, shear stresses are low and around the same value for every sample and the rheological behavior remains similar until 100 rad/s where shear stress of CF reinforced deviates from the expected behavior, indicating a processability limit around that angular frequency. Similar behavior is also seen in complex viscosities of the samples in Figure 38b, where the addition of reinforcing materials increased the complex viscosity of the melt by preventing the movement of polymer chains by reinforcing materials [86]. Furthermore, as with neat PA6,10, exhibit shear-thinning behavior as well, which implies that the viscosity decreases as the shear frequency increases. Moreover, there is no presence of a plateau region where the viscosity remains constant regardless of the frequency. This characteristic signifies non-Newtonian behavior, which differs from the Newtonian behavior observed in other polyamides like PA6, PA11, and PA12 [164–167].

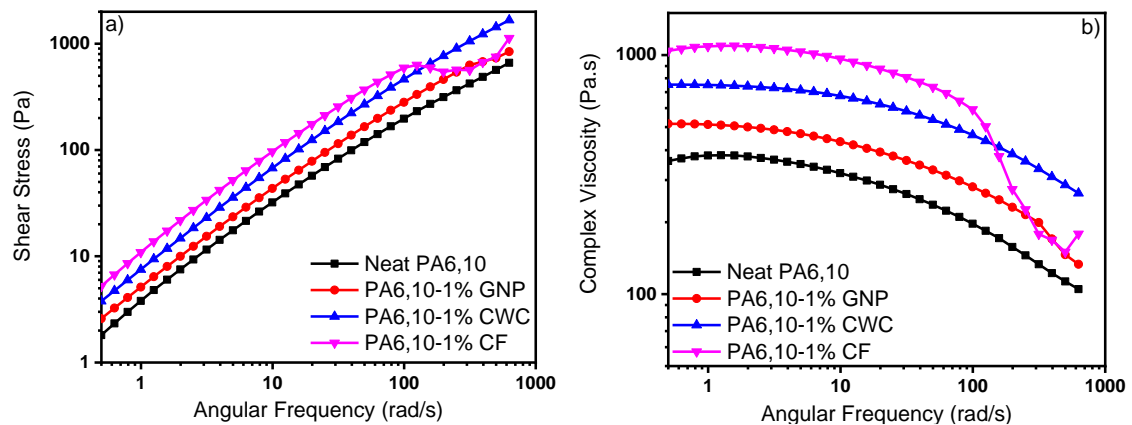


Figure 38. Changes in shear stresses (a) and complex viscosity (b) with the addition of 1 wt.% waste-derived reinforcements as a function of angular frequency

Figure 39a and Figure 39b display the storage and loss moduli of the neat polymer and 1 wt.% reinforced composites, respectively. The storage modulus demonstrates the elastic portion of the viscoelastic behavior which indicates the energy stored before permanent deformation, while the loss modulus corresponds to the viscous portion and indicates the energy dissipated (lost) as heat. Incorporating waste-derived reinforcements into the matrix led to a general increase in complex viscosity, storage modulus, and loss modulus. This indicates the creation of a significant filler network that hinders the mobility of polymer chains [75]. Similarly, CF reinforced composite displays a significant decrease

in storage modulus, while the decrease in loss modulus is not so pronounced. This can be attributed to stronger carbon fibers breaking the bonds between polymer chains and removing their ability to store energy [113]. Furthermore, behaviors of GNP and CWC reinforced composites can be explained by the exfoliation of GNP and separation of CWC spheres aiding to the slip of polymer chains in the event of hard phase-soft phase encounter.

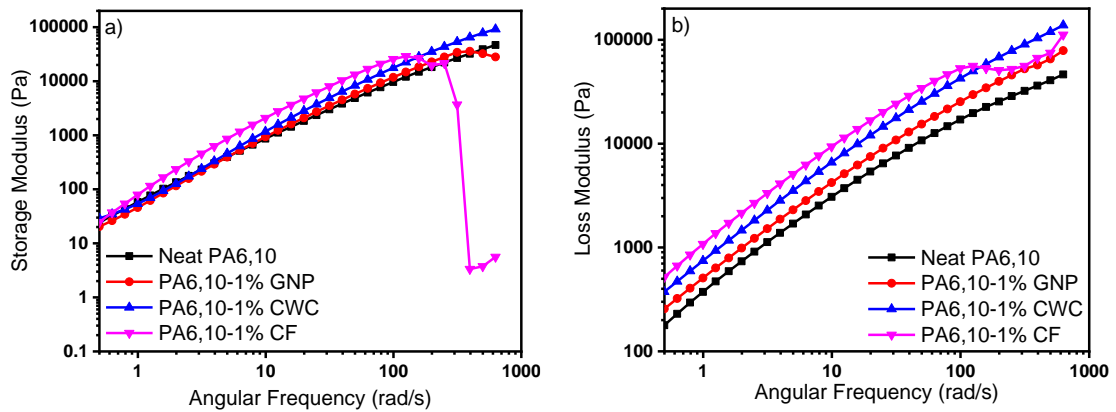


Figure 39. Changes in storage moduli (a) and loss moduli (b) with the addition of 1 wt.% waste-derived reinforcements as a function of angular frequency

In addition to rheological properties, the effect of aspect ratio and morphology of the waste-derived reinforcing materials on crystallinity and lightweighting potential in terms of specific flexural and tensile properties is summarized in Figure 40 where the improvement percentages compared to neat PA6,10 are presented in the spider chart at 1 wt.% loadings. Herein, specific flexural properties are improved significantly when high aspect ratio CF reinforcement is used, whereas platelet structure of GNP became more efficient in improving specific tensile properties. Moreover, spherical CWC displayed highest crystallinity together with CF. Overall, this window of improvement creates a guideline for reinforcement selection with regards to requirements demanded from the compound. Considering the cost of virgin GF (1-32 \$/kg), waste CF (5 \$/kg) becomes a strong contender in the market in terms of both economic and environmental aspects [168, 169].

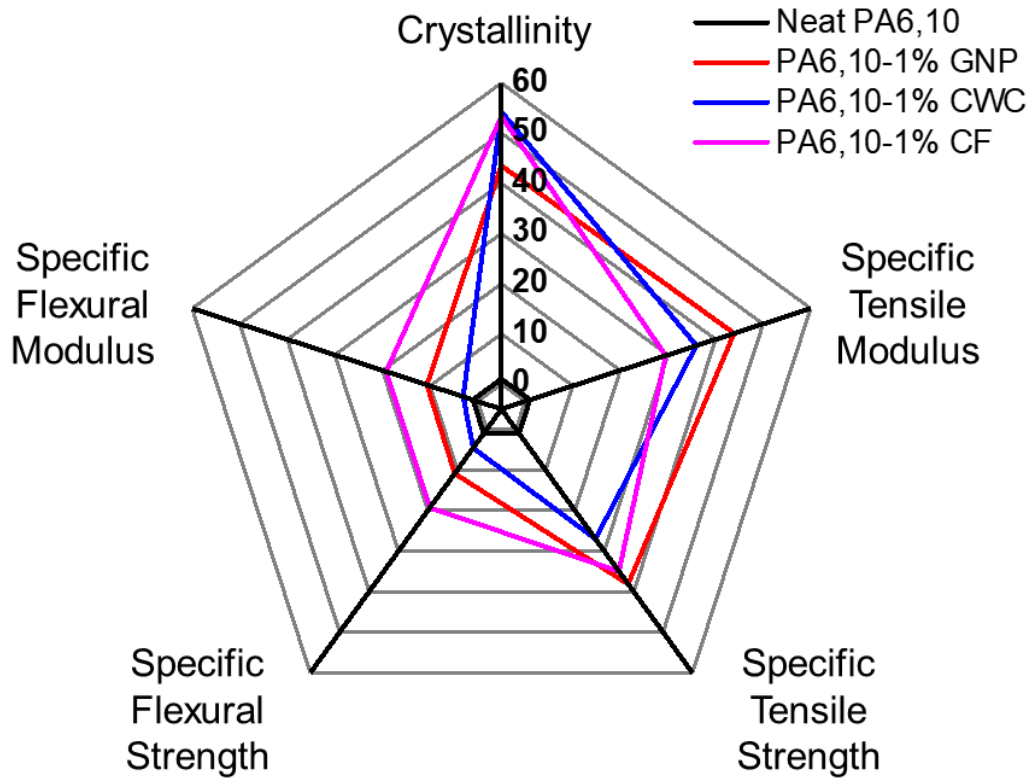


Figure 40. The window of improvement in crystallinity and lightweighting potential of sustainable compounds

4.4.6. Morphological analysis of waste-derived reinforcements and cross-sectional analysis of PA6,10-based sustainable composites

The morphology and the size of the reinforcing materials for composites is critical in terms of load transfer, interfacial interactions, and overall reinforcement efficiency. Therefore, scanning electron microscopy (SEM) analysis is carried out to investigate the morphological parameters of waste-derived reinforcing materials. Moreover, fracture surface analysis of the tensile test specimens provides an important insight on the distribution of reinforcing materials in the composite, strengthening mechanism, and failure mode [91, 92]. SEM images of the GNP, CWC, and CF are provided in Figure 41a, Figure 41c, and Figure 41e, respectively, while the tensile fracture surfaces of the corresponding composites with 0.5 wt.% GNP, 20 wt.% CWC, and 20 wt.% CF are provided in Figure 41b, Figure 41d (with magnified inset image, scale bar is 200 nm) and Figure 41f, respectively. Figure 41 indicates that the platelet structure of GNP, spherical morphology of CWC, and waste carbon fibers have led to different strengthening and fracture mechanisms in the composite structure. Previously, Wang *et al.* provided a multiscale atomistic simulation approach for SiC/Graphene composites where graphene displays a crack bridging mechanism for toughening effect under tensile loads [170].

Herein, Figure 41b clearly shows that bridging is indeed a strengthening mechanism in PA6,10-GNP composites. Furthermore, due to low concentration of GNP in the structure, matrix failure is the dominant failure mode. On the other hand, CWC and CF show a fine distribution in the composite as seen in Figure 41d, and Figure 41f, respectively. The inset image in Figure 41d indicates that spherical morphology is maintained, and polymer melt crystallized around the individual spheres, which later on fractured during the test. Additionally, protrusions of the matrix phase, which is evident for both cases, is an indication of ductile behavior of the polymer. Similar cases were observed for PA6,10-based composites [102, 103]. Moreover, reinforcements are nested in the polymer matrix indicating strong interfacial interactions which are confirmed by the mechanical test results.

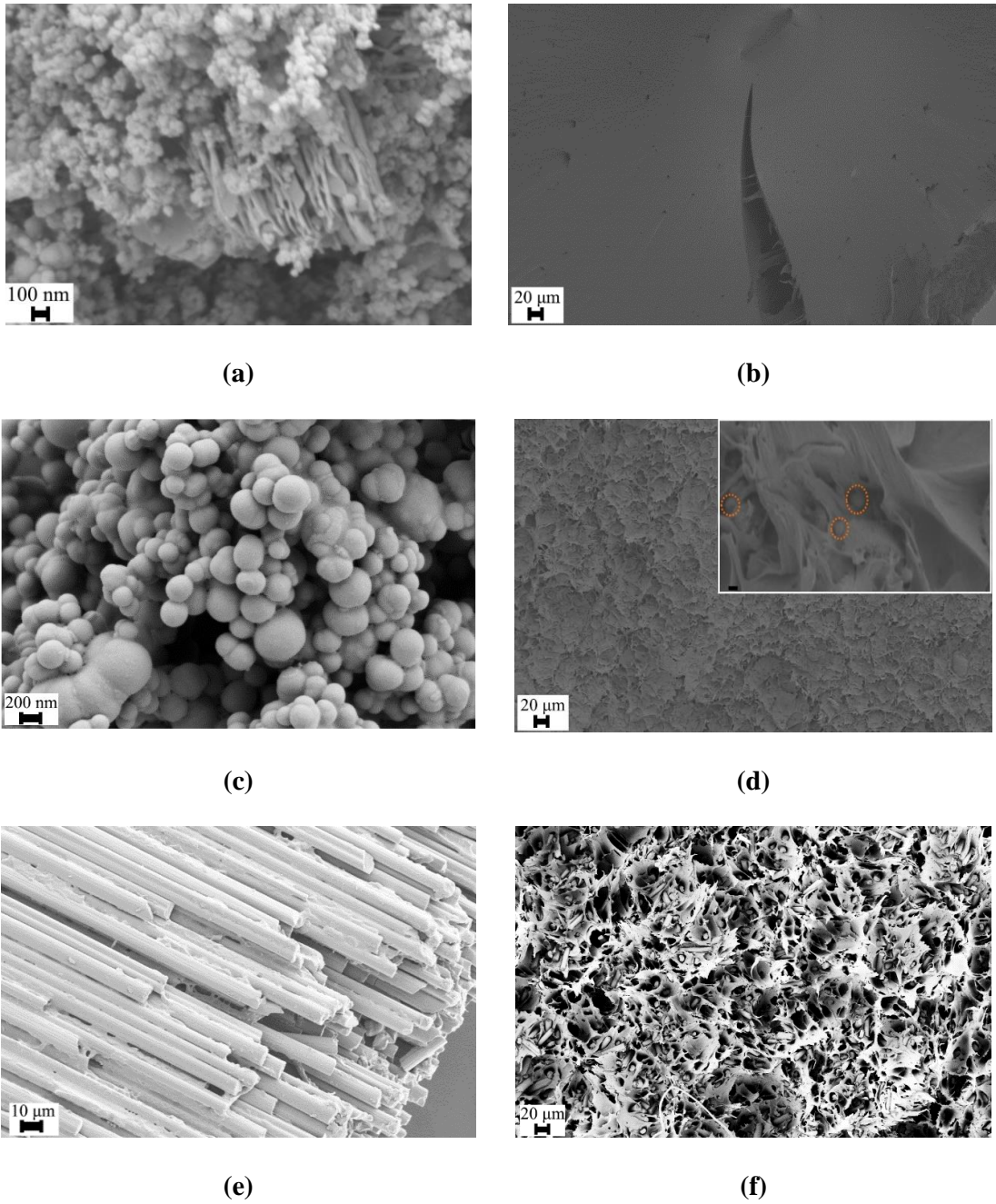


Figure 41. SEM images of GNP (a), 0.5 wt.% GNP-PA6,10 (b), CWC (c), 20 wt.% CWC-PA6,10 (d), CF (e), 20 wt.% CF-PA6,10 (f)

4.5. Conclusions

Environmental concerns and production costs drive the automotive industry towards sustainable approaches such as semi-bio-based polymers and waste-derived reinforcing materials. However, a gap exists in the literature regarding the incorporation of multiscale reinforcements with diverse morphologies and understanding the interface connection with aspect ratios into PA6,10 to enhance performance. This study successfully

incorporated waste-derived reinforcing materials such as waste tire-driven GNP, carbonized waste coffee, and waste carbon fiber with varying size, morphology, and aspect ratios into the PA6,10 matrix, resulting in significant improvements in mechanical properties. In terms of performance outcomes while maintaining the same loading ratios, a substantial improvement in specific flexural properties is observed when employing high aspect ratio CF reinforcement. In contrast, the platelet structure of GNP proves more effective in enhancing specific tensile properties. Furthermore, CWC's spherical graphene exhibits the highest crystallinity, on par with CF. Moreover, maximum improvements in yield strength and tensile modulus were observed with 20 wt.% CF by 40% and 20 wt.% CWC by 87%, respectively, while flexural strength and modulus improved by 24% and 48%, respectively, with the addition of 20 wt.% CF. In addition, a benchmark investigation is carried out for the lightweighting potential in terms of specific strength and specific modulus of the fabricated sustainable compounds against selected commercial automotive grade synthetic compounds. Evidently, sustainable compounds developed in this work performed better against commercial products in terms of lightweighting potential. Moreover, thermal properties indicated that nucleation and crystal growth is triggered by the waste-derived materials and nucleation behavior is dependent on the size and aspect ratio of these reinforcing materials. In addition, fracture surface analysis provided insight into strengthening mechanisms and failure characteristics of the composites.

Consequently, this study presents a sustainable method for utilizing multiscale waste-derived reinforcements by establishing correlations between carbon-based materials' aspect ratio, morphology, and size. This research enables the incorporation of recycled additives into compound formulations, supporting sustainability initiatives and offering lightweight, circular economy-driven solutions. This approach holds particular significance in applications such as automotive, sports and leisure, and the plastics industry, where synthetic PAs reinforced with virgin materials can be replaced.

Future investigations can build upon this study by further exploring characterization techniques that assess flow behavior and impact properties, as well as optimizing composite performance through suitable strategies. It will also be crucial to examine the long-term durability and environmental impact of these composites. Embracing these research avenues will pave the way for the successful integration of waste-derived

reinforcing materials in compound formulations, ultimately promoting sustainability in the industry.

CHAPTER 5: General Conclusion

The pioneering outcome of this research includes significantly superior composites based on synthetic PA6,6 towards semi-synthetic PA6,10 as matrix, reinforced with waste-derived reinforcing materials by highlighting the sustainable aspects and lightweighting philosophy. The transformation from synthetic to semi-synthetic matrix provides much desired sustainability in the automotive industry, together with the use of waste tire, waste coffee, and waste carbon fiber a tailorability to properties of final composite is introduced by utilizing the effect of various aspect ratios and sizes of the reinforcing materials. Furthermore, a benchmarking study in terms of lightweight potential proves that these novel sustainable composites can already outperform their synthetic counterparts reinforced with virgin materials such as glass fibers, glass beads, and mineral fillings. Key materials and findings of this thesis are summarized in Figure 42.

Integration of Waste-based Reinforcing Materials into PA-based Matrices

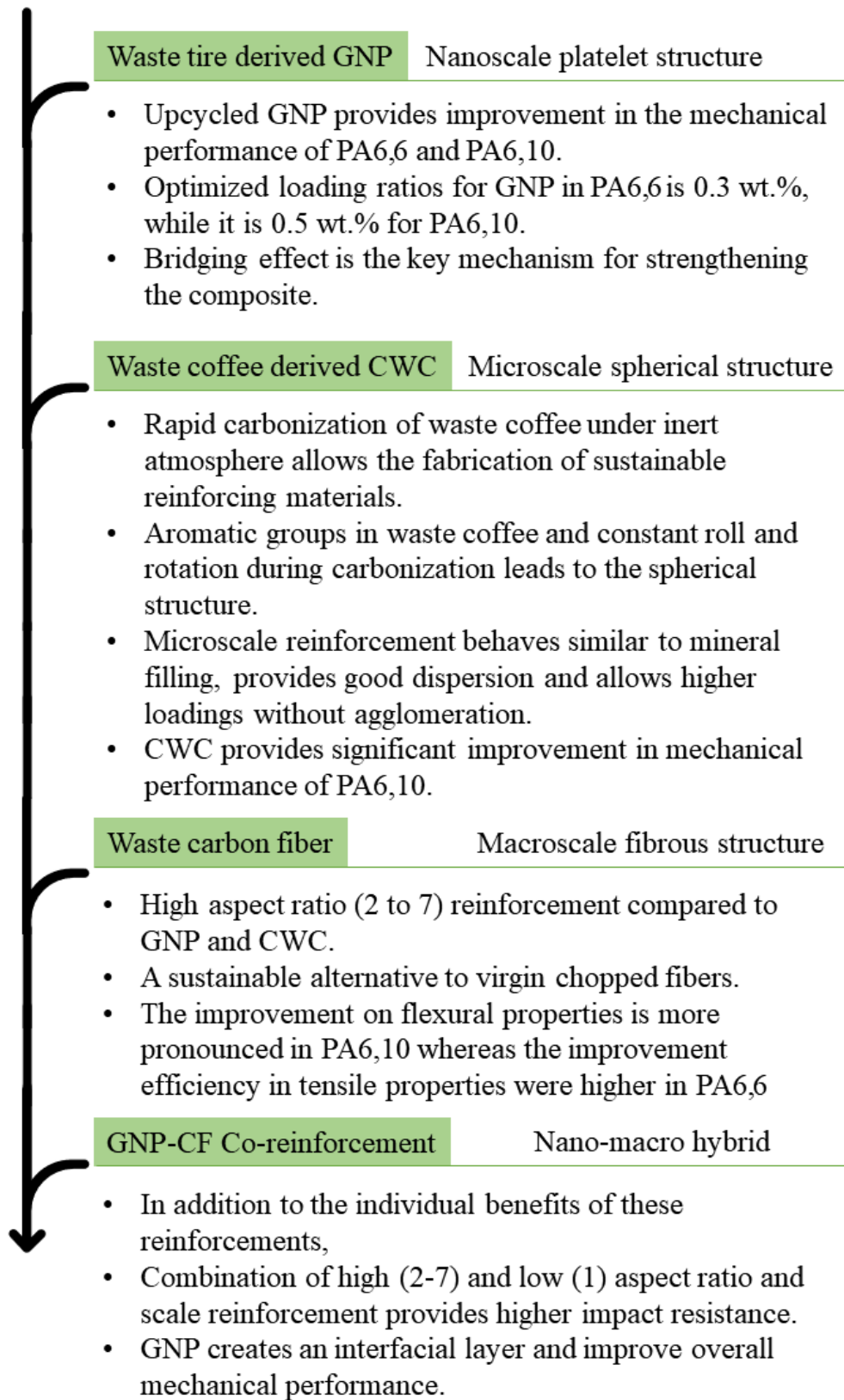


Figure 42. Key materials and findings of this thesis

In the first chapter, an optimal loading ratio for PA6,6/GNP nanocomposites is determined through extensive characterization methods and noteworthy performance

improvement in mechanical properties is obtained. Graphene, despite its exceptional qualities, encounters challenges when incorporated into polymer matrices. These challenges involve uneven dispersion in the polymer matrix and a lack of surface functional groups to effectively enhance the reinforcement/matrix interface. Despite numerous studies on graphene/PA composites, these primary obstacles persist. In this study, graphene nanoplatelets (GNP) containing surface oxygen functional groups efficiently dispersed and intercalated in PA6,6 during the melt phase. The homogeneous intercalation of GNP in the PA6,6 matrix is confirmed through mechanical, crystalline, and rheological characterizations. It's crucial to recognize that even slight modifications in the nanocomposite formulation at these low loading amounts can lead to undesired outcomes, making quality control challenging, particularly concerning thermal and X-ray diffraction. In summary, this extensive interdisciplinary investigation establishes waste tire-derived graphene as a promising reinforcement material. At lower loadings, substantial improvements in mechanical properties are achieved. Tensile strength and modulus of PA6,6 nanocomposites were improved at 30% and 42%, respectively, by the addition of 0.3 wt.% GNP. Flexural strength and modulus were reached at 20% and 43%, respectively. This paves the way for scalable technologies that introduce graphene into polymer matrices through conventional compounding techniques like extrusion and injection processes, facilitated by waste tire derived graphene. Additionally, the conversion of waste materials into value-added substances addresses circular economy concerns and reduces graphene costs by utilizing waste tires as a starting material through recycling and upcycling technologies for mass production in the plastic industry.

In the second chapter, by using previously optimized GNP/PA6,6 nanocomposite, co-reinforcement with high aspect ratio waste carbon fiber (CF) is developed. Furthermore, the effect of CF at high loading ratios as well as hybrid reinforcement are investigated through extensive characterization methods such as mechanical tests, thermal and crystallinity analysis, rheological survey, and cross-sectional analysis which demonstrated significantly higher mechanical performance, indicating potential for load-bearing structural applications for the novel compound. In detail, this study successfully integrated recycled carbon fibers and GNP into the PA6,6 matrix, resulting in substantial enhancements in mechanical properties. The combined effect of incorporating 20 wt.% recycled carbon fibers and 0.3 wt.% GNP led to an 86.6% increase in flexural modulus and a 35.4% increase in strength compared to the neat polymer. Tensile strength and

modulus values also saw improvements of 43.3% and 94.8%, respectively. Additionally, the inclusion of 0.3% GNP boosted Charpy notched impact energy by 7.7% compared to the composite with 20% recycled carbon fiber. This work opens avenues for integrating recycled additives into compound formulations, supporting sustainability approaches, and improving the injection molding process by providing lightweight, circular economy-based solutions, especially in applications such as automotive, sports and leisure, and the plastics sector. Future research can build upon this foundation by delving deeper into characterization techniques and optimization strategies for composite performance. Investigating the long-term durability and environmental impact of these composites is crucial. Moreover, scaling up the experimental data will contribute to the practical implementation of these materials. Embracing these future directions establishes a groundwork for incorporating recycled additives into compound formulations and promoting sustainability across diverse applications.

In the third chapter, by switching to semi-bio-based PA6,10 and using waste-derived reinforcing materials such as GNP, carbonized waste coffee (CWC), and CF, the sustainability aspect of these compounds was promoted. Furthermore, novel reinforcing material from waste coffee was synthesized and characteristics of this material and the sustainable composites were investigated in detail in terms of structural, morphological, elemental properties, and mechanical, thermal, rheological properties, respectively. In addition, market-readiness of these sustainable composites in terms of lightweighting potential is analyzed by benchmarking with synthetic PA6-based compounds reinforced with virgin materials. Environmental considerations and cost factors are propelling the automotive industry towards sustainable practices, including the use of semi-bio-based polymers and reinforcing materials derived from waste. However, a gap exists in the current literature regarding the integration of multiscale reinforcements with diverse morphologies and understanding their interface connection, particularly with aspect ratios, into PA6,10 to enhance performance. This study successfully introduced waste-derived reinforcing materials, such as GNP, CWC, and CF with varying sizes, morphologies, and aspect ratios into the PA6,10 matrix, resulting in significant improvements in mechanical properties. In terms of performance outcomes, a considerable enhancement in specific flexural properties is noted when utilizing high aspect ratio CF reinforcement, while the platelet structure of GNP proves more effective in enhancing specific tensile properties. Furthermore, CWC's spherical graphene exhibits

the highest crystallinity, comparable to CF. The study also observes maximum improvements in yield strength and tensile modulus with 20 wt.% CF by 40% and 20 wt.% CWC by 87%, respectively, while flexural strength and modulus improve by 24% and 48%, respectively, with the addition of 20 wt.% CF. Additionally, a benchmark investigation is conducted to assess the lightweighting potential of the sustainable compounds in terms of specific strength and specific modulus against selected commercial automotive-grade synthetic compounds. The sustainable compounds developed in this study outperform commercial products in terms of lightweighting potential. Thermal properties indicate that waste-derived materials trigger nucleation and crystal growth, with nucleation behavior dependent on the size and aspect ratio of these reinforcing materials. Fracture surface analysis provides insight into the strengthening mechanisms and failure characteristics of the composites. Figure 43 displays the compound formulations and major achievements within the scope of the thesis.

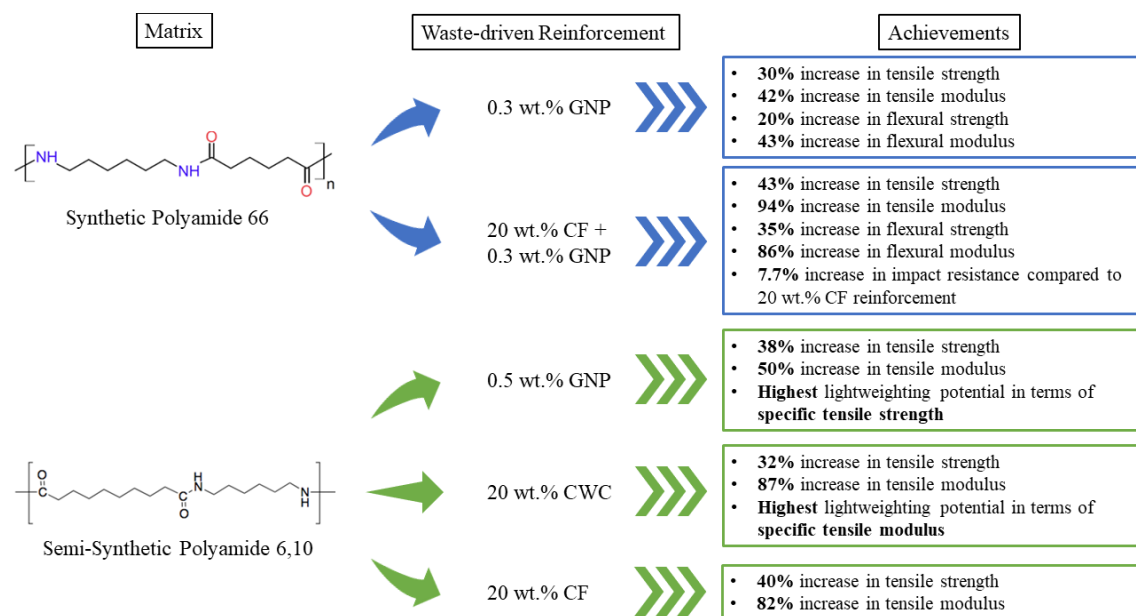


Figure 43. Compound formulations and major achievements within the scope of the thesis

In particular, within this study waste tire-derived graphene nanoplatelets (GNPs) were dispersed in the PA6,6 matrix using a thermokinetic mixer during the melt phase. This was achieved by controlling GNP ratios and reducing loading ratios to as low as 0.3 wt.%. The comprehensive characterization included monitoring the impact of GNP on the mechanical, thermal, crystallinity and rheological properties of PA6,6-based nanocomposites. Throughout this study, extensive characterization of PA6,6 and its GNP-based nanocomposites provided a significant advantage for understanding the interfacial

interaction between polymer chains and nano/hybrid additives during extrusion and injection processes.

Furthermore, in the present study, the adoption of recycled carbon fibers and waste tire-derived graphene nanoplatelets (GNP) was preferred for economic and environmental reasons, in contrast to the expensive and energy-intensive production methods associated with virgin fiber reinforcement. Recycled and upcycled reinforcements were combined in the PA6,6 matrix through melt compounding in a thermokinetic shear mixer, with controlled weight ratios of GNP and recycled carbon fiber. The interactions among GNPs, recycled carbon fibers, and PA6,6 polymer chains during melt compounding and injection molding were examined through extensive characterization. In addition, the influence of the fillers' aspect ratio on the mechanical properties and the polymer/fiber interface was comparatively studied, considering both high aspect ratio fibers and mixed aspect ratio GNP/recycled carbon fiber reinforcement. The focus was on understanding their effects on the crystallinity, mechanical, thermal, and viscoelastic properties of PA6,6-based composites. Additionally, the use of waste tire-derived GNPs and recycled carbon fibers could offer more environmentally friendly solutions for the composite industry, supported by efficient processing design tools.

Later on, the preference was given to the incorporation of waste-derived reinforcing materials, including graphene nanoplatelets (GNP) derived from waste tires, carbonized waste coffee (CWC), and waste carbon fibers (CF), in conjunction with a semi-bio-based PA6,10 matrix. This choice was motivated by the economic and environmental benefits associated with these waste-derived materials, as opposed to utilizing a synthetic PA matrix with virgin reinforcements, which is costly and involves energy-intensive production methods. Consequently, recycled and upcycled reinforcements were melt-blended with the PA6,10 matrix, maintaining controlled ratios of GNP, CWC, and CF, employing a thermokinetic shear mixer. This study delves into the interactions at the interfaces of waste-derived reinforcements and the PA6,10 matrix, exploring the influence of the reinforcing materials' aspect ratio, size, and morphology on mechanical and thermal properties in a comparative manner. The investigation encompasses mechanical and thermal properties, along with the study of interfacial interactions. Subsequently, a benchmarking study is conducted to assess the lightweighting potential of the developed sustainable compounds against selected commercial synthetic compounds of automotive grade, considering specific strength and specific modulus. The

findings suggest that the sustainable compounds produced have the potential to replace several products in the automotive industry market. This not only supports sustainability initiatives but also provides lightweight, circular economy-driven solutions.

To provide a holistic approach, a comparative life cycle assessment (LCA) analysis is carried out for polymers, reinforcements, and compounds in order to evaluate the ecological impact of the developed sustainable reinforcements, switching to a semi-synthetic matrix, and novel sustainable compounds using global warming potential (GWP) as an index, and provided in Figure 44. Data for the PA6, and PA6,6 is obtained from the Ecoinvent database in SimaPro LCA analysis program. Data for PA6,10 and waste CF is obtained from sources in the literature [51, 171–173]. GWP of GNP, CWC, virgin GF (E-glass), and compounds were calculated using a combination of data from the Ecoinvent database and literature [174, 175]. As expected, GWP of semi-synthetic PA6,10 is significantly less compared to synthetic PAs. Additionally, waste-derived reinforcements offer up to 49% reduced GWP compared to virgin GF which complements the performance aspects by providing sustainability index of only the material selection. Furthermore, when compounded, semi-synthetic PA6,10 and waste-derived reinforcing materials offer up to 55% reduction in GWP, in addition to the mechanical properties and lightweighting potential, compared to the selected commercial PA6-based compounds in the market. Consequently, this study introduces a sustainable approach to incorporate multiscale waste-derived reinforcements by establishing correlations between carbon-based materials' aspect ratio, morphology, and size. This research facilitates the integration of recycled additives into compound formulations, supporting sustainability initiatives and providing lightweight, circular economy-driven solutions. Particularly valuable in applications like automotive, sports and leisure, and the plastics industry, this approach offers the potential to replace synthetic PAs reinforced with virgin materials.

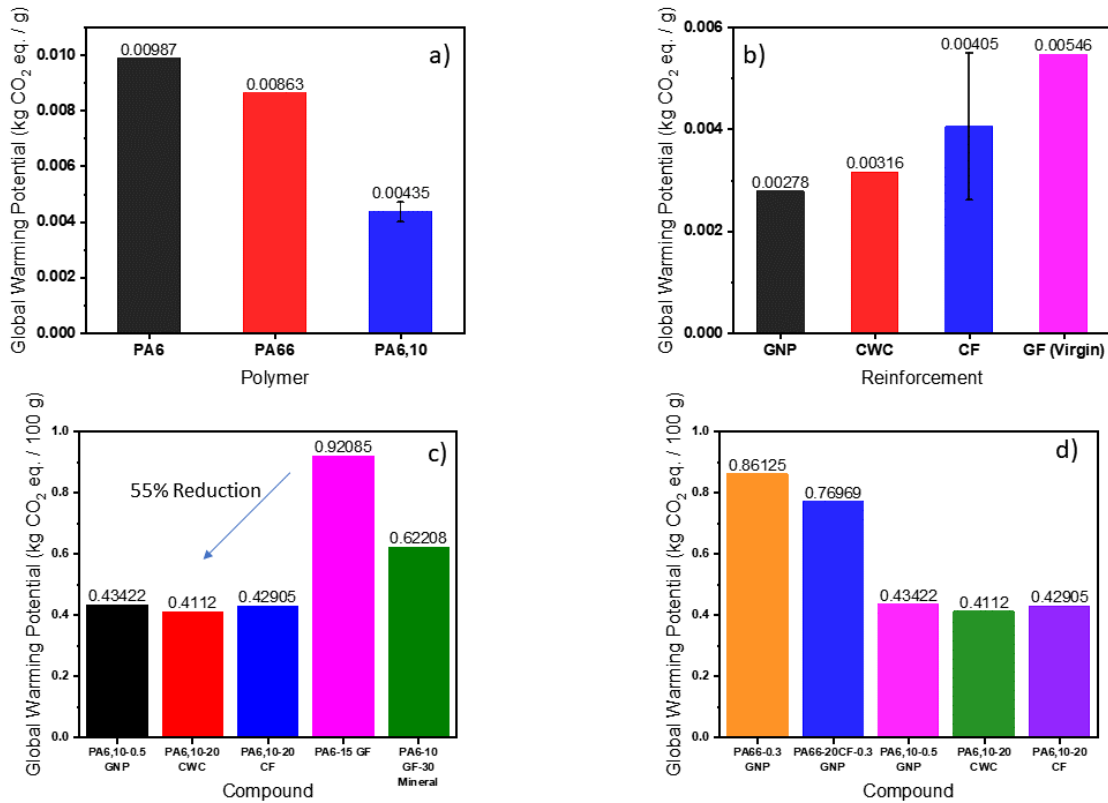


Figure 44. Global warming potential of matrix materials (a), reinforcing materials (b), comparative analysis of developed PA6,10-based compounds and commercial PA6-based compounds (c), and developed PA6,6-based and PA6,10-based compounds (d)

The comparison of fabricated sustainable compounds in terms of tensile properties against the state of the art presented in Figure 45, which indicates that although there are edge cases both in terms of yield strength and tensile modulus, through tailored selection of reinforcing material and also promoting sustainability, these novel compounds are placed among the better half in terms of tensile performance. In this context, state of the art compounds include cellulose nanofibers [97], natural halloysite nanotubes [99], commercial graphene nanoplatelets [75], rice husk ash and nanoclay [106], MWCNT [102], small cellulose microcrystals, large cellulose microcrystals and cellulose nanocrystals [103], functionalized MWCNT [176], and biocarbon obtained from pyrolyzed *mischantus* fibers [105] reinforcements, where among all, only a handful utilize natural sources.

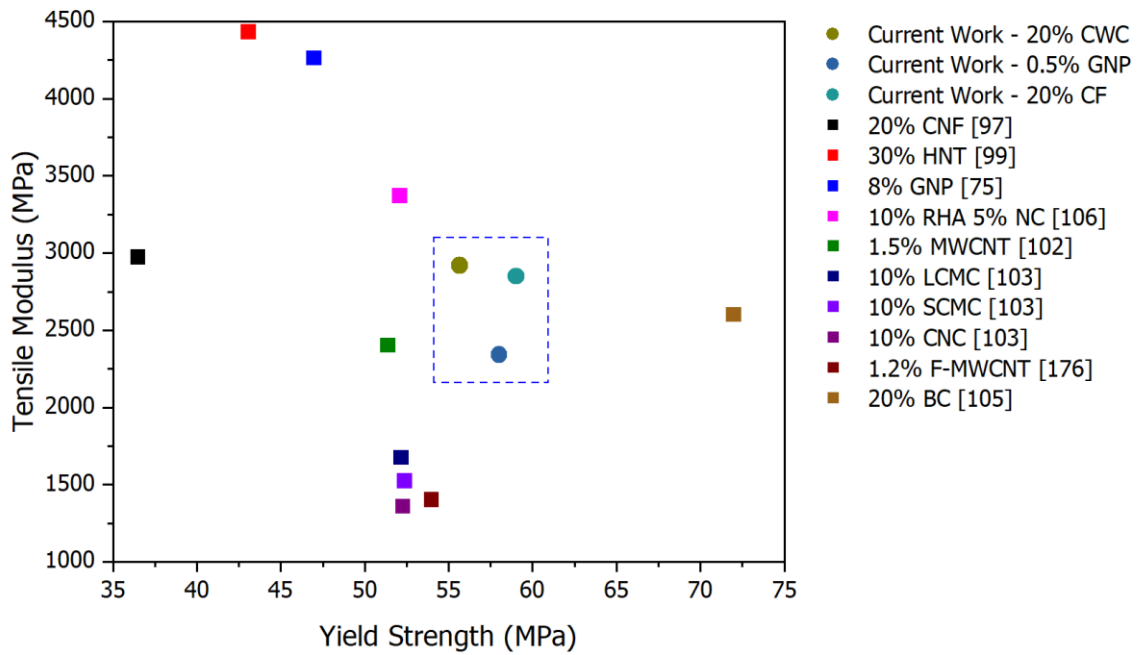


Figure 45. Comparison of sustainable compounds against state of the art

In conclusion, this thesis provides significant contributions to the current research through extensive analysis of the dispersion behavior of waste-based reinforcements, the effect of reinforcement scale and aspect ratio, interfacial interactions, damage mechanisms, mechanical performance, thermal properties, and rheological behavior of PA6,6 and PA6,10-based composites. Furthermore, detailed elemental, structural, chemical, and morphological characterization of carbonized waste coffee was carried out to evaluate the performance of this waste-based material as a composite reinforcement.

Future investigations can expand on this study by exploring characterization techniques for flow behavior and impact properties, optimizing composite performance, and examining the long-term durability of these composites. In addition, the effect of integrating higher aspect ratio reinforcements with different structures and surface areas such as single-walled or multi-walled CNTs on thermal and mechanical properties can provide unusual properties to the composites can be investigated in detail. As the interfacial interactions between the reinforcing material and the polymer matrix is dominated by surface chemistry (functional groups, porosity, size, and surface area) and crystal structure of the reinforcement, a detailed survey with regards to these aspects of waste-derived reinforcements is also necessary to establish a basis on composite development for future studies. Embracing these research avenues will contribute to the successful integration of waste-derived reinforcing materials in compound formulations, ultimately advancing sustainability in the industry.

REFERENCES

- [1] Navik, R.; Tan, H.; Zhang, H.; Liu, Z.; Xiang, Q.; Shi, L.; Lu, S.; Zhao, Y. (2023). Scalable production of polyamide-6/graphene composites with enhanced electromagnetic shielding and thermal conductivity, *Chemical Engineering Journal*, Vol. 471, No. November 2022, 144445. doi:10.1016/j.cej.2023.144445
- [2] Tripathy, S.; Singh, B. P.; de Oliveira, S. M.; Kuznetsov, A.; de Araujo, J. R.; Gnaniyah, S.; Dhakate, S. R. (2023). Mechanical and thermal properties of polyamide-6 nanocomposites reinforced by graphene oxide with low loading by double extrusion method, *Polymers for Advanced Technologies*, Vol. 34, No. 8, 2788–2798. doi:10.1002/pat.6102
- [3] Liao, H.; Yu, T.; Li, Y. (2023). Rheological properties of graphene oxide/polyamide 6 composites, *Polymer Composites*, No. August, 1–10. doi:10.1002/pc.27729
- [4] Liu, M.; Lin, K.; Yao, X.; Vallés, C.; Bissett, M. A.; Young, R. J.; Kinloch, I. A. (2023). Mechanics of reinforcement in a hybrid graphene and continuous glass fibre reinforced thermoplastic, *Composites Science and Technology*, Vol. 237, No. November 2022. doi:10.1016/j.compscitech.2023.110001
- [5] Mulqueen, D. W.; Sattar, S.; Kravchenko, O. G. (2023). Mechanical and thermal properties of carbon fiber epoxy composite with interlaminar graphene at elevated temperature, *Composites Part B: Engineering*, Vol. 255, 110609. doi:10.1016/j.compositesb.2023.110609
- [6] Damacena, L. H. C.; Ferreira, E. H. C.; Ribeiro, H.; Fachine, G. J. M.; Souza, A. M. C. (2023). High-performance hierarchical composites based on polyamide 6, carbon fiber and graphene oxide, *Polymer Composites*, Vol. 44, No. 6, 3387–3400. doi:10.1002/pc.27328
- [7] Pietroluongo, M.; Padovano, E.; Frache, A.; Badini, C. (2020). Mechanical recycling of an end-of-life automotive composite component, *Sustainable Materials and Technologies*, Vol. 23, e00143. doi:10.1016/j.susmat.2019.e00143

- [8] Mark, J. E. (1998). *Polymer Data Handbook*, (J. E. Mark, Ed.) (1st ed.), Springer Oxford, New York
- [9] Li, Q.; Li, B.; Zhang, S.; Lin, M. (2012). Investigation on effects of aluminum and magnesium hypophosphites on flame retardancy and thermal degradation of polyamide 6, *Journal of Applied Polymer Science*, Vol. 125, No. 3, 1782–1789. doi:10.1002/app.35678
- [10] Alexandrescu, L.; Sönmez, M.; Georgescu, M.; Nițuică, M.; Fikai, A.; Trusca, R.; Gurău, D.; Tudoroiu, L. (2017). Polyamide/Polypropylene/graphene oxide nanocomposites with functional compatibilizers: Morpho-structural and physico-mechanical characterization, *Procedia Structural Integrity*, Vol. 5, 675–682. doi:10.1016/j.prostr.2017.07.042
- [11] Soulestin, J.; Rashmi, B. J.; Bourbigot, S.; Lacrampe, M. F.; Krawczak, P. (2012). Mechanical and optical properties of polyamide 6/clay nanocomposite cast films: Influence of the degree of exfoliation, *Macromolecular Materials and Engineering*, Vol. 297, No. 5, 444–454. doi:10.1002/mame.201100202
- [12] Xu, Q.; Chen, F.; Li, X.; Zhang, Z. (2013). The effect of surface functional groups of nanosilica on the properties of polyamide 6/SiO₂ nanocomposite, *Polish Journal of Chemical Technology*, Vol. 15, No. 3, 20–24. doi:10.2478/pjct-2013-0039
- [13] Hu, J.; Zhang, H. Bin; Hong, S.; Jiang, Z. G.; Gui, C.; Li, X.; Yu, Z. Z. (2014). Simultaneous improvement in both electrical conductivity and toughness of polyamide 6 nanocomposites filled with elastomer and carbon black particles, *Industrial and Engineering Chemistry Research*, Vol. 53, No. 6, 2270–2276. doi:10.1021/ie4035785
- [14] Li, L.; Li, C. Y.; Ni, C.; Rong, L.; Hsiao, B. (2007). Structure and crystallization behavior of Nylon 66/multi-walled carbon nanotube nanocomposites at low carbon nanotube contents, *Polymer*, Vol. 48, No. 12, 3452–3460. doi:10.1016/j.polymer.2007.04.030
- [15] Fukushima, H.; Drzal, L. T.; Rook, B. P.; Rich, M. J. (2006). Thermal conductivity of exfoliated graphite nanocomposites, *Journal of Thermal Analysis and Calorimetry*, Vol. 85, No. 1, 235–238. doi:10.1007/s10973-005-7344-x

- [16] Chen, Z.; Li, T.; Liu, X.; Lü, R. (2005). Friction and wear mechanisms of polyamide 66/high density polyethylene blends, *Journal of Polymer Science, Part B: Polymer Physics*, Vol. 43, No. 18, 2514–2523. doi:10.1002/polb.20548
- [17] Chen, Z.; Li, T.; Yang, Y.; Liu, X.; Lv, R. (2004). Mechanical and tribological properties of PA/PPS blends, *Wear*, Vol. 257, Nos. 7–8, 696–707. doi:10.1016/j.wear.2004.03.013
- [18] Masood, M. T.; Papadopoulou, E. L.; Heredia-Guerrero, J. A.; Bayer, I. S.; Athanassiou, A.; Ceseracciu, L. (2017). Graphene and polytetrafluoroethylene synergistically improve the tribological properties and adhesion of nylon 66 coatings, *Carbon*, Vol. 123, 26–33. doi:10.1016/j.carbon.2017.07.026
- [19] Fu, X.; Dong, X.; Liu, Y.; Zhao, X.; Zhang, N.; Qi, S.; Wang, D.; Yang, G. (2019). Combined graphene and poly (butylene terephthalate)-block-poly (tetramethylene glycol) enhance the mechanical performance of polyamide-6, *European Polymer Journal*, Vol. 110, No. November 2018, 97–106. doi:10.1016/j.eurpolymj.2018.11.013
- [20] Li, X.; Shao, L.; Song, N.; Shi, L.; Ding, P. (2016). Enhanced thermal-conductive and anti-dripping properties of polyamide composites by 3D graphene structures at low filler content, *Composites Part A: Applied Science and Manufacturing*, Vol. 88, 305–314. doi:10.1016/j.compositesa.2016.06.007
- [21] Duan, X.; Yu, B.; Yang, T.; Wu, Y.; Yu, H.; Huang, T. (2018). In situ polymerization of nylon 66/reduced graphene oxide nanocomposites, *Journal of Nanomaterials*, Vol. 2018. doi:10.1155/2018/1047985
- [22] Sarno, M.; Baldino, L.; Scudieri, C.; Cardea, S.; Ciambelli, P.; Reverchon, E. (2017). SC-CO₂-assisted process for a high energy density aerogel supercapacitor: The effect of GO loading, *Nanotechnology*, Vol. 28, No. 20. doi:10.1088/1361-6528/aa67d9
- [23] Marcano, D. C.; Kosynkin, D. V.; Berlin, J. M.; Sinitskii, A.; Sun, Z.; Slesarev, A.; Alemany, L. B.; Lu, W.; Tour, J. M. (2010). Improved synthesis of graphene oxide, *ACS Nano*, Vol. 4, No. 8, 4806–4814. doi:10.1021/nn1006368
- [24] Scaffaro, R.; Maio, A. (2017). A green method to prepare nanosilica modified graphene oxide to inhibit nanoparticles re-aggregation during melt processing,

- Chemical Engineering Journal*, Vol. 308, 1034–1047.
doi:10.1016/j.cej.2016.09.131
- [25] Wang, Y. Z.; Gao, X. F.; Liu, H. H.; Zhang, J.; Zhang, X. X. (2020). Green fabrication of functionalized graphene via one-step method and its reinforcement for polyamide 66 fibers, *Materials Chemistry and Physics*, Vol. 240, No. October 2019, 122288. doi:10.1016/j.matchemphys.2019.122288
- [26] Hummers, W. S.; Offeman, R. E. (1958). Preparation of Graphitic Oxide, *Journal of the American Chemical Society*, Vol. 80, No. 6, 1339. doi:10.1021/ja01539a017
- [27] Cai, Z.; Meng, X.; Han, Y.; Ye, H.; Cui, L.; Zhou, Q. (2015). Reinforcing polyamide 1212 with graphene oxide via a two-step melt compounding process, *Composites Part A: Applied Science and Manufacturing*, Vol. 69, 115–123. doi:10.1016/j.compositesa.2014.11.011
- [28] Gong, L.; Yin, B.; Li, L. P.; Yang, M. B. (2015). Nylon-6/Graphene composites modified through polymeric modification of graphene, *Composites Part B: Engineering*, Vol. 73, 49–56. doi:10.1016/j.compositesb.2014.12.009
- [29] Pan, Y.; Hong, N.; Zhan, J.; Wang, B.; Song, L.; Hu, Y. (2014). Effect of Graphene on the Fire and Mechanical Performances of Glass Fiber-Reinforced Polyamide 6 Composites Containing Aluminum Hypophosphite, *Polymer - Plastics Technology and Engineering*, Vol. 53, No. 14, 1467–1475. doi:10.1080/03602559.2014.909483
- [30] Cho, B. G.; Lee, J. E.; Hwang, S. H.; Han, J. H.; Chae, H. G.; Park, Y. Bin. (2020). Enhancement in mechanical properties of polyamide 66-carbon fiber composites containing graphene oxide-carbon nanotube hybrid nanofillers synthesized through in situ interfacial polymerization, *Composites Part A: Applied Science and Manufacturing*, Vol. 135, No. May, 105938. doi:10.1016/j.compositesa.2020.105938
- [31] Karatas, E.; Gul, O.; Karsli, N. G.; Yilmaz, T. (2019). Synergetic effect of graphene nanoplatelet, carbon fiber and coupling agent addition on the tribological, mechanical and thermal properties of polyamide 6,6 composites, *Composites Part B: Engineering*, Vol. 163, No. July 2018, 730–739. doi:10.1016/j.compositesb.2019.01.014

- [32] Saner Okan, B.; Menciloğlu, Y.; Ozunlu, B. G.; Yagci, Y. E. (2020). Graphene from waste tire by recycling technique for cost-effective and light-weight automotive plastic part production, *AIP Conference Proceedings*, Vol. 2205, No. January. doi:10.1063/1.5142961
- [33] Yan, D.; Zhang, H. Bin; Jia, Y.; Hu, J.; Qi, X. Y.; Zhang, Z.; Yu, Z. Z. (2012). Improved electrical conductivity of polyamide 12/graphene nanocomposites with maleated polyethylene-octene rubber prepared by melt compounding, *ACS Applied Materials and Interfaces*, Vol. 4, No. 9, 4740–4745. doi:10.1021/am301119b
- [34] Thomas, S.; Sarathchandran, C.; Chandran, N. (2019). *Rheology of Polymer Blends and Nanocomposites: Theory, Modelling and Applications*, *Rheology of Polymer Blends and Nanocomposites: Theory, Modelling and Applications*, Elsevier. doi:10.1016/C2017-0-04410-5
- [35] Mayoral, B.; Harkin-Jones, E.; Khanam, P. N.; Almaadeed, M. A.; Ouederni, M.; Hamilton, A. R.; Sun, D. (2015). Melt processing and characterisation of polyamide 6/graphene nanoplatelet composites, *RSC Advances*, Vol. 5, No. 65, 52395–52409. doi:10.1039/c5ra08509h
- [36] Canales, J.; Fernández, M.; Peña, J. J.; Eugenia Muñoz, M.; Santamaría, A. (2015). Rheological methods to investigate graphene/amorphous polyamide nanocomposites: Aspect ratio, processing, and crystallization, *Polymer Engineering & Science*, Vol. 55, No. 5, 1142–1151. doi:10.1002/pen.23985
- [37] Cho, E. C.; Huang, J. H.; Li, C. P.; Chang-Jian, C. W.; Lee, K. C.; Hsiao, Y. S.; Huang, J. H. (2016). Graphene-based thermoplastic composites and their application for LED thermal management, *Carbon*, Vol. 102, 66–73. doi:10.1016/j.carbon.2016.01.097
- [38] Cakal Sarac, E.; Haghghi Poudeh, L.; Seyyed Monfared Zanjani, J.; Pehlivan, Z. S.; Cebeci, F. Ç.; Aydin, I.; Menciloglu, Y.; Saner Okan, B. (2019). Nano-engineering of high-performance PA6.6 nanocomposites by the integration of CVD-grown carbon fiber on graphene as a bicomponent reinforcement by melt-compounding, *Journal of Applied Polymer Science*, Vol. 136, No. 47. doi:10.1002/app.48347
- [39] Kim, J.; Oh, J.; Lee, K. Y.; Jung, I.; Park, M. (2017). Dispersion of graphene-based nanocarbon fillers in polyamide 66 by dry processing and its effect on mechanical

- properties, *Composites Part B: Engineering*, Vol. 114, 445–456. doi:10.1016/j.compositesb.2017.01.054
- [40] Balani, K.; Verma, V.; Agarwal, A.; Narayan, R. (2015). Physical, Thermal, and Mechanical Properties of Polymers, *Biosurfaces*, 329–344. doi:10.1002/9781118950623.app1
- [41] Zanjani, J. S. M.; Poudeh, L. H.; Ozunlu, B. G.; Yagci, Y. E.; Menciloglu, Y.; Saner Okan, B. (2020). Development of waste tire-derived graphene reinforced polypropylene nanocomposites with controlled polymer grade, crystallization and mechanical characteristics via melt-mixing, *Polymer International*, No. March. doi:10.1002/pi.6012
- [42] Lim, L. T.; Britt, I. J.; Tung, M. A. (1999). Sorption and Transport of Water Vapor in Nylon 6,6 Film, *Journal of Applied Polymer Science*, Vol. 71, No. 2, 197–206. doi:10.1002/(SICI)1097-4628(19990110)71:2<197::AID-APP2>3.0.CO;2-J
- [43] Zhang, J.; Gao, X.; Zhang, X.; Liu, H.; Zhang, H.; Zhang, X. (2019). Polyamide 66 and amino-functionalized multi-walled carbon nanotube composites and their melt-spun fibers, *Journal of Materials Science*, Vol. 54, No. 16, 11056–11068. doi:10.1007/s10853-019-03619-0
- [44] Liu, X.; Wu, Q.; Berglund, L. A. (2002). Polymorphism in polyamide 66/clay nanocomposites, *Polymer*, Vol. 43, No. 18, 4967–4972. doi:10.1016/S0032-3861(02)00331-2
- [45] Göransson, D. J. O.; Borgström, M. T.; Huang, Y. Q.; Messing, M. E.; Hessman, D.; Buyanova, I. A.; Chen, W. M.; Xu, H. Q. (2019). Measurements of strain and bandgap of coherently epitaxially grown wurtzite InAsP-InP core-shell nanowires, *ArXiv*
- [46] Doumeng, M.; Makhlouf, L.; Berthet, F.; Marsan, O.; Delbé, K.; Denape, J.; Chabert, F. (2021). A comparative study of the crystallinity of polyetheretherketone by using density, DSC, XRD, and Raman spectroscopy techniques, *Polymer Testing*, Vol. 93, No. May 2020. doi:10.1016/j.polymertesting.2020.106878
- [47] Xiao, K. Q.; Zhang, L. C.; Zarudi, I. (2007). Mechanical and rheological properties of carbon nanotube-reinforced polyethylene composites, *Composites Science and*

Technology, Vol. 67, No. 2, 177–182. doi:10.1016/j.compscitech.2006.07.027

- [48] Du, F.; Scogna, R. C.; Zhou, W.; Brand, S.; Fischer, J. E.; Winey, K. I. (2004). Nanotube networks in polymer nanocomposites: Rheology and electrical conductivity, *Macromolecules*, Vol. 37, No. 24, 9048–9055. doi:10.1021/ma049164g
- [49] Pötschke, P.; Fornes, T. D.; Paul, D. R. (2002). Rheological behavior of multiwalled carbon nanotube/polycarbonate composites, *Polymer*, Vol. 43, No. 11, 3247–3255. doi:10.1016/S0032-3861(02)00151-9
- [50] Cho, J. W.; Paul, D. R. (2001). Nylon 6 nanocomposites by melt compounding, *Polymer*, Vol. 42, No. 3, 1083–1094. doi:10.1016/S0032-3861(00)00380-3
- [51] Meng, F.; Olivetti, E. A.; Zhao, Y.; Chang, J. C.; Pickering, S. J.; McKechnie, J. (2018). Comparing Life Cycle Energy and Global Warming Potential of Carbon Fiber Composite Recycling Technologies and Waste Management Options, *ACS Sustainable Chemistry and Engineering*, Vol. 6, No. 8, 9854–9865. doi:10.1021/acssuschemeng.8b01026
- [52] Wellekötter, J.; Resch, J.; Baz, S.; Gresser, G. T.; Bonten, C. (2020). Insights into the processing of recycled carbon fibers via injection molding compounding, *Journal of Composites Science*, Vol. 4, No. 4. doi:10.3390/jcs4040161
- [53] Francis, S. (n.d.). CW Collections: Recycled Composites, *Gardner Business Media, Inc.*, 23
- [54] Utekar, S.; V K, S.; More, N.; Rao, A. (2021). Comprehensive study of recycling of thermosetting polymer composites – Driving force, challenges and methods, *Composites Part B: Engineering*, Vol. 207, No. December 2020, 108596. doi:10.1016/j.compositesb.2020.108596
- [55] Kawajiri, K.; Kobayashi, M. (2022). Cradle-to-Gate life cycle assessment of recycling processes for carbon fibers: A case study of ex-ante life cycle assessment for commercially feasible pyrolysis and solvolysis approaches, *Journal of Cleaner Production*, Vol. 378, No. July, 134581. doi:10.1016/j.jclepro.2022.134581
- [56] Feng, H.; Xu, X.; Wang, B.; Su, Y.; Liu, Y.; Zhang, C.; Zhu, J.; Ma, S. (2023). Facile preparation, closed-loop recycling of multifunctional carbon fiber reinforced polymer composites, *Composites Part B: Engineering*, Vol. 257, No.

February. doi:10.1016/j.compositesb.2023.110677

- [57] Sathler, C. R. D. L. J. F.; Reis, Y. H. Q. J. M. L.; Costa, H. S. (2021). Thermal aging of a polyamide 66 — experimental analysis and modeling, *Journal of the Brazilian Society of Mechanical Sciences and Engineering*, Vol. 2. doi:10.1007/s40430-021-02810-2
- [58] Chekkour, R.; Benaarbia, A.; Chatzigeorgiou, G.; Meraghni, F.; Robert, G. (2023). Effect of thermo-hygro glycol aging on the damage mechanisms of short glass-fiber reinforced polyamide 66, *Composites Part A: Applied Science and Manufacturing*, Vol. 165, No. September 2022, 107358. doi:10.1016/j.compositesa.2022.107358
- [59] Chen, Q.; Chatzigeorgiou, G.; Robert, G.; Meraghni, F. (2022). Viscoelastic-viscoplastic homogenization of short glass-fiber reinforced polyamide composites (PA66/GF) with progressive interphase and matrix damage: New developments and experimental validation, *Mechanics of Materials*, Vol. 164, No. September 2021, 104081. doi:10.1016/j.mechmat.2021.104081
- [60] Le Gac, P. Y.; Fayolle, B. (2018). Impact of fillers (short glass fibers and rubber) on the hydrolysis-induced embrittlement of polyamide 6.6, *Composites Part B: Engineering*, Vol. 153, No. April, 256–263. doi:10.1016/j.compositesb.2018.07.028
- [61] Holmström, P. H.; Hopperstad, O. S.; Clausen, A. H. (2020). Anisotropic tensile behaviour of short glass-fibre reinforced polyamide-6, *Composites Part C: Open Access*, Vol. 2, No. August. doi:10.1016/j.jcomc.2020.100019
- [62] Hriberšek, M.; Kulovec, S. (2022). Study of the glass fibres and internal lubricants influence in a polyamide 66 matrix on the wear evolution of polyacetal and polyamide 66 based gears in a meshing process, *Engineering Failure Analysis*, Vol. 134, No. January. doi:10.1016/j.engfailanal.2022.106071
- [63] Bondy, M.; Rodgers, W.; Altenhof, W. (2019). Tensile fatigue characterization of polyamide 66/carbon fiber direct/in-line compounded long fiber thermoplastic composites, *Composites Part B: Engineering*, Vol. 173, No. May, 106984. doi:10.1016/j.compositesb.2019.106984
- [64] Gao, X.; Yu, W.; Zhang, X.; Zhang, J.; Liu, H.; Zhang, X. (2019). Facile

- Fabrication of PA66/GO/MWNTs-COOH Nanocomposites and Their Fibers, *Fibers*, Vol. 7, No. 8, 69. doi:10.3390/fib7080069
- [65] Hendrix, J. W.; Szeto, R.; Nosker, T.; Lynch-Branzoi, J.; Emge, T. J. (2018). Evaluation of exfoliated graphite to graphene in polyamide 66 using novel high shear elongational flow, *Polymers*, Vol. 10, No. 12. doi:10.3390/polym10121399
- [66] Li, J.; Qian, L.; Xi, W.; Qiu, Y.; Tang, W.; Li, S. (2022). Alloying synergistic flame retardant effect improving fire resistance and mechanical properties of polyamide 6, *Journal of Applied Polymer Science*, Vol. 139, No. 48. doi:10.1002/app.53226
- [67] Zhang, T.; Xu, Y.; Li, H.; Zhang, B. (2019). Interfacial adhesion between carbon fibers and nylon 6: Effect of fiber surface chemistry and grafting of nano-SiO₂, *Composites Part A: Applied Science and Manufacturing*, Vol. 121, No. September 2018, 157–168. doi:10.1016/j.compositesa.2019.03.029
- [68] Fernandez-Barranco, C.; Yebra-Rodriguez, A.; La Rubia-Garcia, M. D.; Navas-Martos, F. J.; Alvarez-Lloret, P. (2015). Mechanical and crystallographic properties of injection-molded polyamide 66/sepiolite nanocomposites with different clay loading, *Polymer Composites*, Vol. 36, No. 12, 2326–2333. doi:10.1002/pc.23146
- [69] Ghadami Jadval Ghadam, A.; Karimi, H. (2015). Synthesis and Characterization of Polyamide-66/Calcium Carbonate Composites, *Journal of Chemical and Petroleum Engineering*, Vol. 49, No. 1, 63–78. doi:10.22059/jchpe.2015.9962
- [70] Shao, X. L.; Wei, Y. F.; Wu, L.; He, D. M.; Mo, H.; Zhou, N. L.; Zhang, J.; Shen, J. (2012). Studies on Crystal Morphology and Crystallization Kinetics of Polyamide 66 Filled with CaCO₃ of Different Sizes and Size Distribution, *Polymer - Plastics Technology and Engineering*, Vol. 51, No. 6, 590–596. doi:10.1080/03602559.2012.659308
- [71] Qi, S.; Gao, X.; Su, Y.; Zhou, Y.; Dong, X.; Wang, D. (2022). Effect of carbon nanotubes on mechanical properties of polyamide 12 parts by fused filament fabrication, *Polymer*, Vol. 247, No. December 2021, 124784. doi:10.1016/j.polymer.2022.124784
- [72] Li, B.; Song, G.; Peng, Z.; Zhang, W.; Zheng, H.; Zhu, J.; Wang, C.; Wang, J.; Ma,

- R.; Zhu, S.; Yang, X.; Huang, Y.; Ma, L. (2023). Improving mechanical and thermal properties of short carbon fiber/polyamide 6 composites through a polydopamine/nano-silica interface layer, *Journal of Applied Polymer Science*, Vol. 140, No. 6. doi:10.1002/app.53457
- [73] Ciampaglia, A.; Ciardiello, R.; Cesano, F.; Belingardi, G.; Brunella, V. (2023). Multifunctional material design for strain sensing: Carbon black effect on mechanical and electrical properties of polyamides, *Composite Structures*, Vol. 304, No. P2, 116373. doi:10.1016/j.compstruct.2022.116373
- [74] Mardlin, K.; Osazuwa, O.; Kontopoulou, M.; Leelapornpisit, W. (2022). Polyamide composites containing graphene nanoplatelets produced via thermomechanical exfoliation, *Composites Science and Technology*, Vol. 225, No. May, 109493. doi:10.1016/j.compscitech.2022.109493
- [75] Kiziltas, A.; Liu, W.; Tamrakar, S.; Mielewski, D. (2021). Graphene nanoplatelet reinforcement for thermal and mechanical properties enhancement of bio-based polyamide 6, 10 nanocomposites for automotive applications, *Composites Part C: Open Access*, Vol. 6, 100177. doi:10.1016/j.jcomc.2021.100177
- [76] Wu, J.; Gan, H.; Liu, H. (2021). Coagulation-assisted preparation of graphene oxide/polyamide 6 composites, *Materials Chemistry and Physics*, Vol. 266, No. August 2020, 124579. doi:10.1016/j.matchemphys.2021.124579
- [77] Minář, J.; Brožek, J.; Michalcová, A.; Hadravová, R.; Slepíčka, P. (2019). Functionalization of graphene oxide with poly(ϵ -caprolactone) for enhanced interfacial adhesion in polyamide 6 nanocomposites, *Composites Part B: Engineering*, Vol. 174, No. May. doi:10.1016/j.compositesb.2019.107019
- [78] Surace, R.; Pagano, C.; Bellantone, V.; Gatti, S.; Castellani, L.; Vighi, M.; Stoclet, G.; Sechi, S.; Fassi, I.; Baldi, F. (2021). Injection vs micro-injection molding of nano-particle filled polyamide 6: Moldability and structuring, *Polymer*, Vol. 230, No. March. doi:10.1016/j.polymer.2021.124035
- [79] Deepa Urs, M. V.; Suresha, B.; Hemanth, G.; Kulkarni, G.; Shiva Charan, M. R. (2020). Influence of graphene nanoplatelets on tribological properties of short carbon fibre reinforced PA-66/TCE composites, *Materials Today: Proceedings*, Vol. 43, 1640–1646. doi:10.1016/j.matpr.2020.10.013

- [80] Padhi, P. K.; Satapathy, A.; Nakka, A. M. (2015). Processing, characterization, and wear analysis of short glass fiber-reinforced polypropylene composites filled with blast furnace slag, *Journal of Thermoplastic Composite Materials*, Vol. 28, No. 5, 656–671. doi:10.1177/0892705713486142
- [81] He, D.; Soo, V. K.; Kim, H. C.; Doolan, M. (2021). Life Cycle Primary Energy Demand and Greenhouse Gas Emission benefits of vehicle lightweighting with recycled carbon fibre, *Procedia CIRP*, Vol. 98, No. March, 43–48. doi:10.1016/j.procir.2021.01.003
- [82] Li, Y.; Liu, K.; Zhang, J.; Xiao, R. (2018). Preparation and characterizations of inherent flame retarded polyamide 66 containing the phosphorus linking pendent group, *Polymers for Advanced Technologies*, Vol. 29, No. 2, 951–960. doi:10.1002/pat.4206
- [83] Wang, C.; Li, M.; WANG, H.; Wang, X.; FILIPPINI, F. R. (2009). Monte Carlo technique to simulate amide interchange reactions: an improved model of PA6/PA66 blending system
- [84] Kurima, A.; Kinashi, K.; Sakai, W.; Tsutsumi, N. (2022). Spin-Trapping Analysis of the Thermal Degradation Reaction of Polyamide 66, *Polymers*, Vol. 14, No. 21. doi:10.3390/polym14214748
- [85] Mark, H. F.; Kroschwitz, J. I. (n.d.). *Encyclopedia of Polymer Science and Engineering*, TA - TT - (2nd ed.), Wiley, New York SE -. doi:LK - <https://worldcat.org/title/11158119>
- [86] Dericiler, K.; Sadeghi, H. M.; Yagci, Y. E.; Sas, H. S.; Okan, B. S. (2021). Experimental and numerical investigation of flow and alignment behavior of waste tire-derived graphene nanoplatelets in PA66 matrix during melt-mixing and injection, *Polymers*, Vol. 13, No. 6. doi:10.3390/polym13060949
- [87] Li, Y. Y.; Liu, K.; Xiao, R. (2017). Preparation and characterizations of flame retardant polyamide 66 fiber, *IOP Conference Series: Materials Science and Engineering*, Vol. 213, No. 1. doi:10.1088/1757-899X/213/1/012040
- [88] Güllü, A.; Özdemir, A.; Özdemir, E. (2006). Experimental investigation of the effect of glass fibres on the mechanical properties of polypropylene (PP) and polyamide 6 (PA6) plastics, *Materials and Design*, Vol. 27, No. 4, 316–323.

doi:10.1016/j.matdes.2004.10.013

- [89] Zanjani, J. S. M.; Poudeh, L. H.; Ozunlu, B. G.; Yagci, Y. E.; Menciloglu, Y.; Saner Okan, B. (2020). Development of waste tire-derived graphene reinforced polypropylene nanocomposites with controlled polymer grade, crystallization and mechanical characteristics via melt-mixing, *Polymer International*, No. April. doi:10.1002/pi.6012
- [90] Batista, N. L.; Olivier, P.; Bernhart, G.; Rezende, M. C.; Botelho, E. C. (2016). Correlation between degree of crystallinity, morphology and mechanical properties of PPS/carbon fiber laminates, *Materials Research*, Vol. 19, No. 1, 195–201. doi:10.1590/1980-5373-MR-2015-0453
- [91] Cetiner, B.; Sahin Dundar, G.; Yusufoglu, Y.; Saner Okan, B. (2023). Sustainable Engineered Design and Scalable Manufacturing of Upcycled Graphene Reinforced Polylactic Acid/Polyurethane Blend Composites Having Shape Memory Behavior, *Polymers*, Vol. 15, No. 5. doi:10.3390/polym15051085
- [92] Dündar, G. Ş.; Saner Okan, B. (2023). An efficient interface model to develop scalable methodology of melt processing of polypropylene with graphene oxide produced by an improved and eco-friendly electrochemical exfoliation, *Journal of Applied Polymer Science*, Vol. 140, No. 2, 1–14. doi:10.1002/app.53282
- [93] Aoki, R.; Yamaguchi, A.; Hashimoto, T.; Urushisaki, M.; Sakaguchi, T.; Kawabe, K.; Kondo, K.; Iyo, H. (2019). Preparation of carbon fibers coated with epoxy sizing agents containing degradable acetal linkages and synthesis of carbon fiber-reinforced plastics (CFRPs) for chemical recycling, *Polymer Journal*, Vol. 51, No. 9, 909–920. doi:10.1038/s41428-019-0202-7
- [94] Alderliesten, R. C. (2013). Critical review on the assessment of fatigue and fracture in composite materials and structures, *Engineering Failure Analysis*, Vol. 35, No. December 2013, 370–379. doi:10.1016/j.engfailanal.2013.03.022
- [95] Saravanakumar, K.; Arumugam, V.; Souhith, R.; Santulli, C. (2020). Influence of milled glass fiber fillers on mode I & mode II interlaminar fracture toughness of epoxy resin for fabrication of glass/epoxy composites, *Fibers*, Vol. 8, No. 6. doi:10.3390/FIB8060036
- [96] Bastioli, C.; Magistrali, P.; Gestí Garcia, S. (2013). *Bio-Based Plastics*, (S.

- Kabasci, Ed.) *Bio-Based Plastics: Materials and Applications*, Wiley.
doi:10.1002/9781118676646
- [97] Zhu, J. H.; Kiziltas, A.; Lee, E. C.; Mielewski, D. (2015). Bio-based polyamides reinforced with cellylose nanofibers - processing and characterization, *Spe Acce*, No. November
- [98] Maizel', N. S.; Zezina, L. A.; Zagorskaya, Z. G.; Kazaryan, L. G.; Abramova, I. M.; Vasil'eva, V. A.; Maslova, Y. V.; Balabanova, V. A. (1990). Influence of composition and irradiation of the structure and mechanical properties of compositions based on polyamide-610, *Polymer Science U.S.S.R.*, Vol. 32, No. 3, 495–501. doi:10.1016/0032-3950(90)90137-U
- [99] Quiles-Carrillo, L.; Boronat, T.; Montanes, N.; Balart, R.; Torres-Giner, S. (2019). Injection-molded parts of fully bio-based polyamide 1010 strengthened with waste derived slate fibers pretreated with glycidyl- and amino-silane coupling agents, *Polymer Testing*, Vol. 77, No. April, 105875. doi:10.1016/j.polymertesting.2019.04.022
- [100] Lee, J.; Yun, Y. S.; Kim, B.; Cho, S. Y.; Jin, H. J. (2014). Nylon 610/graphene oxide composites prepared by in-situ interfacial polymerization, *Journal of Nanoscience and Nanotechnology*, Vol. 14, No. 8, 5703–5707. doi:10.1166/jnn.2014.8793
- [101] Marset, D.; Dolza, C.; Boronat, T.; Montanes, N.; Balart, R.; Sanchez-Nacher, L.; Quiles-Carrillo, L. (2020). Injection-Molded parts of partially biobased polyamide 610 and biobased halloysite nanotubes, *Polymers*, Vol. 12, No. 7, 1–15. doi:10.3390/polym12071503
- [102] Kang, M.; Myung, S. J.; Jin, H. J. (2006). Nylon 610 and carbon nanotube composite by in situ interfacial polymerization, *Polymer*, Vol. 47, No. 11, 3961–3966. doi:10.1016/j.polymer.2006.03.073
- [103] Tian, Y.; Kim, W.; Kowalski, E.; Kiziltas, A.; Mielewski, D.; Argento, A. (2022). Damping of micro- and nanocellulose reinforced PA610 composites and influences of moisture absorption, *Materials Today Communications*, Vol. 33, No. May, 104325. doi:10.1016/j.mtcomm.2022.104325
- [104] Nagel, J.; Hanemann, T.; Rapp, B. E.; Finnah, G. (2022). Enhanced PTC Effect in

- Polyamide/Carbon Black Composites, *Materials*, Vol. 15, No. 15, 1–13. doi:10.3390/ma15155400
- [105] Ogunsona, E. O.; Misra, M.; Mohanty, A. K. (2017). Sustainable biocomposites from biobased polyamide 6,10 and biocarbon from pyrolyzed miscanthus fibers, *Journal of Applied Polymer Science*, Vol. 134, No. 4, 1–11. doi:10.1002/app.44221
- [106] Battezzore, D.; Salvetti, O.; Frache, A.; Peduto, N.; De Sio, A.; Marino, F. (2016). Thermo-mechanical properties enhancement of bio-polyamides (PA10.10 and PA6.10) by using rice husk ash and nanoclay, *Composites Part A: Applied Science and Manufacturing*, Vol. 81, 193–201. doi:10.1016/j.compositesa.2015.11.022
- [107] Wyzgoski, M. G.; Novak, G. E. (1995). Fatigue fracture of long fiber reinforced nylon 66, *Polymer Composites*, Vol. 16, No. 1, 38–51. doi:10.1002/pc.750160107
- [108] Wyzgoski, M. G.; Novak, G. E. (1991). Fatigue fracture of nylon polymers - Part II Effect of glass-fibre reinforcement, *Journal of Materials Science*, Vol. 26, No. 23, 6314–6324. doi:10.1007/BF02387810
- [109] KUCIEL, S.; KUZNIAR, P.; LIBER-KNEC, A. (2012). Polyamides from renewable sources as matrices of short fiber reinforced biocomposites, *Polimery*, Vol. 57, No. 9, 627–634. doi:10.14314/polimery.2012.627
- [110] Artykbaeva, E.; Ucpinar Durmaz, B.; Aksoy (Golshaei), P. (Parisa); Aytac, A. (2022). Investigation of the properties of PA6/PA610 blends and glass fiber reinforced PA6/PA610 composites, *Polymer Composites*, Vol. 43, No. 10, 7514–7525. doi:10.1002/pc.26840
- [111] Nikiforov, A. A.; Okhotina, N. A.; Fayzullin, I. Z.; Volfson, S. I.; Rinberg, R.; Kroll, L. (2016). Stress-strain properties of composites based on bio-based polyamide 1010 filled with cut fibers, *AIP Conference Proceedings*, Vol. 1785, No. November 2016. doi:10.1063/1.4967039
- [112] Caltagirone, P. E.; Ginder, R. S.; Ozcan, S.; Li, K.; Gay, A. M.; Stonecash, J.; Steirer, K. X.; Cousins, D.; Kline, S. P.; Maxey, A. T.; Stebner, A. P. (2021). Substitution of virgin carbon fiber with low-cost recycled fiber in automotive grade injection molding polyamide 66 for equivalent composite mechanical performance

with improved sustainability, *Composites Part B: Engineering*, Vol. 221, No. September 2020, 109007. doi:10.1016/j.compositesb.2021.109007

- [113] Dericiler, K.; Zafar, S.; Sas, H. S.; Saner Okan, B. (2023). The effect of reinforcement aspect ratio on the performance of PA66 composites with recycled carbon fiber and upcycled graphene nanoplatelets: An interface characterization from process to modeling, *Journal of Applied Polymer Science*, Vol. 140, No. 35, 1–14. doi:10.1002/app.54352
- [114] Ferrari, A. C. (2007). Raman spectroscopy of graphene and graphite: Disorder, electron-phonon coupling, doping and nonadiabatic effects, *Solid State Communications*, Vol. 143, Nos. 1–2, 47–57. doi:10.1016/j.ssc.2007.03.052
- [115] Bandi, S.; Ravuri, S.; Peshwe, D. R.; Srivastav, A. K. (2019). Graphene from discharged dry cell battery electrodes, *Journal of Hazardous Materials*, Vol. 126, No. 1, 358–369. doi:10.1016/j.jhazmat.2018.12.005
- [116] Sayah, A.; Habelhames, F.; Bahloul, A.; Nessark, B.; Bonnassieux, Y.; Tendelier, D.; El Jouad, M. (2018). Electrochemical synthesis of polyaniline-exfoliated graphene composite films and their capacitance properties, *Journal of Electroanalytical Chemistry*, Vol. 818, No. April, 26–34. doi:10.1016/j.jelechem.2018.04.016
- [117] Guardia, L.; Fernández-Merino, M. J.; Paredes, J. I.; Solís-Fernández, P.; Villar-Rodil, S.; Martínez-Alonso, A.; Tascón, J. M. D. (2011). High-throughput production of pristine graphene in an aqueous dispersion assisted by non-ionic surfactants, *Carbon*, Vol. 49, No. 5, 1653–1662. doi:10.1016/j.carbon.2010.12.049
- [118] Wang, H. S.; Tian, S. Y.; Yang, S. W.; Wang, G.; You, X. F.; Xu, L. X.; Li, Q. T.; He, P.; Ding, G. Q.; Liu, Z.; Xie, X. M. (2018). Anode coverage for enhanced electrochemical oxidation: A green and efficient strategy towards water-dispersible graphene, *Green Chemistry*, Vol. 20, No. 6, 1306–1315. doi:10.1039/c7gc03345a
- [119] Kumaresan, T. K.; Masilamani, S. A.; Raman, K.; Karazhanov, S. Z.; Subashchandrabose, R. (2021). High performance sodium-ion battery anode using biomass derived hard carbon with engineered defective sites, *Electrochimica Acta*, Vol. 368, 137574. doi:10.1016/j.electacta.2020.137574

- [120] Wang, K.; Xu, Y.; Li, Y.; Dravid, V.; Wu, J.; Huang, Y. (2019). Sodium storage in hard carbon with curved graphene platelets as the basic structural units, *Journal of Materials Chemistry A*, Vol. 7, No. 7, 3327–3335. doi:10.1039/C8TA11510A
- [121] Weaving, J. S.; Lim, A.; Millichamp, J.; Neville, T. P.; Ledwoch, D.; Kendrick, E.; McMillan, P. F.; Shearing, P. R.; Howard, C. A.; Brett, D. J. L. (2020). Elucidating the sodiation mechanism in hard carbon by operando raman spectroscopy, *ACS Applied Energy Materials*, Vol. 3, No. 8, 7474–7484. doi:10.1021/acsaem.0c00867
- [122] Athanasiou, M.; Samartzis, N.; Sygellou, L.; Dracopoulos, V.; Ioannides, T.; Yannopoulos, S. N. (2021). High-quality laser-assisted biomass-based turbostratic graphene for high-performance supercapacitors, *Carbon*, Vol. 172, 750–761. doi:10.1016/j.carbon.2020.10.042
- [123] Luna-Lama, F.; Rodríguez-Padrón, D.; Puente-Santiago, A. R.; Muñoz-Batista, M. J.; Caballero, A.; Balu, A. M.; Romero, A. A.; Luque, R. (2019). Non-porous carbonaceous materials derived from coffee waste grounds as highly sustainable anodes for lithium-ion batteries, *Journal of Cleaner Production*, Vol. 207, 411–417. doi:10.1016/j.jclepro.2018.10.024
- [124] Li, Z. Q.; Lu, C. J.; Xia, Z. P.; Zhou, Y.; Luo, Z. (2007). X-ray diffraction patterns of graphite and turbostratic carbon, *Carbon*, Vol. 45, No. 8, 1686–1695. doi:10.1016/j.carbon.2007.03.038
- [125] Yakobson, B. I.; Tour, J. M.; Stanford, M. G.; Bets, K. V.; Luong, D. X.; Advincula, P. A.; Chen, W.; Li, J. T.; Wang, Z.; McHugh, E. A.; Algozeeb, W. A. (2020). Flash graphene morphologies, *ACS Nano*, Vol. 14, No. 10, 13691–13699. doi:10.1021/acsnano.0c05900
- [126] Lyman, D. J.; Benck, R.; Dell, S.; Merle, S.; Murray-Wijelath, J. (2003). FTIR-ATR analysis of brewed coffee: Effect of roasting conditions, *Journal of Agricultural and Food Chemistry*, Vol. 51, No. 11, 3268–3272. doi:10.1021/jf0209793
- [127] Barbin, D. F.; Felicio, A. L. de S. M.; Sun, D. W.; Nixdorf, S. L.; Hirooka, E. Y. (2014). Application of infrared spectral techniques on quality and compositional attributes of coffee: An overview, *Food Research International*, Vol. 61, 23–32. doi:10.1016/j.foodres.2014.01.005

- [128] Keller, R. (1986). *The Sigma Library of FT-IR Spectra*. (1st ed.), John Wiley and Sons (WIE), St. Louis
- [129] Dericiler, K.; Alishah, H. M.; Bozar, S.; Güneş, S.; Kaya, F. (2020). A novel method for graphene synthesis via electrochemical process and its utilization in organic photovoltaic devices, *Applied Physics A: Materials Science and Processing*, Vol. 126, No. 11, 1–9. doi:10.1007/s00339-020-04091-3
- [130] Kang, H.; Choi, S.; Lee, J. H.; Kim, K. T.; Song, Y. H.; Lee, D. H. (2020). Plasma jet assisted carbonization and activation of coffee ground waste, *Environment International*, Vol. 145, 106113. doi:10.1016/j.envint.2020.106113
- [131] Hontoria-Lucas, C.; López-Peinado, A. J.; López-González, J. de D.; Rojas-Cervantes, M. L.; Martín-Aranda, R. M. (1995). Study of oxygen-containing groups in a series of graphite oxides: Physical and chemical characterization, *Carbon*, Vol. 33, No. 11, 1585–1592. doi:10.1016/0008-6223(95)00120-3
- [132] Luo, W.; Zhang, B.; Zou, H.; Liang, M.; Chen, Y. (2017). Enhanced interfacial adhesion between polypropylene and carbon fiber by graphene oxide/polyethyleneimine coating, *Journal of Industrial and Engineering Chemistry*, Vol. 51, 129–139. doi:10.1016/j.jiec.2017.02.024
- [133] Marsden, A. J.; Brommer, P.; Mudd, J. J.; Dyson, M. A.; Cook, R.; Asensio, M.; Avila, J.; Levy, A.; Sloan, J.; Quigley, D.; Bell, G. R.; Wilson, N. R. (2015). Effect of oxygen and nitrogen functionalization on the physical and electronic structure of graphene, *Nano Research*, Vol. 8, No. 8, 2620–2635. doi:10.1007/s12274-015-0768-0
- [134] Chia, C. H.; Joseph, S. D.; Rawal, A.; Linser, R.; Hook, J. M.; Munroe, P. (2014). Microstructural characterization of white charcoal, *Journal of Analytical and Applied Pyrolysis*, Vol. 109, 215–221. doi:10.1016/j.jaap.2014.06.009
- [135] Rojas, J. V.; Toro-Gonzalez, M.; Molina-Higgins, M. C.; Castano, C. E. (2016). Facile radiolytic synthesis of ruthenium nanoparticles on graphene oxide and carbon nanotubes, *Materials Science and Engineering B: Solid-State Materials for Advanced Technology*, Vol. 205, 28–35. doi:10.1016/j.mseb.2015.12.005
- [136] Inagaki, M. (1996). Carbon materials structure, texture and intercalation, *Solid State Ionics*, Vols 86–88, No. PART 2, 833–839. doi:10.1016/0167-

- [137] Inagaki, M. (1997). Discussion of the formation of nanometric texture in spherical carbon bodies, *Carbon*, Vol. 35, No. 5, 711–713. doi:10.1016/S0008-6223(97)86645-6
- [138] Sun, X.; Li, Y. (2004). Colloidal Carbon Spheres and Their Core/Shell Structures with Noble-Metal Nanoparticles, *Angewandte Chemie - International Edition*, Vol. 43, No. 5, 597–601. doi:10.1002/anie.200352386
- [139] Pol, V. G.; Motiei, M.; Gedanken, A.; Calderon-Moreno, J.; Yoshimura, M. (2004). Carbon spherules: Synthesis, properties and mechanistic elucidation, *Carbon*, Vol. 42, No. 1, 111–116. doi:10.1016/j.carbon.2003.10.005
- [140] Wang, Q.; Li, H.; Chen, L.; Huang, X. (2001). Monodispersed hard carbon spherules with uniform nanopores, *Carbon*, Vol. 39, No. 14, 2211–2214. doi:10.1016/S0008-6223(01)00040-9
- [141] Boo, W. J.; Sun, L.; Warren, G. L.; Moghbelli, E.; Pham, H.; Clearfield, A.; Sue, H. J. (2007). Effect of nanoplatelet aspect ratio on mechanical properties of epoxy nanocomposites, *Polymer*, Vol. 48, No. 4, 1075–1082. doi:10.1016/j.polymer.2006.12.042
- [142] Chong, H. M.; Hinder, S. J.; Taylor, A. C. (2016). Graphene nanoplatelet-modified epoxy: effect of aspect ratio and surface functionality on mechanical properties and toughening mechanisms, *Journal of Materials Science*, Vol. 51, No. 19, 8764–8790. doi:10.1007/s10853-016-0160-9
- [143] Sinclair, A.; Zhou, X.; Tangpong, S.; Bajwa, D. S.; Quadir, M.; Jiang, L. (2019). High-performance styrene-butadiene rubber nanocomposites reinforced by surface-modified cellulose nanofibers, *ACS Omega*, Vol. 4, No. 8, 13189–13199. doi:10.1021/acsomega.9b01313
- [144] Siraj, S.; Al-Marzouqi, A. H.; Iqbal, M. Z.; Ahmed, W. (2022). Impact of Micro Silica Filler Particle Size on Mechanical Properties of Polymeric Based Composite Material, *Polymers*, Vol. 14, No. 22. doi:10.3390/polym14224830
- [145] Dericiler, K.; Kocanali, A.; Buldu-Akturk, M.; Erdem, E.; Saner Okan, B. (2022). Upcycling process of transforming waste coffee into spherical graphene by flash pyrolysis for sustainable supercapacitor manufacturing with virgin graphene

- electrodes and its comparative life cycle assessment, *Biomass Conversion and Biorefinery*. doi:10.1007/s13399-022-02447-8
- [146] Yu, B.; Feng, Y.; Zhu, W.; Wang, R.; Qi, S. (2019). Self-healing electromagnetic interference shielding composite based on Diels–Alder chemistry, *Journal of Materials Science: Materials in Electronics*, Vol. 30, No. 22, 19994–20001. doi:10.1007/s10854-019-02366-x
- [147] Bhingardive, V.; Kar, G. P.; Bose, S. (2016). Lightweight, flexible and ultra-thin sandwich architectures for screening electromagnetic radiation, *RSC Advances*, Vol. 6, No. 74, 70018–70024. doi:10.1039/c6ra14154d
- [148] Karakassides, A.; Karakassides, A.; Konstantinidou, M.; Paipetis, A. S.; Papakonstantinou, P. (2020). Enhanced out of plane electrical conductivity in polymer composites induced by CO₂ laser irradiation of carbon fibers, *Applied Sciences (Switzerland)*, Vol. 10, No. 10. doi:10.3390/app10103561
- [149] Jones, R. M. (1976). Apparent Flexural Modulus and Strength of Multimodulus Materials, *Journal of Composite Materials*, Vol. 10, No. 4, 342–354. doi:10.1177/002199837601000407
- [150] Winnacker, M.; Rieger, B. (2016). Biobased Polyamides: Recent Advances in Basic and Applied Research, *Macromolecular Rapid Communications*, Vol. 37, No. 17, 1391–1413. doi:10.1002/marc.201600181
- [151] Nofar, M. (2021). *PLA Binary Bioblends with Other Biopolymers, Multiphase Polylactide Blends*. doi:10.1016/b978-0-12-824150-9.00005-4
- [152] Stevens, C. V. (2013). *Bio-Based Plastics: Materials and Applications*, John Wiley & Sons
- [153] AKROMID® B28 GM 10/20 1 LA black (4790). (2022), from <https://akroplastic.com/productfilter/details/4790/>
- [154] AKROMID® B3 GF 10 1 black (3658). (2022), from <https://akroplastic.com/productfilter/details/3658/>
- [155] AKROMID® B28 GFM 10/30 7 black (8106). (2022), from <https://akroplastic.com/productfilter/details/8106/>
- [156] AKROMID® B3 GF 15 S3 black (2345). (2022), from <https://akroplastic.com/productfilter/details/2345/>

plastic.com/productfilter/details/2345/, accessed 10-6-2023

- [157] ZHANG, S.; ZHAO, Y.; SUN, X.; JIANG, Z.; WU, Z.; WANG, G. (2007). Crystallization Kinetics and Melting Behavior of PA1010/Ether-based TPU Blends, *Chemical Research in Chinese Universities*, Vol. 23, No. 3, 370–373. doi:10.1016/S1005-9040(07)60078-6
- [158] Inoue, M. (1963). Studies on crystallization of high polymers by differential thermal analysis, *Journal of Polymer Science Part A: General Papers*, Vol. 1, No. 8, 2697–2709. doi:10.1002/pol.1963.100010813
- [159] Brandrup, J.; Immergut, E. H.; Grulke, E. A. (2003). *Polymer Handbook*, John Wiley & Sons, Inc (4th Editio.)
- [160] Pagacz, J.; Raftopoulos, K. N.; Leszczyńska, A.; Pielichowski, K. (2016). Bio-polyamides based on renewable raw materials: Glass transition and crystallinity studies, *Journal of Thermal Analysis and Calorimetry*, Vol. 123, No. 2, 1225–1237. doi:10.1007/s10973-015-4929-x
- [161] Wunderlich - Macromolecular Physics - Crystal Melting. Volume 3-Academic Press .pdf. (n.d.)
- [162] Cakal Sarac, E.; Haghghi Poudeh, L.; Berktaş, I.; Saner Okan, B. (2020). Scalable fabrication of high-performance graphene/polyamide 66 nanocomposites with controllable surface chemistry by melt compounding, *Journal of Applied Polymer Science*, No. August, 1–12. doi:10.1002/app.49972
- [163] Nagarajan, V.; Zhang, K.; Misra, M.; Mohanty, A. K. (2015). Overcoming the fundamental challenges in improving the impact strength and crystallinity of PLA biocomposites: Influence of nucleating agent and mold temperature, *ACS Applied Materials and Interfaces*, Vol. 7, No. 21, 11203–11214. doi:10.1021/acsami.5b01145
- [164] Scaffaro, R.; Maio, A. (2019). Optimization of two-step techniques engineered for the preparation of polyamide 6 graphene oxide nanocomposites, *Composites Part B: Engineering*, Vol. 165, No. June 2018, 55–64. doi:10.1016/j.compositesb.2018.11.107
- [165] Faghihi, M.; Shojaei, A.; Bagheri, R. (2015). Characterization of polyamide 6/carbon nanotube composites prepared by melt mixing-effect of matrix molecular

- weight and structure, *Composites Part B: Engineering*, Vol. 78, 50–64. doi:10.1016/j.compositesb.2015.03.049
- [166] Huang, S.; Wang, M.; Liu, T.; Zhang, W.-D.; Tjiu, W. C.; He, C.; Lu, X. (2009). Morphology, thermal, and rheological behavior of nylon 11/multi-walled carbon nanotube nanocomposites prepared by melt compounding, *Polymer Engineering & Science*, Vol. 49, No. 6, 1063–1068. doi:10.1002/pen.21349
- [167] Versavaud, S.; Régnier, G.; Gouadec, G.; Vincent, M. (2014). Influence of injection molding on the electrical properties of polyamide 12 filled with multi-walled carbon nanotubes, *Polymer*, Vol. 55, No. 26, 6811–6818. doi:10.1016/j.polymer.2014.10.038
- [168] Oliveux, G.; Dandy, L. O.; Leeke, G. A. (2015). Current status of recycling of fibre reinforced polymers: Review of technologies, reuse and resulting properties, *Progress in Materials Science*, Vol. 72, 61–99. doi:10.1016/j.pmatsci.2015.01.004
- [169] Vo Dong, P. A.; Azzaro-Pantel, C.; Cadene, A. L. (2018). Economic and environmental assessment of recovery and disposal pathways for CFRP waste management, *Resources, Conservation and Recycling*, Vol. 133, No. January, 63–75. doi:10.1016/j.resconrec.2018.01.024
- [170] Wang, Y. C.; Zhu, Y. B.; He, Z. Z.; Wu, H. A. (2020). Multiscale investigations into the fracture toughness of SiC/graphene composites: Atomistic simulations and crack-bridging model, *Ceramics International*, Vol. 46, No. 18, 29101–29110. doi:10.1016/j.ceramint.2020.08.082
- [171] Brehmer, B. E. I. (2008). Life Cycle Assessment of biobased polyamides, 2
- [172] Ligthart, R. (2011). EcoPaXX the green performer DSM Engineering Plastics
- [173] Witik, R. A.; Teuscher, R.; Michaud, V.; Ludwig, C.; Månson, J. A. E. (2013). Carbon fibre reinforced composite waste: An environmental assessment of recycling, energy recovery and landfilling, *Composites Part A: Applied Science and Manufacturing*, Vol. 49, 89–99. doi:10.1016/j.compositesa.2013.02.009
- [174] Gardiner, G. (2020). The making of glass fiber, *Composites World*, from <https://www.compositesworld.com/articles/the-making-of-glass-fiber>, accessed 20-12-2023
- [175] Muller, O.; Mercier, J.; Flores, C. E. R. (2023). *Life cycle assessment of CFGF –*

- [176] Jeong, J.-Y.; Lee, H.-J.; Kang, S.-W.; Tan, L.-S.; Baek, J.-B. (2008). Nylon 610/functionalized multiwalled carbon nanotube composite prepared from in-situ interfacial polymerization, *Journal of Polymer Science Part A: Polymer Chemistry*, Vol. 46, No. 18, 6041–6050. doi:10.1002/pola.22916